

Investigating the Continuous Circuit Coprecipitation of Arsenic(V) with Ferric Iron in Sulphate Media

Richard Jack De Klerk, McGill University, Montreal

September 2008

“A thesis submitted to McGill University in partial fulfillment
of the requirements of the degree of Master of Engineering”

© Richard J. De Klerk, 2008

Abstract

This thesis presents the results of an investigation on the impact of continuous circuit and solution parameters on coprecipitation of arsenic with ferric iron from acidic sulphate solution. The techniques employed were selected, or developed, to emulate industrial practice. The concept behind the work was to better understand the link between the process of precipitation and the stability of arsenic in the resultant coprecipitates. This was performed by examining the role of circuit design and co-ions on both arsenic removal during coprecipitation and arsenic retention during ageing. The parameters/factors investigated included continuous versus batch operation, number of stages (pH profile), recycling and Ca^{2+} , Ni^{2+} and Al^{3+} as co-ions.

Arsenic removal was found to be greatly improved by continuous rather than batch coprecipitation. In addition, the presence of calcium (introduced as slaked lime) was found to be instrumental in the removal and retention of arsenic. Arsenic retention during ageing (up to 300 days) at various temperatures (3, 22, 40 and 70°C) was observed to reach an “equilibrium” that was strongly affected by the continuous circuit design, as well as the co-ions present during coprecipitation. Evidence is presented of the partitioning of arsenic within the coprecipitates in two principal phases, namely ferric arsenate ($\text{FeAsO}_4 \cdot x\text{H}_2\text{O}$) and arsenic adsorbed ferrihydrite. Continuous circuit design parameters, such as staging, that resulted in enhanced stability appear to yield coprecipitates with higher ferric arsenate content. Analysis of the kinetic and “equilibrium” arsenic retention data yielded activation energy (~ 60 kJ/mol) and enthalpy (~ -38.5 kJ/mol) values that suggest a reaction controlled exothermic dissolution mechanism.

Ce mémoire de maîtrise présente les résultats d'une étude portée sur la co-précipitation de l'arsenic et des ions ferriques en solution aqueuse sulfatée. L'utilisation d'un procédé continu et les paramètres de la solution ont été considérés comme cibles d'étude. Les techniques employées ont été sélectionnées ou développées afin de simuler les méthodes opératoires industrielles. L'idée directrice de ce travail était d'aboutir à une meilleure compréhension sur les liens entre les mécanismes de précipitation et la stabilité de l'arsenic dans les co-précipités formés. Aussi, le rôle du design du procédé ainsi que celui des co-ions sur l'extraction, respectivement la stabilisation de l'arsenic ont fait l'objet d'un examen approfondi à court terme soit au stade de co-précipitation, respectivement à long terme durant le vieillissement de la solution. Les paramètres/facteurs étudiés incluaient le caractère continu du procédé (en comparaison avec un procédé discontinu), le nombre d'étapes (le profile pH), le recyclage des produits solides et la nature (Ca^{2+} , Ni^{2+} et Al^{3+}) des co-ions introduits dans le système.

Cette étude a montré que l'utilisation d'un procédé continu (en comparaison avec un procédé discontinu) améliorerait considérablement l'extraction de l'arsenic à partir de solutions aqueuses sulfatées. Aussi, la présence de calcium (introduit sous forme de chaux hydratée) s'est avérée profitable à l'extraction de l'arsenic à court et à long terme. Il a été observé que la stabilisation de l'arsenic dans le cas des expériences de vieillissement (d'une durée de 300 jours) effectuées à différentes températures (3, 22, 40 et 70°C) atteignait un état d'équilibre fortement influencé par le design du procédé continu ainsi que par les co-ions présents lors de la co-précipitation. Il a été mis en évidence que lors de la phase de co-précipitation, l'arsenic était réparti sous forme de deux phases solides d'arséniate de fer ($\text{FeAsO}_4 \cdot x\text{H}_2\text{O}$) et d'arsenic adsorbé à la ferrihydrite. Les co-précipités issus de procédés dont la stabilité était améliorée par control des paramètres d'un design continu, tel que l'introduction d'étapes successives, contenaient un taux plus élevé d'arséniate de fer. L'analyse des données cinétiques et thermodynamiques de stabilisation de l'arsenic ont permis de calculer des valeurs approximatives pour l'énergie ($\sim 60 \text{kJ/mol}$) et l'enthalpie d'activation ($\sim 38.5 \text{kJ/mol}$) correspondant à celles d'une réaction dont le mécanisme de dissolution exothermique est stable.

Acknowledgements

I would like to thank NSERC for providing funding for the research through a Strategic Projects Grant, which was sponsored by: Areva Resources, Barrick Gold, Cameco Corporation, Hatch & Teck Cominco.

I am gratefully indebted to George Demopoulos for providing the opportunity to study and perform research at McGill as well as for his support and guidance during this research. I thank him for his often critical reviews of my ideas, which were instrumental in helping me to identify and pursue those with learning and practical potential.

I would like to thank Ranjan Roy and Glenna Keating for their assistance in performing solution analyses as well as Monique Riendeau, Helen Campbell and Petr Fiurasek, for their assistance in performing solids characterization. I am grateful to all of them for their advice, tips and answers to my inquisitive questions.

I would like to acknowledge Amani Al-Othman, for her role in procuring equipment necessary for the project prior to my arrival. In addition, I would like to thank the Hydromet group who often acted as a sounding board for ideas and a source of knowledge when my own reached its limits; including: Levente, Yongfeng, Jeff, Vincent, Vera, Cecile, Karl, Mario, Nick and Sebastian. Special thanks to Cecile for the abstract translation.

I would also like to thank the people at the Cameco Research Centre for the role that they played in my undergraduate education and for providing both the experience and the direction which eventually lead me to McGill in pursuit of graduate studies.

Finally, I would like to thank my parents for teaching me the value of hard work, as well as my wife Susan, for her encouragement and support during our adventures here in Montreal.

Table of Contents

Abstract.....	ii
Acknowledgements.....	iv
Introduction.....	1
Chapter 1 Literature Review.....	3
1.1 The Electrical Double Layer.....	3
1.1.1 Measurement of the Chemical Properties of Material Surfaces	5
1.2 Precipitation	6
1.2.1 Nucleation.....	6
1.2.2 Growth	7
1.2.3 Step-wise Precipitation Control	7
1.2.4 Metastable Phases (Ostwald Law of Stages vs. Stranski’s Rule).....	8
1.2.5 Solubility and the Gibbs-Thompson Effect (or Kelvin Effect).....	8
1.3 Adsorption (a.k.a. Surface Complexation)	10
1.3.1 Surface Coordination of Adsorbed Ions	10
1.3.2 Physical Adsorption (Outer-sphere complexation).....	12
1.3.3 Chemical Adsorption (Inner-sphere complexation).....	12
1.4 Review of Published Fe(III)-As(V) Coprecipitation Literature.....	13
1.4.1 Summary of the Current Understanding of Coprecipitation.....	13
1.4.2 Effect of Fe/As Molar Ratio on Arsenic Removal.....	14
1.4.3 Effect of pH on Arsenic Stability.....	15
1.4.4 Tabulation and Classification of Coprecipitation Research.....	16
Chapter 2 Methods & Materials	27
2.1 A Note Regarding Ageing “Equilibrium”.....	27
2.2 Heterogeneous Reactions and Concentration Gradients.....	27
2.3 Continuous Circuit Design.....	28
2.3.1 Reactor Dimensions	28
2.3.2 Steady-State Operation	29
2.4 Feed Solution Preparation.....	31
2.5 Batch Coprecipitation	31
2.6 Continuous Coprecipitation Circuit	32
2.7 Continuous Coprecipitation Operation	34
2.8 Coprecipitate Ageing	35
2.9 Arsenic Analysis	36
Chapter 3 Coprecipitate Production	37
3.1 Effect of Base.....	40
3.2 Effect of Circuit Design.....	41
3.2.1 Conceptual Reaction Mechanism	42
3.3 Effect of Co-ions.....	47
3.4 Characterization	48
3.4.1 Settling Rate.....	48
3.4.2 Particle Size Distribution	49

3.4.3	X-Ray Diffraction	51
3.4.4	Measurement of PZC via Batch Equilibration.....	52
3.4.5	Fourier Transform Infrared Spectroscopy	54
3.4.6	Scanning Electron Microscopy.....	55
3.5	Discussion.....	58
Chapter 4	Coprecipitate Ageing	59
4.1	Ageing with pH Control.....	60
4.1.1	Effect of Base.....	62
4.1.2	Effect of Coprecipitation Circuit Design	63
4.1.3	Effect of Aluminium.....	63
4.1.4	Effect of Nickel.....	64
4.2	Ageing without pH Control: “Drift”	66
4.2.1	Effect of Circuit Design on Equilibrium pH.....	70
4.2.2	Effect of Aluminium.....	72
4.2.3	Effect of Nickel.....	72
4.3	Evaluation of Transformation to Crystalline Phases	74
4.4	Discussion.....	76
Chapter 5	Modelling of Coprecipitate Ageing	77
5.1	Calculation of Kinetic & Thermodynamic Terms	78
5.2	Model Selection	81
5.3	Discussion.....	84
Chapter 6	Global Conclusions.....	85
6.1	Recommendations for Future Research.....	87
References	89
Appendix I	Effect of Ionic Strength (on As retention)	94
Appendix II	Equilibrium Constants (As Speciation)	96
Appendix III	Additional Data from Coprecipitate Production and Ageing	100

List of Figures

Figure 1	SG model of the electrical double layer [Fuerstenau & Han, 2003]	4
Figure 2	Solubility-nucleation graph indicating the “metastable zone” or operating region by which to design and control staged precipitation processes	7
Figure 3	Schematic representation of the surface coordination of different adsorbed complexes [Davis & Kent, 1990]	11
Figure 4	Effect of Fe/As molar ratio on arsenic removal during batch coprecipitation (with NaOH) [Robins et al., 1988].....	15
Figure 5	Effect of pH on arsenic stability in coprecipitates (Fe/As =4, 25°C) [Krause & Ettel, 1989].....	16
Figure 6	(a) Recommended dimensions for agitated reactor with baffles and (b) dimensions of reactor used in this continuous coprecipitation work.	29
Figure 7	Theoretical and actual tracer test response curves for a three reactor circuit with (A) 1.5” marine type impellers and (B) 2.5” Lighnin A-310 type impellers.....	30
Figure 8	Schematic diagram of continuous coprecipitation circuit set-up	33
Figure 9	Theoretical solubility of Fe and/or As with respect to FA or FH (assuming congruent dissolution, not including Fe-SO ₄ aqueous complexes)	44
Figure 10	Calculated saturation index of FH and FA as a function of pH (1400 mg/L As, Fe/As=4, instantaneous pH change, no dilution).....	45
Figure 11	Aqueous speciation of Fe and As in equilibrium with FA (assuming congruent dissolution, not including Fe-SO ₄ aqueous complexes).....	46
Figure 12	Initial settling rate of coprecipitates	49
Figure 13	Particle size distribution of coprecipitates A) effect of base, B) effect of circuit design and C) effect of co-ions.....	50
Figure 14	XRD pattern of 2 stage coprecipitates (experiment RP-5, patterns obtained before and after washing to remove gypsum)	51
Figure 15	Bulk PZC of coprecipitates (as indicated by the plateau in pH(final) after batch equilibration at 22°C).....	53
Figure 16	FTIR spectra of coprecipitates.....	54
Figure 17	SEM images of coprecipitates.....	57
Figure 18	Coprecipitate arsenic retention during ageing.....	61
Figure 19	Arsenic retention differences resulting from the type of base (pH 8, 22°C)	62
Figure 20	Arsenic retention differences resulting from the type of base (pH 8, 22°C)	65
Figure 21	Coprecipitate arsenic retention during ageing (pH unadjusted and temperatures of 3, 22, 40 & 70 °C)	67

Figure 22	Solution pH during coprecipitate ageing (pH unadjusted and temperatures of 3, 22, 40 & 70 °C)	68
Figure 23	Nickel & arsenic retention during constant pH and drift ageing (pH 8.0 and 7.1 (3°C), 6.9 (22°C), 6.6 (40°C), and 6.4 (70°C) respectively).....	73
Figure 24	HCl digestion of two-stage coprecipitate solids aged at 70°C, indicating the extent of transformation of iron to crystalline phases	75
Figure 25	Effect of temperature on A) the initial reaction rate (Arrhenius plot) and B) the “equilibrium” concentration (van’t Hoff plot)	78
Figure 26	First-order model fits to the results of coprecipitate ageing (1- 2- and 3-stage respectively).....	83

List of Tables

Table 1	PZC of some common metal (hydrous) oxides [Parks, 1965, Han, 2002]	5
Table 2	Summary of conditions and major observations of published arsenic coprecipitation and adsorption experimental work	17
Table 3	Summary of coprecipitate ageing and tailings monitoring programs	22
Table 4	Summary of coprecipitate ageing and tailings monitoring programs	24
Table 5	Normalized time required to achieve steady-state for a continuous circuit	31
Table 6	Results of continuous circuit coprecipitation experiments (residence time 1 hr)	38
Table 7	Stage removal percentages (absolute basis, to account for dilution effect of base)	39
Table 8	Comparison of effect of base on coprecipitation final stage arsenic concentrations (from Table 6)	40
Table 9	Comparison of batch and continuous circuit final stage arsenic concentrations, for NaOH neutralization (from Table 6)	41
Table 10	Comparison of batch and continuous circuit final stage arsenic concentrations, for Ca(OH) ₂ neutralization (from Table 6)	42
Table 11	Comparison of batch and continuous circuit final stage arsenic concentrations (from Table 6)	47
Table 12	FTIR absorption frequencies for various functional groups	55
Table 13	Summary of equilibrium stability concentration data observed during ageing of coprecipitates (pH 8)	65
Table 14	Calculated FA content of coprecipitates (assuming $\text{pH}_{\text{PZC,FA}}=3.5$, $\text{pH}_{\text{PZC,FH}}=8$)	71
Table 15	Initial rate data and calculated apparent activation energy (E_A) for coprecipitate ageing	78
Table 16	“Equilibrium” concentration data and calculated enthalpy (ΔH) for coprecipitate ageing	79
Table 17	First-order model fit parameter (k) values	81

Introduction

Arsenic is a common impurity in copper, nickel, gold and uranium ores that eventually reports to aqueous processing effluents [Harris & Krause, 1993]. To minimize the risk of environmental impact, the arsenic must be converted to a stable form before disposal. There are several processes which produce an acceptable solid [Harris, 2003], including, but not limited to, coprecipitation with ferric iron. Much research has investigated the effect of the Fe/As ratio during coprecipitation, [Krause & Ettel, 1989, Robins et al. 1988, Langmuir et al. 1999] with indications that a ratio greater than three provides acceptable arsenic stability.

Recent characterization research has indicated that the coprecipitates contain a mixture of two poorly crystalline phases: ferric arsenate, a precursor of scorodite, as well as arsenic adsorbed ferrihydrite, an iron(III) oxyhydroxide commonly utilized to adsorb variable amounts of cations and/or anions [Cutler et al. 2003, Jia et al. 2003, 2005, Chen et al. in review, Paktunc et al. 2008]. The contribution of these two phases to the stability of arsenic under oxidizing disposal conditions is not yet known, nor is it known how the circuit design influences the partitioning of arsenic between the two phases. To date, only one study has used continuous circuit coprecipitation [Moldovan & Hendry, 2005]. All other coprecipitation work has been batch.

Other coprecipitation research has indicated that the aqueous chemistry surrounding the coprecipitation process can have a significant effect on arsenic removal and retention. Sulphate media [Jia & Demopoulos, 2005, 2008] and calcium [Jia & Demopoulos, 2005, Wilkie & Hering, 1996] have been shown to provide improved arsenic removal, while calcium [Jia & Demopoulos, 2005], nickel [Mahoney et al. 2006, Jia & Demopoulos, 2008] and other cations including magnesium, zinc and lead [Emett & Khoe, 1994] and copper, cadmium and zinc [Harris & Monette, 1988, 1989] have all been shown to provide improved arsenic retention.

The first objective of this research was to investigate the continuous circuit coprecipitation process, to evaluate the role of circuit design on arsenic removal, as well

as to clarify the role of co-ions present in the feed solution prior to neutralization. The second objective was to evaluate the effect of both the circuit design and the co-ions on arsenic retention. This was accomplished through ageing of the continuous circuit coprecipitates at various temperatures. The third and final objective of this work was to provide a basis for the development of predictive tools. The premise encompassing this research was the desire to understand the link between the process and arsenic stability.

The research has been divided into chapters to facilitate assimilation and separate concepts. Chapter 1 briefly reviews the subject fields related to the process of coprecipitation, which includes (but is not limited to) colloid chemistry, precipitation and adsorption. It also provides a technical summary of current Fe/As coprecipitation literature, as well as a summary of coprecipitate ageing and tailings monitoring related articles. Chapter 2 outlines the methods and materials used to perform this research. Chapter 3 shows the results of coprecipitate production campaigns and discusses the results with respect to arsenic removal behavior. Characterization of fresh coprecipitates is also briefly discussed in this section. Chapter 4 shows the results of ageing coprecipitates and discusses them with respect to arsenic retention behavior. Chapter 5 begins to interpret the rate and equilibrium data into kinetic and thermodynamic terms suitable for use in a predictive model. In addition, trends are identified which provide an indication of the contribution of the two phases to the stability of arsenic. Finally, some global conclusions are drawn from the work and recommendations for future research are identified.

Chapter 1 Literature Review

The following chapter introduces behavior characteristics of solids in an aqueous environment. In addition, it outlines concepts relevant to the formation of these solids, through precipitation and adsorption phenomena. Finally, literature concerning arsenic removal is considered.

1.1 The Electrical Double Layer

The interface of a solid and a liquid involves the abrupt termination of the solid structure, resulting in unsatisfied co-ordination and the presence of potential energy which is manifested as electrical potential [Parks, 1990]. To preserve electroneutrality, the surface has a tendency to accumulate counter-charge from the ions in solution, or diffuse layer [James & Parks, 1982]. The term electrical double layer (EDL) identifies the presence of the two charged layers at the solid | liquid interface.

Gouy & Chapman first derived equations which served to describe the distribution of counter ions accumulated near the surface. Stern & Grahame refined the model, by recognizing the finite distance of approach which could be achieved, due to either the ionic radius or the hydration layer. The result is known as the GC (or SG or GCSG) model illustrated in Figure 1, where the surface has a finite potential, Ψ_0 , balanced by the ions located in the diffuse (liquid) layer. Various analytical techniques have been developed to evaluate the potential at specific planes in the diffuse layer, which provide an indication of the potential at the solid | liquid interface. The surface potential can change with pH and one of the most important properties of an (hydr)oxide is the pH value where the surface charge transitions between positive and negative, known as the point of zero charge or PZC. The following Nerstian equation relates the surface potential to solution conditions of pH and temperature [Han, 2002].

$$\Psi_0 = 2.303 \frac{RT}{F} \log \left(\frac{[H^+]}{[H^+]_{st.st.}} \right) \quad 1.1$$
$$\Psi_0 = 2.303 \frac{RT}{F} (\text{pH}_{\text{PZC}} - \text{pH})$$

where $[H^+]_{st.st.}$ represents the steady state concentration of H^+
and is equivalent to the pH_{pZC}
 Ψ_0 represents the potential at the solid surface
R is the constant 8.314 kJ/mol
F is Faradays constant
T is temperature in Kelvin

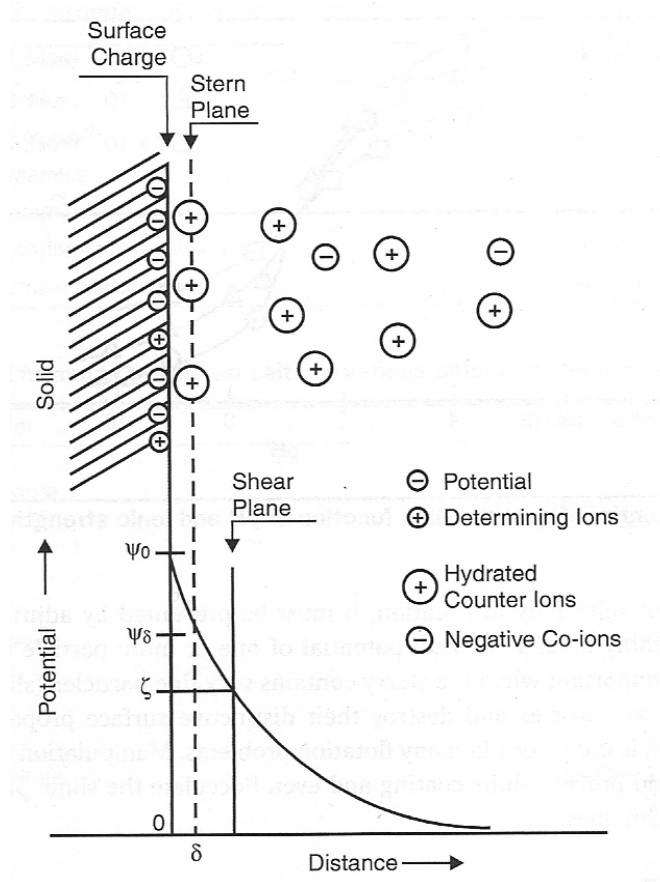


Figure 1 SG model of the electrical double layer [Fuerstenau & Han, 2003]

A more thorough breakdown of EDL properties and behavior, including equations that describe the potential, can be found in the literature. The author recommends the following resources: Parks & De Bruyn, 1962; Parks, 1990 and Han, 2002.

1.1.1 Measurement of the Chemical Properties of Material Surfaces

One of the most commonly encountered methods for quantifying the surface properties at different pH values is the measurement of zeta-potential (the potential at the Shear plane) via electrophoretic techniques. Others include: potentiometric titration, batch equilibration, inert electrolyte titration and mass titration. The details of these and other techniques, as well as tables of the point of zero charge (PZC) of various solids, can be found in literature and have been summarized by Kosmulski [2001].

Table 1 PZC of some common metal (hydrous) oxides [Parks, 1965, Han, 2002]

Metal (Hydrous) Oxides		pH _{PZC}
Iron(III)	Fe(OH) ₃	8.5
	α -Fe ₂ O ₃ (synth)	8.4
	α -Fe ₂ O ₃ (natural)	4.8-6.7
	α -FeOOH (synth)	6.7±0.2
Iron(II)	Fe(OH) ₂	12±0.5
Aluminium	α -Al(OH) ₃	5
	γ - Al(OH) ₃	9.25
	α -Al ₂ O ₃	9
Nickel	Ni(OH) ₂	11.1±0.4
Magnesium	Mg(OH) ₂	12
Calcium	Ca(OH) ₂	12.6
Silica	SiO ₂	2

The PZC of an oxide is a property specific to an oxide, but which can be modified by potential determining ions in the diffuse layer. There are those who argue that evaluation of the PZC can be used as a characterization technique [Fourest et al., 1994] to identify colloids in-situ. The specific nature of the PZC to an oxide is such that a physical mixture of different oxides will develop an apparent “bulk PZC” which is governed by the relative amount of surface area of each of the two phases [De Faria & Trasatti, 2003]

1.2 Precipitation

Precipitation involves the formation of a solid phase from a liquid solution phase. In some cases, such as the system investigated in this work, precipitation can be referred to as reactive crystallization, since the driving force is generated by means of one or more chemical reactions. Generally, precipitation involves the steps of nucleation, crystal growth and agglomeration; all of which are rapid phenomena and can occur simultaneously, making these processes difficult to separate and investigate independently [Wey & Karpinski, 2002]

Wey and Karpinski [2002] identify several important characteristics of precipitation. The “precipitates” are usually sparingly soluble and their formation occurs under relatively high saturation conditions. As a result, nucleation plays a major role in the precipitation process, producing a crystal size between 0.1 and 10 μm . The small particle size then leads to secondary processes such as aggregation; whereby small particles agglomerate, undergo minor growth and become cemented together.

Design of precipitation processes usually center on obtaining appropriate physical properties of the solids, such as crystal size distribution or morphology, which are important for down-stream processing such as thickening, filtration or drying. Precipitation conditions can also be controlled to modify chemical properties such as impurity content or desired morphology.

1.2.1 Nucleation

There are different nucleation mechanisms by which a new solid phase may be formed from solution. The first is called homogeneous nucleation; where solid formation is not caused by the presence of any solid phase. This type of nucleation occurs in three-dimensions. The second type of nucleation is called heterogeneous nucleation; where solid phase formation is induced by the presence of a foreign solid phase (i.e. nucleation occurs on the foreign solid surface). This type of nucleation occurs in less than three dimensions and has a decreased energy barrier (and can occur more easily), as a result of a reduction in the surface tension [Wey & Karpinski, 2002].

1.2.2 Growth

Once nucleation has occurred and a solid phase is present, the process of crystal growth can occur. Growth involves the steps of mass transport through the electrical double layer, as well as surface integration; where dissolved species are incorporated into the crystal structure. The growth rate can be limited by either or both of the two steps. For more details, the reader is directed to the books by Söhnel and Garside [1992] or Myerson [2002].

1.2.3 Step-wise Precipitation Control

Growth and nucleation are competitive mechanisms of precipitation (i.e. both work to reduce the saturation state which drives the precipitation reaction). However, nucleation requires higher supersaturation conditions than growth. From this, a concept of staged (step-wise) precipitation control has been developed by which the saturation conditions are controlled to promote growth. Design and control conditions can be obtained by determination of the metastable zone [Schwartz & Myerson, 2002] where growth is promoted, and is shown in Figure 2 as the grey, bounded region.

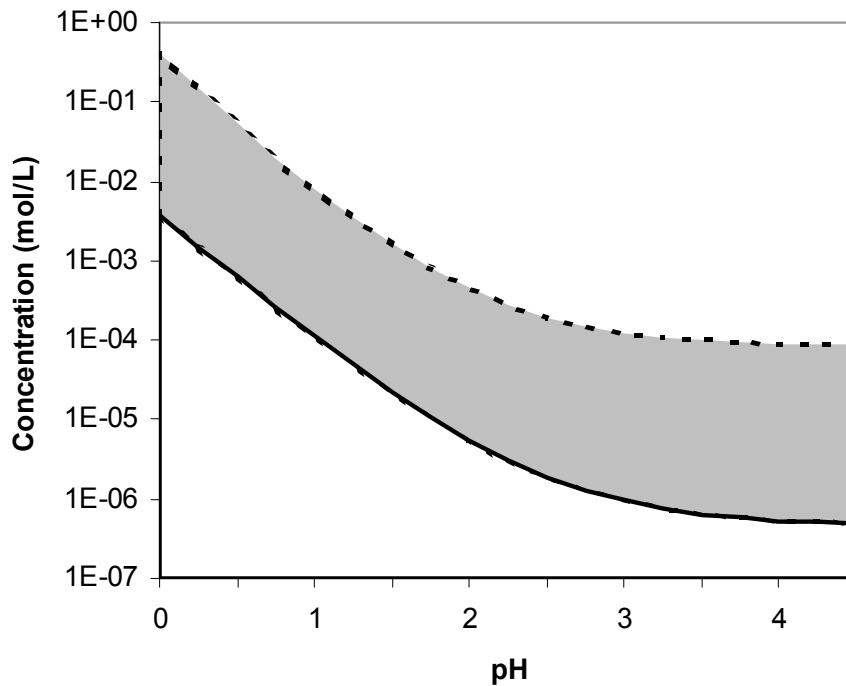


Figure 2 Solubility-nucleation graph indicating the “metastable zone” or operating region by which to design and control staged precipitation processes

In the figure shown, the first (solid) line represents the solubility of the mineral/crystal, or the absence of driving force for precipitation. The second (dashed) line represent the “critical homogenous nucleation line”, defined by a series of points at which homogeneous nucleation occurs. In this instance, since the reaction controlling crystallization is that of acid/base neutralization, pH is used as the x-axis.

In staged precipitation, it is possible to control the saturation conditions by a variety of reactions; including pH, redox, complexation or dissolution [Demopoulos, *accepted*], allowing innovative design of the precipitation process.

1.2.4 Metastable Phases (Ostwald Law of Stages vs. Stranski’s Rule)

Ostwald was the first to comment on the formation of metastable phases during precipitation, formulating the statement: “If the supersaturated state has been spontaneously removed then, instead of a solid phase which under the given conditions is thermodynamically stable, a less stable phase will be formed.” To simplify, the formation of metastable phases, having greater energy, will precede the formation of the most thermodynamically favored phase (provided that the formation of solid proceeds sufficiently quickly) [Söhnle & Garside, 1992].

While Ostwald’s law of stages can be applied to many systems, it has some exceptions and is more of an observation than an explanation stemming from any precipitation mechanisms. For this reason, Stranski instead claimed that the type of solid phase is determined by the kinetics, rather than the thermodynamics, of nucleation. The implication is that the preferential phase formed has the lowest nucleation energy barrier, and thus the highest nucleation rate [Söhnle & Garside, 1992]. That is to say, when homogeneous nucleation dominates, the least stable phase nucleates first. [Blesa & Matijevic, 1989].

1.2.5 Solubility and the Gibbs-Thompson Effect (or Kelvin Effect)

Parks [1990] reports that the magnitude of equilibrium constant can change when significant change in surface area accompanies the reaction. He goes on to derive a general relationship between the equilibrium constant and the free energy of the interface,

at constant pressure and temperature, given below. The specific equation can take several named forms, such as Kelvin, Freundlich-Ostwald or Gibbs-Thompson.

$$\ln(K^S) = \ln(K) + \frac{1}{RT} \sum_j \gamma_j \frac{dA_j}{dn_\phi} \quad 1.2$$

where $\ln(K^S)$ is the equilibrium constant as influenced by the interface
 $\ln(K)$ is the equilibrium constant of the phase without influence

R is the constant 8.314 kJ/mol

T is the temperature in Kelvin

γ_j is the surface free energy of component j

dA_j is the change in area of component j

dn_ϕ is the amount of reacted species ϕ

For solids with small particle size, the amount of surface area (dA_j) changes rapidly with respect to an amount of reacting species (dn_ϕ). The second term in the equation becomes significant, increasing the equilibrium constant $\ln(K^S)$ (i.e. less negative). The end result is a higher solubility for solids with small particle size.

The major significance to arsenic coprecipitation with ferric iron, is that poorly crystalline ferric arsenate and ferrihydrite, which both have a small particle size (and correspondingly large surface areas), exhibit higher solubilities than their more crystalline, lower surface area analogues (scorodite and hematite respectively).

1.3 Adsorption (a.k.a. Surface Complexation)

The phenomenon of adsorption is the result of both electrostatic and chemical forces [Davis & Kent, 1990]. For ions which adsorb at the Stern plane (or outer Helmholtz plane) the sum of the binding energy can be expressed by: [Lyklema, 1987]

$$g_i + zF\Psi_\delta \quad 1.3$$

where g_i is the force of the specific chemical interaction

z is the charge of the sorbing ion

Ψ_δ is the potential of the adsorbing surface

F is Faradays constant

Adsorption can be broken down into two broad categories, depending on the relative contribution of the electrostatic and chemical forces. The first category is physical adsorption (non-specific), and the second category is chemical adsorption (specific). The mechanism of adsorption is dependant on the character of the bond between the adsorbing molecule and the solid surface, which results in the formation of an identifiable surface complex.

Parks mentions that cations and anions adsorb with opposite pH dependence, where each can be modified by ionic strength, hydrolysis, complex formation and the ratio of total adsorbate present to total adsorbent surface area [Parks, 1990].

1.3.1 Surface Coordination of Adsorbed Ions

When an ion adsorbs onto a solid, it does so in a very specific manner, characteristic of the molecular structure of the ion. Spectroscopic techniques are particularly useful in evaluating the nature, and hence manner, of adsorption. A summarization is shown in Figure 3.

A complex adsorbed in the EDL is referred to as an outer-sphere when the hydration shell surrounding the ion (or the solid) remains intact. These complexes are generally weaker than inner-sphere complexes, which bond directly to the surface metal or oxygen groups. In addition, there are a variety of inner-sphere complexes, depending

on the number of bonds formed (dentate) and the number of surface atoms involved (nuclear). Molecules with a single bond to the surface atoms (metal or oxygen) are monodentate, while those with two bonds are bidentate. Similarly, molecules bonding to a single surface atom (metal or oxygen) are mononuclear, while those bonding to two atoms are binuclear.

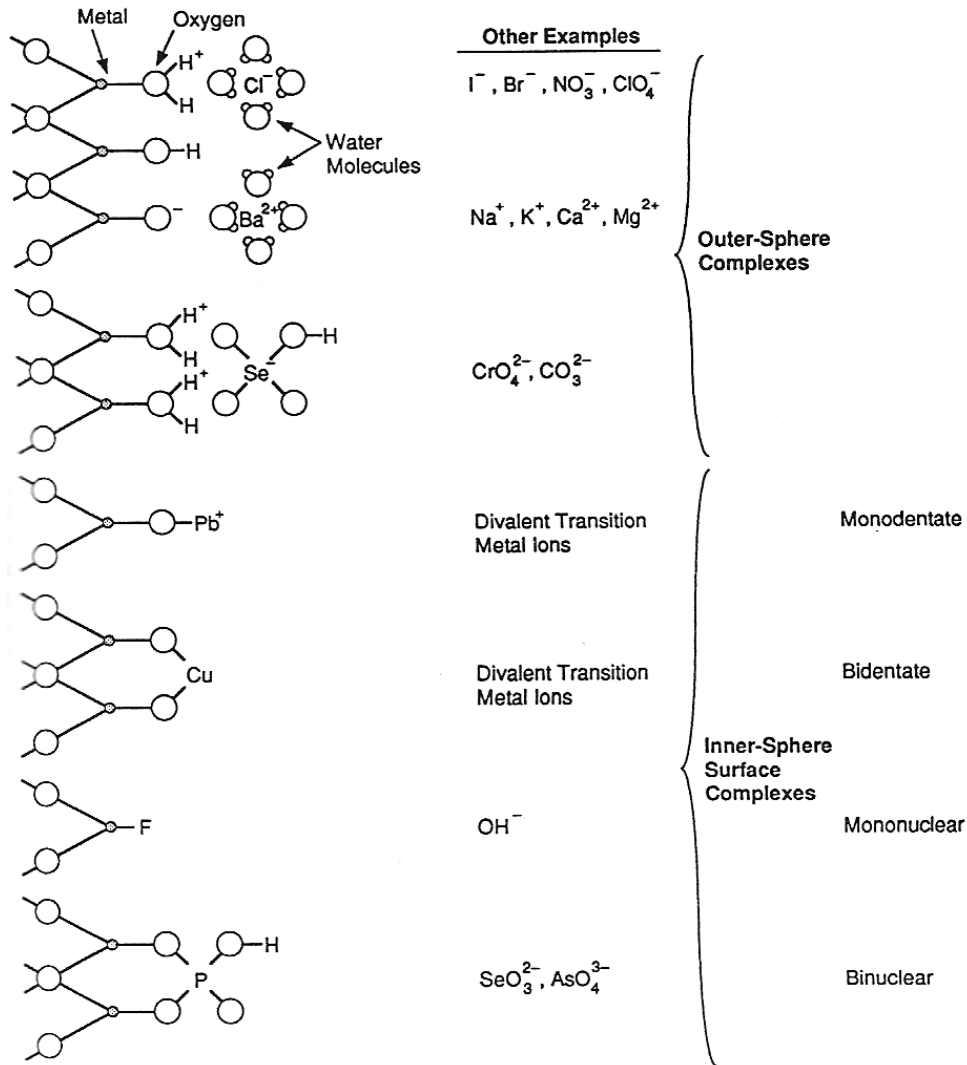


Figure 3 Schematic representation of the surface coordination of different adsorbed complexes [Davis & Kent, 1990]

1.3.2 Physical Adsorption (Outer-sphere complexation)

Physical adsorption is largely electrostatically driven, where ions sorb onto surfaces of opposite charge. The identity of the sorbing ion is relatively unimportant, and the principle controlling factor is the surface charge. No true physical bond forms between the adsorbing ion (adion) and the surface. The result is usually a weak outer-sphere complex, with the hydration (solvation) shell remaining intact, between the ion and the surface; see Figure 3 [Davis & Kent, 1990].

1.3.3 Chemical Adsorption (Inner-sphere complexation)

The dominant mechanism occurring in chemical adsorption (chemisorption) is chemical attraction. The separation from physical adsorption is necessary as chemisorption can occur even when surface and ion charges are identical, (i.e. occurs against mild repulsive forces). The chemisorption contribution to “bond strength,” (specific adsorption potential) is finite and can be prevented if the magnitude of the repulsive force is sufficiently high, (i.e. sufficiently above/below the PZC). The chemical contribution to adsorption occurs as a result of the exchange of hydration water for the surface functional group, forming an inner-sphere complex, as shown in Figure 3. Parks suggests that adsorbing surfaces are most commonly composed of multivalent cations, having a tendency to hydrolyze significantly and are capable of forming strong aqueous complexes with the chemisorbing anions (at different conditions, most commonly at low pH).

Recent characterization research has revealed that the identity of surface complexes formed during chemical adsorption can be dependent on conditions such as pH, with dentate, protonation and charge being variable (similar to aqueous complexes). Surface complexation modeling has been employed to evaluate complexation constants that can be used to predict the distribution of complexes at various conditions. Sverjenski has proposed the following surface complexes for arsenate and developed complexation constants for a number of adsorbents, including ferrihydrite [Keisuke & Sverjenski, 2007]: $(\equiv \text{SO})_2 \text{AsOOH}$, $(\equiv \text{SO})_2 \text{AsO}_2^-$, $\equiv \text{SOAsO}_3^{2-}$

1.4 Review of Published Fe(III)-As(V) Coprecipitation Literature

The following section provides a review of relevant coprecipitation literature that deals with arsenic coprecipitation and adsorption experimental work. While it is not comprehensive, it summarizes the methods and materials, as well as some of the significant observations and conclusions presented by the researchers.

1.4.1 Summary of the Current Understanding of Coprecipitation

Coprecipitation of arsenic with ferric iron, with an Fe/As molar ratio greater than or equal to three, provides effective arsenic removal to mildly alkaline conditions [Twidwell et al. 2005, Krause & Ettl, 1989, Harris & Monette, 1988]. The role of the Fe/As ratio in controlling the arsenic removal has led a number of researchers to believe that the process involves an adsorption mechanism [Robins et al. 1988]. While adsorption is involved in the process, it may not be the only active mechanism; precipitation of arsenic bearing compounds may also be involved. It has been demonstrated that coprecipitation, at higher arsenic concentrations, is capable of producing ferric arsenate (FA), a poorly crystalline material analogous to scorodite [Jia et al., 2003, 2005, 2006, 2007, Langmuir et al. 2006, Le Berre et al. 2007]. While the current body of evidence for the formation of FA is not very large, advanced characterization techniques are currently being used to identify the nature of the solids produced via low temperature coprecipitation [Cutler et al. 2003, Chen et al. in review].

While the coprecipitation process is effective for arsenic removal, its retention at neutral to mildly alkaline conditions remains a matter of debate. While scorodite and FA are both less thermodynamically stable than iron phases at mildly acidic and alkaline conditions, their dissolution (and hence arsenic release) appears to be controlled by solubility and kinetics [Bluteau & Demopoulos, 2007]. In addition, the stability of adsorbed material is questionable, as transformation of FH to more thermodynamically stable (and lower surface area phases) is predicted to occur [Cornell & Schwertmann, 2003]. However, physical evidence indicates that the transformation of ferrihydrite (FH) is severely retarded by adsorbed ions, including multivalent metal ions and oxoanions [Stumm, 1997, Baltpurvins et al. 1997, Jambor & Dutrizac 1998, Ford 2002].

Current industrial evidence from tailings monitoring programs indicates that arsenic contained in coprecipitates is stable, with equilibrium pH values near 7.5 and arsenic concentrations near 0.8 mg/L in tailings pits [Moldovan et al., 2003, Mahoney et al. 2005, Harris & Krause, 1993]. This evidence indicates that there is a gap in the current understanding of the coprecipitation process and the nature of the product.

1.4.2 Effect of Fe/As Molar Ratio on Arsenic Removal

One of the most commonly investigated first order variables in the coprecipitation process is effect of the Fe/As molar ratio on arsenic removal. There have been a variety of techniques selected, including coprecipitation and adsorption onto pre-synthesized solids as well as choice of reagents and concentration ranges (as shown in Table 2). The variability of technique has contributed to a large scatter (or low precision) in the results of various researchers. In general, it can be said that the more ferric iron present, the more complete the arsenic removal. This is illustrated well by the results of Robins et al. [1988], shown in Figure 4. It is worthy to note that the maximum removal of arsenic via coprecipitation appears to reach a plateau near 0.01 mg/L.

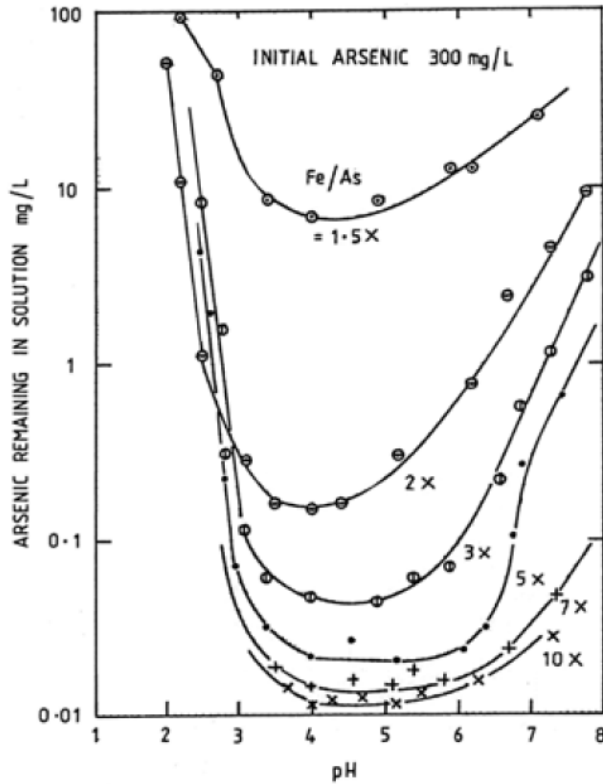


Figure 4 Effect of Fe/As molar ratio on arsenic removal during batch coprecipitation (with NaOH) [Robins et al., 1988]

1.4.3 Effect of pH on Arsenic Stability

Another common topic in coprecipitation research, relates to the effect of pH on the stability of arsenic in the coprecipitates. This effect can be observed on either the process of arsenic removal or the evaluation of long-term stability of arsenic containing coprecipitates. The first is demonstrated by the results of Robins et al., Figure 4, while the second has been the focus of a large amount of industrial research to evaluate the stability of arsenic within the tailings (as shown in Table 4). In general both processes demonstrate similar trends, where arsenic concentrations exhibit a minimum near pH 4 and rise with increasing pH. This is illustrated by the results of Krause & Ettel [1988], shown in Figure 5. In most cases, a shift in solution pH during ageing has been documented. For laboratory studies, which have looked to control the solution pH during ageing, this has been handled by routine adjustment (with acid or base) or the addition of a buffer.

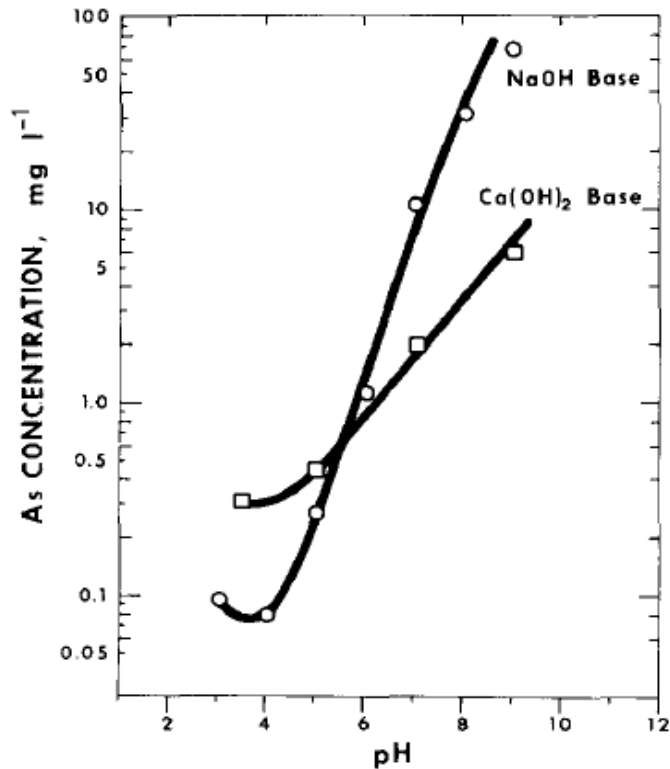


Figure 5 Effect of pH on arsenic stability in coprecipitates (Fe/As =4, 25°C) [Krause & Ettel, 1989]

1.4.4 Tabulation and Classification of Coprecipitation Research

A comprehensive discussion of the most important coprecipitation studies is given in Table 2. The table provides details about the concentration range, method of precipitation/conditions/preparation, as well as the major observations and conclusions drawn from the research.

As a result of increased pressure by provincial and federal licensing bodies, much research has been invested into understanding the stability of tailings and the toxic elements present, in particular, arsenic. Most of this research has been site specific; however generalizations and behavioral trends can be identified. Table 3 presents some of the published research on mineralogical characterization and monitoring of the long-term stability of arsenic in industrial and synthetic tailings. The list of references for all these studies is given in Table 4.

Table 2 Summary of conditions and major observations of published arsenic coprecipitation and adsorption experimental work

Nature	Author	Initial Arsenic Valence & Conc.	Fe/As Ratio	Reagents	Acid & Base	Co-ions	pH	Prep. Method	Char.	Observations & Conclusions	Notes
Cpt	Paktunc, Dutrizac & Gertsman (2008) <i>GCA</i> .	As(V) - 1500 to 15000 mg/L Fe(III) - 11.2 g/L	1 to 10	Na-As(V), Fe-SO ₄	H ₂ SO ₄ , NaOH	---	1 to 4.5	Cont (pre-SS) (70°C, 0.2µm)	XRD EXAFS TEM	Color changes indicate coprecipitates are a heterogeneous mixture of multiple phases. Minor FA formed with an Fe/As ratio of 4 (at these conditions)	
Cpt	Jia & Demopoulos (2008) <i>Water Res.</i>	As(V) - 700 to 2800 mg/L Fe(III) - 4000 mg/L	2, 4	Na-As(V), Fe-SO ₄	HNO ₃ NaOH or Ca(OH) ₂	Ca, Ni	2, 4, 8	Batch (21°C, 0.2µm, 6-12 mth equil ⁿ)	XRD	Coprecipitate product stability was improved by the presence of Ca ²⁺ and Ni ²⁺ ions. Sulphate incorporation into the solids decreased with increasing pH. Yukonite was formed during ageing of Fe/As=2 product at pH 7.5-8 and 75°C (time unknown).	
Cpt	Jia & Demopoulos (2005) <i>ES&T</i>	As(V) - 700 to 2800 mg/L Fe(III) - 4000 mg/L	2, 4, 8	Na-As(V), Fe-SO ₄	HNO ₃ NaOH	---	2, 4, 8	Batch (21°C, 0.2µm, 6-12 mth equil ⁿ)	---	Enhanced removal of As via coprecipitation vs. adsorption (~10x lower at Fe/As=4).	Comparable adsorption experiments
Ads	Jia & Demopoulos (2005) <i>ES&T</i>	As(V) - 700 to 2800 mg/L Fe(III) - 4000 mg/L	2, 4, 8	Na-As(V), Fe-SO ₄ or Fe-NO ₃	HNO ₃ , NaOH	CaSO ₄ at 0 g/L or 1.1 g/L	3 to 8	Batch (21°C, 0.2µm, 15 day equil ⁿ)	---	Enhanced As adsorption in SO ₄ vs. NO ₃ media. Improved ads. with presence of Ca ions as well as with staged adsorption (pH 8 to 4 to 8). Evidence for sulphate ads. on FH.	Comparable coprecip. experiments
Cpt	Jia et al. (2005) <i>As Met '05</i>	As(V) - 700 to 2800 mg/L Fe(III) - 4000 mg/L	1 to 8	Na-As(V), Fe-SO ₄	HNO ₃ , NaOH, Ca(OH) ₂	---	2 to 8	Batch (10 min)	XRD EXAFS X-ray MP	Enhanced removal of As with Ca(OH) ₂ vs. NaOH. XRD similarities with poorly crystalline ferric arsenate.	Comparable adsorption experiments
Ads	Jia et al. (2005) <i>As Met '05</i>	As(V) - 1400 mg/L Fe(III) - 4000 mg/L	4	Na-As(V), Fe-SO ₄	NaOH	---	4, 6, 8	Batch	XRD EXAFS X-ray MP	Enhanced As(V) removal during coprecipitation vs. adsorption.	Comparable coprecip. experiments
Cpt	Jia et al. (2003) <i>Hydromet '03</i>	As(V) - 700 to 2800 mg/L Fe(III) - 4000 mg/L	1 to 8	Na-As(V), Fe-SO ₄ or Fe-NO ₃	HNO ₃ , NaOH	---	2 to 8	Batch (10 min)	XRD EXAFS	Enhanced removal of As via coprecipitation vs. adsorption as well as in SO ₄ media vs. NO ₃ media	Comparable adsorption experiments
Ads	Jia et al. (2003) <i>Hydromet '03</i>	As(V) - 700 to 2800 mg/L Fe(III) - 4000 mg/L	1 to 8	Na-As(V), Fe-SO ₄ or Fe-NO ₃	NaOH	---	4, 8	Batch	XRD EXAFS	Enhanced adsorption of As with Fe-SO ₄ vs. Fe-NO ₃ at low pH	Comparable coprecip. experiments
Cpt	Krause & Ettel (1989) <i>Hydromet</i>	As(V) - 7500 mg/L	1 to 16	Na-As(V), Fe-SO ₄	H ₂ SO ₄ , NaOH, Ca(OH) ₂	---	5 to 8	Batch & semi-cont. (1 hr, 25 and 80°C, 0.2 or 0.45µm)	XRD	As removal attributed to basic ferric arsenates. Improved As removal with slaked lime at higher pH as well as improved As removal at lower temp.	Also involves ageing

Nature	Author	Initial Arsenic Valence & Conc.	Fe/As Ratio	Reagents	Acid & Base	Co-ions	pH	Prep. Method	Char.	Observations & Conclusions	Notes
Cpt	Harris & Monette (1988) As Met '88	As(V) - 7500 mg/L	1.5 to 8	Na-As(V), Fe-SO ₄ , or Fe-Cl	H ₂ SO ₄ , NaOH, Ca(OH) ₂ , CaMgO ₂ (calcined dolomite)	Cu+Cd+Zn	4 to 10	Semi-cont. (1 hr, 25 and 80°C, 0.45µm)	---	No significant difference in the As stability of high Fe "ferric arsenates" depending on precipitation pH (either 5 or 8). Arsenic removal attributed to formation of "high iron ferric arsenates".	Also involves ageing
Cpt	Moldovan & Hendry (2005) <i>ES&T</i>	ΣAs - 526 mg/L Fe(II) - 86 mg/L Fe(III) - 776 mg/L Al - 498 mg/L	2.2	U mill raffinate	H ₂ SO ₄ , Ca(OH) ₂	Na, Ca, SO ₄ , Al, Ni, Mg, and more	1 to 11	Cont., 3 reactors (τ = 3.5 hr)	---	Regions of As control: pH<3.1 - precipitation as scorodite 3.1<pH<11 - ads on ferrihydrite 5<pH<8 - Al hydroxide	Articles available on tailings pit monitoring
Cpt	Langmuir, Mahoney et al. (2006, 2006, 2007)	ΣAs - 668 mg/L As(III) - 447 mg/L As(V) - 221 mg/L Fe(II) - 685 mg/L Fe(III) - 1169 mg/L Al - 200 mg/L	3.6	U mill raffinate (spiked w/ Fe-SO ₄ , As ₂ O ₅ & Ni-SO ₄)	H ₂ SO ₄ , CaO, Ca(OH) ₂ , NaOH	Na, Ca, K, SO ₄ , Al, Ni, Mg, and more	2 to 8	Staged Batch (pH 2-3 for 90 min, then to target)	XRD SEM EM XM EXAFS	As controlled by poorly crystalline scorodite and amorphous ferric oxide, As(III) rapidly oxidized to As(V) during neutralization.	Articles available on tailings pit monitoring
Cpt	Langmuir & Mahoney (1999) <i>GCA</i> .	ΣAs - >140 mg/L As(III) - >30 mg/L As(V) - >110 mg/L ΣFe - >430 mg/L Al - >400 mg/L	3 to 7.7	Various U mill raffinate	H ₂ SO ₄ , Ca(OH) ₂ , CaO	Na, Ca, K, SO ₄ , Al, Ni, Mg, and more	7 to 9	Batch (3 hr)	---	Precipitation of poorly crystalline scorodite at pH 1, ferrihydrite may precipitate at pH 3-4	Also involves kinetic ageing
Cpt Ptn	Hohn, Twidwell, Robins (2006) COM '06	As(V) - 1 or 10 mg/L	Al:Fe 0:1, 1:1 M:As 5 to 10	As(V) acid, Fe-SO ₄ , Al-SO ₄ ,	H ₂ SO ₄ , NaOH	---	4 to 8	Batch (21°C, 0.22µm)	---	Phys char of FH and Al-modified-FH (AMF) similar. AMF more effective at lower loading ratios. More rapid partitioning of As to oxalate insol for AMF during ageing (25 & 70°C)	
Cpt	Robins, Singh, Das (2005) As Met '05	As(III) - <10 mg/L or As(V) - <10 mg/L	5 to 10	As ₂ O ₃ , Na-As(V), Fe-Cl, Al-Cl,	HCl, NaOH	---	2 to 10	Batch (30 min/pH unit inc., 0.45µm)	XRD FT-IR	Enhanced removal of As with Fe-Al vs. Fe system at low As concentrations (Al:Fe 1:1 most beneficial)	
Cpt	Nishimura & Umetsu (2000) Minor Ele.	As(III) - 380 mg/L	1 to 10	As ₂ O ₃ , Fe-SO ₄	NaOH	---	3 to 11	Batch (25°C, 1hr reaction time)	XRD	Most effective removal of As(III) at pH 8. Ferric arsenite can be formed at pH 2.6, 0.1 M.	
Cpt	Wang, Nishimura & Umetsu (2000) Minor Elem. '00	As(V) and/or As(III) <37.5 mg/L	2 to 10	Fe(II)-SO ₄ , Fe(III)-SO ₄ , As(III)- As(V)-?	acid & base not reported	---	3 to 11	Batch (30 min, 25°C, 0.65µm)	---	Oxidation of As(III) by H ₂ O ₂ or SO ₂ /O ₂ most effective with Fe(II) or Fe(III) present at Fe/As>5.	

Nature	Author	Initial Arsenic Valence & Conc.	Fe/As Ratio	Reagents	Acid & Base	Co-ions	pH	Prep. Method	Char.	Observations & Conclusions	Notes
Cpt	Robins, Huang, Nishimura & Khoe (1988) As Met '88	As(V) - 1 to 300 mg/L	1.5 to 10	As ₂ O ₅ , Fe-SO ₄	HNO ₃ , NaOH	1 M NaNO ₃	2 to 8	Batch (6 day equil ⁿ)	FT-IR TEM	Arsenic inhibited FH transformation. Optimum removal in pH 4-5 region. SO ₄ (and Cl) can be incorporated into FH crystals during formation, but released during ageing.	
Cpt	Emmet & Khoe (1994) EPD Cong. '94	As(V) - 200 mg/L Fe(III) - 720 mg/L	5	As(V) acid, Fe-NO ₃	NaOH	Cu, Cd, Pb, Zn, Ca, Mg, SO ₄ , SiO ₄		Batch (0.05μm)	---	Ca provides increased stability to product, as well as Pb, Mg Cd. Increased electrolyte conc can increase dissolved As.	
Cpt Age	Waychunas, et al. (1993) GCA	As(V) - 0.0375 to 375 mg/L Fe(III) - 28 mg/L	0.1 to 100	Na-As(V), Fe- Cl	HCl, NaOH	0.1 M NaNO ₃ ~0.025 M Cl	8	Batch (21°C, Fe & As added to soln kept at target pH, 7 day equil ⁿ)	EXAFS	Less monodentate As in cpt vs ads. indicating greater As bonding strength, and improved stability from coprecip. Formation of FH poisoned by presence of As, resulting in reduced polymerization. Ageing results in further polymerization of FH, causing a release of ads. As.	Comparable adsorption and ageing experiments.
Ads Age	Waychunas, et al. (1993) GCA	As(V) - 0.0375 to 375 mg/L Fe(III) - 28 mg/L	0.1 to 100	Na-As(V) Fe- Cl	HCl, NaOH	0.1 M NaNO ₃ ~0.025 M Cl	8	Batch (21°C, 7 day equil ⁿ)	EXAFS	As(V) adsorbs primarily as an inner-sphere bidentate bridging complex, sharing oxygens of two adjacent Fe oxyhydroxyl-octahedra. Monodentate As(V) also observed (about 30%). Ageing results in further polymerization of FH, causing a release of ads. As.	Comparable coprecip. and ageing experiments
Cpt	Fuller et al. (1993) GCA	As(V) - 0.3 to 150 mg/L Fe(III) - 11 to 28 mg/L	0.1 to 125	Na-As(V) Fe-NO ₃ or Fe-SO ₄	HCl NaOH	0.1 M NaNO ₃	7.5 to 9	Batch (10 min, 21°C)	---	As(V) removal most effective as As may adsorb as FH crystallites form. As(V) may also bridge FH crystallites.	Comparable adsorption experiments
Ads	Fuller et al. (1993) GCA	As(V) - 0.3 to 750 mg/L Fe(III) - 11 to 28 mg/L	0.1 to 125	Na-As(V) Fe-NO ₃	HNO ₃ NaOH	0.1 M NaNO ₃	7.5 to 9	Batch (21°C, 8 day equil ⁿ)	---	As(V) adsorption becomes diffusion limited as exterior sites become occupied. FH ageing rapidly reduces the sorption capacity.	Comparable coprecipitation experiments
Cpt Ptn	Ford et al. (2002) ES&T	As(V) - 0 to 0.7 mM Fe - 0.1M	20 to 200	Na-As(V), Fe-NO ₃	HCl, NaOH		6	Batch	XRD	As(V) preferentially partitioned to more crystalline Fe phase during ageing. Higher As loading results in lower rates of transformation to more crystalline phases.	

Nature	Author	Initial Arsenic Valence & Conc.	Fe/As Ratio	Reagents	Acid & Base	Co-ions	pH	Prep. Method	Char.	Observations & Conclusions	Notes
Cpt	Richmond, et al. (2004) <i>ES&T</i>	As(V) - 18 to 1400 mg/L Fe(III) - 170 to 13000 mg/L	12	Na-As(V), Fe-SO ₄	? acid, NaOH	---	3.5, 5.5, 7.0	Batch (<1 min, 85°C, 0.2µm)	XRD TEM	Increased FH crystallinity with decreased supersaturation (i.e. lower Fe conc.) resulting in more effective As removal. By corollary, increased Fe conc. to remove As at higher pH values. TEM & XRD characterization. (implications to neutralization circuit staging)	
Ads	Jia et al. (2007) <i>GCA</i>	As(V) - 700 to 2800 mg/L Fe(III) - 4000 mg/L	2, 4, 8	Na-As(V), Fe-SO ₄ or Fe-NO ₃	HNO ₃ NaOH	---	3 to 8	Batch (21°C, 0.2µm, 14 day equil ⁿ)	XRD FT-IR	Surface precipitation of poorly-crystalline ferric-arsenate at pH 3 to 4 while bidentate surface complex dominant mode at neutral to high pH.	
Ads	Jia et al. (2006) <i>ES&T</i>	As(V) - 700 to 2800 mg/L Fe(III) - 4000 mg/L	2, 4, 8	Na-As(V), Fe-SO ₄	HNO ₃ , NaOH	---	3 to 8	Batch (21°C, 0.2µm, 14 day equil ⁿ)	XRD Raman	XRD evidence for surface precipitation of ferric arsenate from As ads on FH at high conc As, low pH.	
Ads	Raven, Jain & Loeppert (1998) <i>ES&T</i>	As(III) or As(V) 40 or 2000 mg/L	<1 to 42 (13.3 to 0.267 mol _{As} /kg _{FH})	Na-As(V) Na-As(III) Fe-NO ₃	HCl, NaOH (KOH for FH synth.)	0.1 M NaCl	2.5 to 10	Batch (N ₂ purge, <96 hr contact, 0.45µm)	---	Possibility of surface precipitate formation. Increased sorption capacity of As(III) vs. As(V), with better retention of As(III) at higher pH. Higher As(V) sorption capacity at lower pH.	
Ads	Jain, Raven & Loeppert (1999) <i>ES&T</i>	As(III) or As(V) 10 to 1000 mg/L	<1 to 85 (13.3 to 0.133 mol _{As} /kg _{FH})	Na-As(V) Na-As(III) Fe-NO ₃	HCl, NaOH	0.1 M NaCl	3 to 11	Batch (N ₂ purge, 24 hr contact, 0.45µm)	---	Shift in As(V) sorption mechanism from monodentate to bidentate with 1) increased surface coverage and/or, 2) increasing pH, resulting in weaker ads. bond strength.	
Ads	Jain & Loeppert (2000) <i>J. En. Q.</i>	As(III) and/or As(V) - 74 to 520 mg/L	3 to 20	Na-As(V) Na-As(III) Fe-NO ₃ Na-PO ₄ Na-SO ₄	HCl, NaOH	0.1 M NaCl, varying PO ₄ and SO ₄ (<10 g/L PO ₄ , <10 g/L SO ₄)	4 to 10.5	Batch (N ₂ purge, 24 hr contact, 0.2µm)	---	Improved As(V) adsorption with SO ₄ :As of 50:1. Reduced As(V) ads. with PO ₄ and AsO ₃ (in dec. order). Reduced As(III) ads. with PO ₄ , AsO ₄ and SO ₄ (in dec. order).	
Ads	Masue, Loeppert & Kramer (2007) <i>ES&T</i>	As(III) or As(V) 1 up to 10 mg/L	Al:Fe 0:1, 1:4, 1:1, 1:0 M:As 10 to 20	Na-As(V) Na-As(III) Al-NO ₃ , Fe-NO ₃ , Ca-NO ₃ , Na-NO ₃	HCl, NaOH or Ca(OH) ₂	0.1 M NaCl varying Na and Ca (<3 g/L Na, <4 g/L Ca)	3 to 10	Batch (N ₂ purge, 24 hr contact, 0.45µm)	XRD	Significantly improved As(V) adsorption/retention at higher pH with Ca present, with both Fe and Al:Fe hydroxides. Reduced As(III) adsorption with any Al substitution. Reduced As(V) adsorption beyond Al:Fe of 1:4.	

Nature	Author	Initial Arsenic Valence & Conc.	Fe/As Ratio	Reagents	Acid & Base	Co-ions	pH	Prep. Method	Char.	Observations & Conclusions	Notes
Ads	Wilkie & Hering (1996) <i>Col. & Surf.</i>	As(III) or As(V) 0.025 to 1 mg/L Fe - 2.8 mg/L	40 to 1500	As ₂ O ₃ , Na-As(V), Fe-NO ₃ , Ca-NO ₃ , Na-SO ₄	HNO ₃ , NaOH	0.01 M NaNO ₃ , varying SO ₄ and Ca (<1 g/L SO ₄ , <120 mg/L Ca)	4 to 9	Batch (5-10 min, 25°C)	---	Significantly improved As(V) adsorption at higher pH with Ca present, that is not explained by electrostatic effects. Reduced As(V) and As(III) adsorption in the presence of SO ₄ .	
Cpt Ads Ptn	Violante, et al. (2007) <i>ES&T</i>	As(V) - 0 to 374 mg/L Fe(III) - 2800 mg/L	10 or 100	Na-As(V) Fe-NO ₃	HNO ₃ , NaOH	---	4, 7, 10	Batch (21°C, 10min, 0.22µm)	XRD FT-IR XPS PZC	Lower pH and longer ageing resulted in lower As desorption (by PO ₄). Coprecipitation resulted in lower As desorption (by PO ₄) than adsorption. The PZC of adsorbed samples was lower than for coprecipitated samples.	
Cpt Ptn	Violante, et al. (2006) <i>ES&T</i>	As(V) - 0 to 374 mg/L Al(III) - 1350 mg/L	10 or 100	Na-As(V) Al-NO ₃	HNO ₃ , NaOH	---	4, 7, 10	Batch (21°C, 10min, 0.22µm)	XRD FT-IR	Lower pH and longer ageing resulted in lower As desorption (by PO ₄) as well as by oxalate/HCl digestion.	
Ads	Pigna, Krishnamurti, Violante (2006) <i>Soil. Sci. S.</i>	As(V) - 5E-4 to 5E-2 M	0.2-0.6 mol/kg	Fe-NO ₃ , K-As(V)	HCl, KOH, NaOH	---	6	Batch (21°C, 10min, 0.22µm)	XRD FT-IR	Adsorption kinetics & capacity greatest for ferrihydrite, followed by Al(OH) _x , goethite, gibbsite. Desorption of As (by PO ₄) reduced during ageing.	

Cpt Co-precipitation - Neutralization of acidic solution containing both Fe and As to target pH

Ads Adsorption - Neutralization of Fe solution (to generate ferrihydrite, as per Cornell & Schwertman) followed by contact with aqueous As at target pH

Ptn Partitioning - Evaluation of arsenic phase partitioning during ageing via either extraction with 0.4 M HCl or oxalic acid digestion

Age Ageing - Monitoring of solids (dissolved arsenic) during ageing

Table 3 Summary of coprecipitate ageing and tailings monitoring programs

Coprecip. Prod. Technique	Author	Location	Article Topic	Fe/As Ratio	Arsenic Conc.	Age & Conditions	Observations & Conclusions	Notes
Industrial soln, mill-scale, cont.	Langmuir & Mahoney (1999) <i>GCA</i>	JEB TMF Saskatchewan, Canada	Prediction of arsenic concentrations in TMF into long term future via ageing of coprecipitate tailings.	3-5	predicted	5-49 day ageing pH 7 to 9 4, 25 & 50°C	Arsenic concentrations should not exceed 1 mg/L between pH 7-8 and 50 to 10,000 years.	
Industrial soln, mill-scale, cont.	Mahoney et al. (2005) <i>App. Geochem</i>	JEB TMF Saskatchewan, Canada	Equilibrium partitioning in closed system (EPICS) – measure As releases from the solids under conditions as similar to those of disposal site	>3	<3mg/L	pH = 7-8	0.2% of total arsenic could be readily released to pore waters	
Industrial soln, mill-scale, cont.	Donahue & Hendry (2003) <i>App. Geochem</i>	Rabbit Lake In-pit TMF Saskatchewan, Canada	PHREEQC calculation of pore water saturation state and sequential extraction of tailings core	>4	9.6-71 mg/L	pH = 9.3 to 10.3 Eh = 58 to 213 mV 3.1°C	High arsenic concentrations associated with low Fe/As ratio coprecipitates. Fe/As ratio largely depended on ore body being processed ranged from <2 to >8.	
Industrial soln, mill-scale, cont.	Modovan, Jiang & Hendry (2003) <i>ES&T</i>	Rabbit Lake In-pit TMF Saskatchewan, Canada	Mineralogical characterization EXAFS XANES	5.3-303	---	10 yrs pH = 9.79 Eh = 162 mV 2.8 °C	FH did not convert to more crystalline phases after ~10 years of ageing. XANES showed arsenic to be in As(V) oxidation state.	
Industrial soln, mill-scale, cont.	Donahue, Hendry & Landine (2000) <i>App. Geochem</i>	Rabbit Lake In-pit TMF Saskatchewan, Canada	Describes bulk neutralization process, mill feed records, TMF design & TMF sampling program	---	---	---	71% of As in historical mill feed dissolved during leaching. SEM suggested Ca ²⁺ , Fe ³⁺ and Ni ²⁺ arsenates present.	
Industrial soln, mill-scale cont.	Pichler, Hendry & Hall (2001) <i>Env. Geology</i>	Rabbit Lake In-pit TMF Saskatchewan, Canada	Tailings mineralogy investigation through selective extraction and characterization	---	---	---	Identification of secondary minerals inconclusive. Association of As to HFO demonstrated. Fe, As, Ni & Al appear to be associated together.	
Synthetic soln, bench-scale batch	Krause & Ettel (1985) <i>COM 1985</i>	---	Evaluation of the stability of coprecipitated “basic ferric arsenates”	2-17	varied	1 week @ 100°C, pH 5 (pre-stability test)	Coprecipitation provided better arsenic retention than a mixture of FA and FH. “Accelerated ageing” showed no effect for Fe/As>8, but for Fe/As<4, structure changes may have an affect	
Synthetic soln, bench-scale batch	Krause & Ettel (1989) <i>Hydromet</i>	---	Uses “accelerated ageing” to evaluate effect of phase changes on As retention	8	1.8 mg/L	up to 222 days at 100°C, pH 5	Arsenic not released despite transformation to more crystalline phases (Hematite). Goethite formation suppressed.	

Coprecip. Prod. Technique	Author	Location	Article Topic	Fe/As Ratio	Arsenic Conc.	Age & Conditions	Observations & Conclusions	Notes
Industrial soln, mill-scale, cont.	Krause et al. (2006) COM2006	Copper Cliff TMA Ontario, Canada	Selection of As disposal strategy for WATP sludge, refers to historical TMA monitoring program results	~10 excess FeS	<0.001 to 0.238 mg/L	14 yrs (~1990) ORP = -50 to 90 pH = 6.2 to 9.6 13-19°C	Monitoring indicated that As is stable, higher range pore water concentrations were located near waste wood dump (pressure treated wood)	
Synthetic soln, bench-scale batch	Harris & Monette (1988) As Met '88	---	Production and ageing of various metal arsenate compounds as well as "high iron ferric arsenate" solids	1-8	varied	up to 5 months pH = 4 to 10 25°C	CO ₂ did not have a significant adverse effect on high iron and mixed base metal arsenates. Gypsum had a stabilizing effect. Arsenic stable (<5 mg/L) between pH 4-7 if Fe/As > 3, or pH 4-10 if mixed base metals present (Cu+Cd+Zn).	
Synthetic soln, bench-scale batch & industrial smelter solids	Harris & Monette (1989) Prod Tech	Various Noranda plant residues	Ageing and stability testing of various high iron ferric arsenate solids and arsenic bearing plant residues	2-8	varied	up to 18 months pH = 4 to 10 25°C	Sulphate medium provided better stability, possibly due to the presence of gypsum. Arsenic continued to remain stable in solids between pH 4-7 if Fe/As molar ratio > 3 or pH 4-10 if mixed base metals present (Cu+Cd+Zn).	
Synthetic soln, bench-scale batch	Ford et al. (2002) ES&T	---	Monitor As partitioning during transformation of HFO to more crystalline phases	20 to 200	N/A	125 days pH = 6.0 40°C shaker bath	Overall HFO transformation rate is reduced at higher loadings, (VERY low at Fe/As ratio of 20). Hematite formation becomes promoted over goethite.	
Industrial soln, mill-scale, cont.	Paktunc et al. (2003) ES&T	Ketza River mine tailings Yukon, Canada	Primarily characterization of mill precipitates and minor arsenic mobilization investigation.	varied	18-34.7 mg/L 0.3-2.6 mg/L	flow through (pH 7-8) or standing water (pH 6.5-7)	Solution not gypsum saturated. Provides evidence for Ca interaction with As in arsenic bearing iron oxyhydroxides	
Industrial soln, mill-scale, cont.	Paktunc et al. (2004) GCA	Ketza River mine tailings Yukon, Canada	Mineralogical characterization of mill precipitates including:	varied	---	---	As bearing minerals included iron(III) oxyhydroxides, scorodite, ferric arsenates, arseniosiderite, Ca-Fe arsenates, pharmacosiderite, jarosite and arsenopyrite. Iron(III) oxyhydroxides contain variable levels of arsenic up to 22 wt% and Ca up to 9 wt%. Calcium association correlates well with arsenic.	
Synthetic soln, bench-scale batch	Hohn, Twidwell, Robins (2006) COM '06	---	Monitor As partitioning during transformation of FH and AMF to more crystalline phases	10	---	500 days pH = 7 70°C	As retention with AMF was improved over FH during ageing. AMF transformation considerably slower at 70°C than FH	
Synthetic soln, bench-scale batch	Fuller et al. (1993) GCA	---	Monitor As adsorption kinetics onto FH	5	50% adsorbed (1E-4M initial)	8 days pH 8 21°C	Arsenic release from post-synthesis adsorption data fitted with a pore-space diffusion model.	

Table 4 Summary of coprecipitate ageing and tailings monitoring programs

- Donahue, R.; Hendry, M. J.. (2003) "Geochemistry of arsenic in uranium mine mill tailings, Saskatchewan, Canada," *Applied Geochemistry*, 18(11), 1733-1750.
- Donahue, R.; Hendry, M.J.; Landine, P. (2000) "Distribution of arsenic and nickel in uranium mill tailings, Rabbit Lake, Saskatchewan, Canada," *Applied Geochemistry*, 15(8), 1097-1119.
- Emett, M.T.; Khoe, G.H., (1994) "Environmental stability of arsenic bearing hydrous iron oxide," In *EPD Congress 1994*, (Warren, G., Ed.), TMS, 153-166.
- Ford, R.G., (2002) "Rates of hydrous ferric oxide crystallization and the influence on coprecipitated arsenate," *Environmental Science & Technology*, 36(11), 2459-2463.
- Fuller, C.C.; Davis, J.A.; Waychunas, G.A., (1993) "Surface chemistry of ferrihydrite: Part 2. Kinetics of arsenate adsorption and coprecipitation," *Geochimica et Cosmochimica Acta*, 57, 2271-2282.
- Harris, G. B.; Monette, S., (1988) "The stability of arsenic-bearing residues," In *Arsenic Metallurgy: Fundamentals & Applications*, (Reddy, R.G.; Hendrix, J.L.; Queneau, P.B., Eds.), TMS, 469-488.
- Harris, G. B.; Monette, S. (1989) "The disposal of arsenical solid residues," In *Productivity and Technology in the Metallurgical Industries*, (Koch, M., Taylor, J.C. Eds.), TMS, 545-559.
- Hohn, J.; Twidwell, R.; Robins, R.G., (2006) "A comparison of ferrihydrite and aluminum-modified ferrihydrite for the removal of arsenate from aqueous solution by co-precipitation," In *Iron Control in Hydrometallurgy*, (Dutrizac, J.E., Ed.), CIM, 911-926.
- Jia, Y.F.; Demopoulos, G.P.; Chen, N.; Cutler, J.N.; Jiang, D.-T., (2003) "Preparation, characterization and solubilities of adsorbed and co-precipitated iron (III)-arsenate solids," In *Hydrometallurgy 2003 Volume 2: Electrometallurgy and Environmental Hydrometallurgy*, (Young, C.A.; Alfantazi, A.M.; Anderson, C.G.; Dreisinger, D.B.; Harris, B.; James, A., Eds.), TMS, 1923-1935.
- Jia, Y.F.; Demopoulos, G.P.; Chen, N.; Cutler, J., (2005) "Coprecipitation of As(V) with Fe(III) in sulfate media: solubility and speciation of arsenic," In *Arsenic Metallurgy*, (Reddy, R.G.; Ramachandran, V., Eds.), TMS, 137-148.
- Jia, Y.F.; Demopoulos, G.P., (2005) "Adsorption of arsenate onto ferrihydrite from aqueous solution: Influence of media (sulfate vs. nitrate), added gypsum, and pH alteration," *Environmental Science & Technology*, 39, 9523-9527.
- Jia, Y.F.; Xu, L.; Fang, Z.; Demopoulos, G.P., (2006) "Observation of surface precipitation of arsenate on ferrihydrite," *Environmental Science & Technology*, 40(10), 3248-3253.
- Jia, Y.; Xu, L.; Wang, X.; Demopoulos, G.P., (2007) "Infrared spectroscopic and X-ray diffraction characterization of the nature of adsorbed arsenate on ferrihydrite," *Geochimica et Cosmochimica Acta*, 71(7), 1643-1654.
- Jia, Y.F.; Demopoulos, G.P., (2008) "Coprecipitation of arsenate with iron(III) in aqueous sulfate media: Effect of time, lime as base and co-ions on arsenic retention," *Water Research*, 42(3), 661-668.
- Jain, A.; Loeppert, R.H., (2000) "Effect of competing anions on the adsorption of arsenate and arsenite by ferrihydrite," *Journal of Environmental Quality*, 29(5), 1422-1430.

- Jain, A.; Raven, K.P.; Loeppert, R.H., (1999) "Arsenite and arsenate desorption on ferrihydrite: Surface charge reduction and net OH⁻ release stoichiometry," *Environmental Science & Technology*, 33(8), 1179-1184.
- Krause, E.; Ettl, V.A., (1989) "Solubilities and stabilities of ferric arsenate compounds," *Hydrometallurgy*, 22, 311-337.
- Krause, E.; Ettl, V.A., (1985) "Ferric arsenate compounds: Are they environmentally safe? Solubilities of basic ferric arsenates," In *Impurity Control & Disposal*, (Oliver, A.J.; Ed.), CIM, 5/1-5/20.
- Langmuir, D.; Mahoney, J.; MacDonald, A.; Rowson J., (1999) "Predicting arsenic concentrations in the porewaters of buried uranium mill tailings," *Geochimica et Cosmochimica Acta*, 63(19-20), 3379-3394.
- Langmuir, D.; Mahoney, J.; Rowson, J., (2006) "Solubility products of amorphous ferric arsenate and crystalline scorodite (FeAsO₄•2H₂O) and their application to arsenic behavior in buried mine tailings," *Geochimica et Cosmochimica Acta*, 70(12), 2942-2956.
- Mahoney, J.; Langmuir, D.; Slaughter, M.; Rowson, J., (2007) "Control of As and Ni releases from buried mill tailings: Laboratory neutralization test results, solution chemistry, mineralogy and geochemical modeling," *Applied Geochemistry*, 2758-2776.
- Mahoney, J.; Langmuir, D.; Slaughter, M.; Rowson, J., (2006) "Raffinate neutralization experiment at McClean Lake Mill - Removal of arsenic and nickel," In *Uranium in the Environment: Mining Impact & Consequences*, (Merkel, B.J.; Hasche-Berger, A. Eds.), 225-234.
- Mahoney, J.; Langmuir, D.; Gosselin, N.; Rowson, J., (2005) "Arsenic readily released to pore waters from buried mill tailings," *Applied Geochemistry*, 20(5), 947-959.
- Masue, Y.; Loeppert, R.H.; Kramer, T.A., (2007) "Arsenate and arsenite adsorption and desorption behavior on coprecipitated aluminum:iron hydroxides," *Environmental Science & Technology*, 41(3), 837-842.
- Moldovan, B. J.; Hendry, M. J., (2005) "Characterizing and quantifying controls on arsenic solubility over a pH range of 1-11 in a uranium mill-scale experiment," *Environmental Science & Technology*, 39(13), 4913-4920.
- Moldovan, B.J.; Jiang, D.T.; Hendry, M.J., (2003) "Mineralogical characterization of arsenic in uranium mine tailings precipitated from iron-rich hydrometallurgical solutions," *Environ. Sci. Technol.*, 37(5), 873 -879.
- Nishimura, T.; Umetsu, Y., (2000) "Chemistry on elimination of arsenic, antimony, and selenium from aqueous solution with iron(III) species," In *Minor Elements 2000: Processing and Environmental Aspects of As, Sb, Se, Te, and Bi*, (Young, C., Ed.), SME, 105-112.
- Paktunc, D.; Dutrizac, J.; Gertsman, V., (2008) "Synthesis and phase transformations involving scorodite, ferric arsenate and arsenical ferrihydrite: Implications for arsenic mobility," *Geochimica et Cosmochimica Acta*, doi: 10.1016/j.gca.2008.03.012
- Paktunc, D.; Foster, A.; Heald, S.; Laflamme, G., (2004) "Speciation and characterization of arsenic in gold ores and cyanidation tailings using X-ray absorption spectroscopy," *Geochimica et Cosmochimica Acta*, 68(5), 969-983.

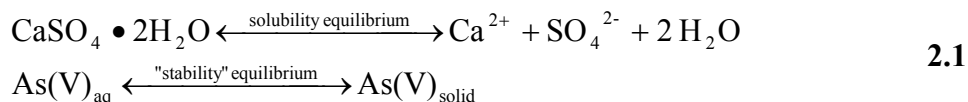
- Paktunc, D.; Foster, A.; Laflamme, G., (2003) "Speciation and characterization of arsenic in Ketz River mine tailings using X-ray absorption spectroscopy," *Environmental Science and Technology*, 37(10), 2067-2074.
- Pichler, T.; Hendry, M.J.; Hall, G.E.M., (2001) "The mineralogy of arsenic in uranium mine tailings at the Rabbit Lake In-pit Facility, northern Saskatchewan, Canada," *Environmental Geology*, 40(4-5), 495-506.
- Pigna, M.; Krishnamurti, G.S.R.; Violante, A., (2006) "Kinetics of arsenate sorption-desorption from metal oxides: effect of residence time," *Soil Science Society of America Journal*, 70(6), 2017-2027.
- Raven, K.P.; Jain, A.; Loeppert, R.H., (1998) "Arsenite and arsenate adsorption on ferrihydrite: Kinetics, equilibrium and adsorption envelopes," *Environmental Science & Technology*, 32(3), 344-349.
- Richmond, W.R.; Loan, M.; Morton, J.; Parkinson, G.M., (2004) "Arsenic removal from aqueous solution via ferrihydrite crystallization control," *Environmental Science & Technology*, 38(8), 2368-2372.
- Robins, R.G.; Singh, P.; Das, R.P., (2005) "Coprecipitation of arsenic with Fe(III), Al(III) and mixtures of both in a chloride system," In *Arsenic Metallurgy*, (Reddy, R.G.; Ramachandran, V., Eds.), TMS, 113-128.
- Robins, R.G.; Huang, J.C.Y.; Nishimura, T.; Khoe, G.H., (1988) "The adsorption of arsenate ion by ferric hydroxide," In *Arsenic Metallurgy: Fundamentals and Applications*, (Geddy, R.G.; Hendrix, J.L.; Queneau, P.B., Eds.), TMS, 99-112.
- Violante, A.; Ricciardella, M.; del Gaudio, S.; Pigna, M., (2006) "Coprecipitation of arsenate with metal oxides: Nature, mineralogy and reactivity of aluminum precipitates," *Environmental Science & Technology*, 40(16), 4961-4967.
- Violante, A.; Ricciardella, M.; del Gaudio, S.; Pigna, M., (2007) "Coprecipitation of arsenate with metal oxides: 2. Nature, mineralogy and reactivity of iron(III) Precipitates," *Environmental Science & Technology*, 41(24), 8275-8280.
- Wang, Q.; Nishimura, T.; Umetsu, Y., (2000) "Oxidative precipitation for arsenic removal in effluent treatment," In *Minor Elements 2000: Processing and Environmental Aspects of As, Sb, Se, Te, and Bi*, (Young, C., Ed.), SME, 39-52.
- Waychunas, G.A.; Rea, B.A.; Fuller, C.C.; Davis, J.A., (1993) "Surface chemistry of ferrihydrite: Part 1. EXAFS studies of the geometry of coprecipitated and adsorbed arsenate," *Geochimica et Cosmochimica Acta*, 57(10), 2251-69.
- Wilkie, J.A.; Hering, J.G., (1996) "Adsorption of arsenic onto hydrous ferric oxide: effects of adsorbate/adsorbent ratios and co-occurring solutes," *Colloids and Surfaces, A: Physicochemical and Engineering Aspects*, 107, 97-110.

Chapter 2 Methods & Materials

This section describes the techniques employed for coprecipitation and ageing of the solids.

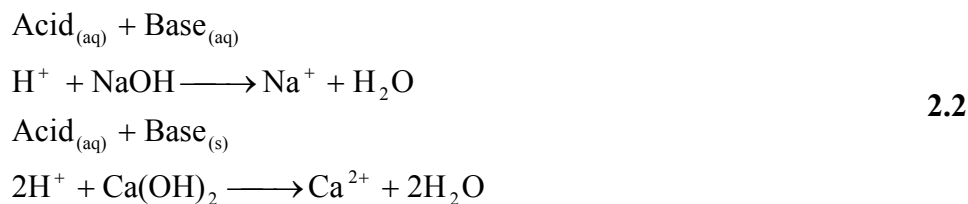
2.1 A Note Regarding Ageing “Equilibrium”

It should be noted that the “equilibrium” observed in the coprecipitation system investigated is not considered a solubility equilibrium but a stability equilibrium. The terminology is deliberate as solubility would imply the presence of a singular solid phase and an equilibrium which does not involve the removal of one or more of the soluble ions via formation of another solid phase (i.e. incongruent dissolution). In the case of this work, the stability equilibrium (eq 2.1) involves only arsenic, between the aqueous and any of multiple solid phases which could be possible, with pathways which could involve mechanisms of dissolution-precipitation and/or adsorption-desorption. In addition, the stability “equilibrium” observed is only that of As(V). In industrial systems, the other oxidation states of arsenic may control the equilibrium arsenic concentrations in solution.



2.2 Heterogeneous Reactions and Concentration Gradients

Heterogeneous reactions are commonly encountered chemical processes. There are inherent difficulties with the blending of different phases, in this case, solids and liquids. In addition, the nature of the reactants in the coprecipitation system can be either homogeneous or heterogenous, depending on the type of base used (i.e. sodium hydroxide or slaked lime, respectively). In either case, there are concentration gradients, which are dispersed via agitation.



For the case of sodium hydroxide at a concentration of 1 molar, the aqueous solution would have a pH of 14. For slaked lime, the concentration gradients are dependant on the rate of dissolution of slaked lime, with a maximum concentration corresponding to the solubility of $\text{Ca}(\text{OH})_2$, 1.65 g/L at 20°C [Perry & Green, 1999] with a solution pH of 12.6.

The purpose of this discussion is to draw attention to the possibility that, despite the use of recommended design, concentration gradients are inherent and diffusion control is a likely operating regime, influencing the phases generated via precipitation. Diffusion controlled processes can be affected by agitation. For arsenic coprecipitation, this phenomenon has been observed and documented [Twidwell, Robins & Hohn, 2005].

In addition, the concentration gradients mentioned can also affect the results of ageing when base is used to adjust the pH of long-term stability experiments. It is possible for these gradients to cause dissolution of solids and release of arsenic, a process that is not entirely reversible. As a result, consideration should be given to the effect of concentration gradients and techniques should be developed that eliminate the variability that can be introduced.

2.3 Continuous Circuit Design

For the laboratory simulation of continuous circuit coprecipitation, three stirred tank reactors were configured in series. The details of reactor dimensions and the results of commissioning tracer tests are provided below.

2.3.1 Reactor Dimensions

The recommended and actual dimensions of a stirred tank reactor with baffles are shown below.

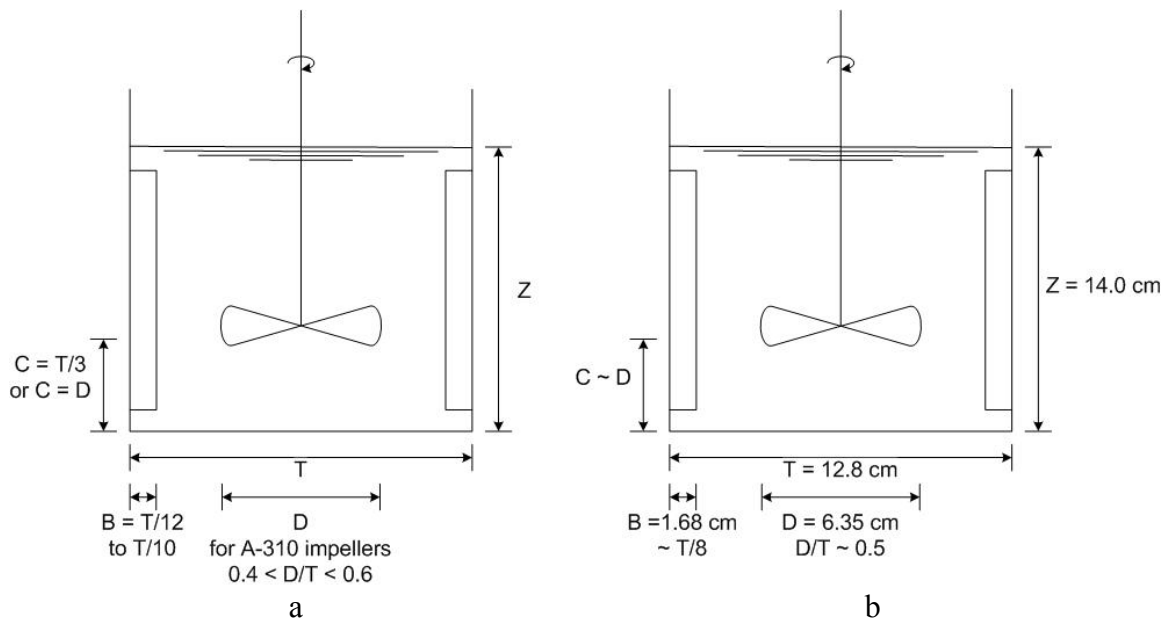


Figure 6 (a) Recommended dimensions for agitated reactor with baffles and (b) dimensions of reactor used in this continuous coprecipitation work.

The dimensions are those recommended by Perry's Chemical Engineers Handbook, Chapter 18 – Liquid-solid operations and equipment [Perry & Green, 1999].

2.3.2 Steady-State Operation

By performing a material balance on each reactor in the circuit, a series of coupled ordinary differential equations are obtained. By solving these equations with the aid of software (Polymath 5.1), it is possible to determine the response of the system to different conditions. The simplified equations are given below.

$$\frac{d(C_1)}{d(t)} = \frac{F}{V}(C_0 - C_1) + r_{a1} \quad 2.3$$

$$\frac{d(C_2)}{d(t)} = \frac{F}{V}(C_1 - C_2) + r_{a2} \quad 2.4$$

$$\frac{d(C_3)}{d(t)} = \frac{F}{V}(C_2 - C_3) + r_{a3} \quad 2.5$$

Where \$t\$ = time (min)

\$V\$ = reactor volume (1650mL)

\$F\$ = flow rate (mL/min)

\$C_1\$ to \$C_3\$ = concentration in each reactor 1 to 3 respectively (mg/mL)

\$r_{a1}\$ to \$r_{a3}\$ = reaction rate in each reactor 1 to 3 respectively (mg/(mL·min))

A pulse input provides the theoretical response of a (pulse) non-reacting tracer test. A test of this nature was performed on the circuit prior to operation to evaluate the mixing conditions within each reactor. The results from a prior tracer test had indicated that mixing was less than ideal. The circuit design was examined and it was found that the impeller was undersized with respect to the reactor dimensions. Consequently, the impeller in each reactor was changed from a 1.5 inch marine type, to a 2.5 inch Lightnin A-310 type. The tracer test performed after replacement of the impeller yielded a profile very close to ideal. The results of both tracer tests are shown below.

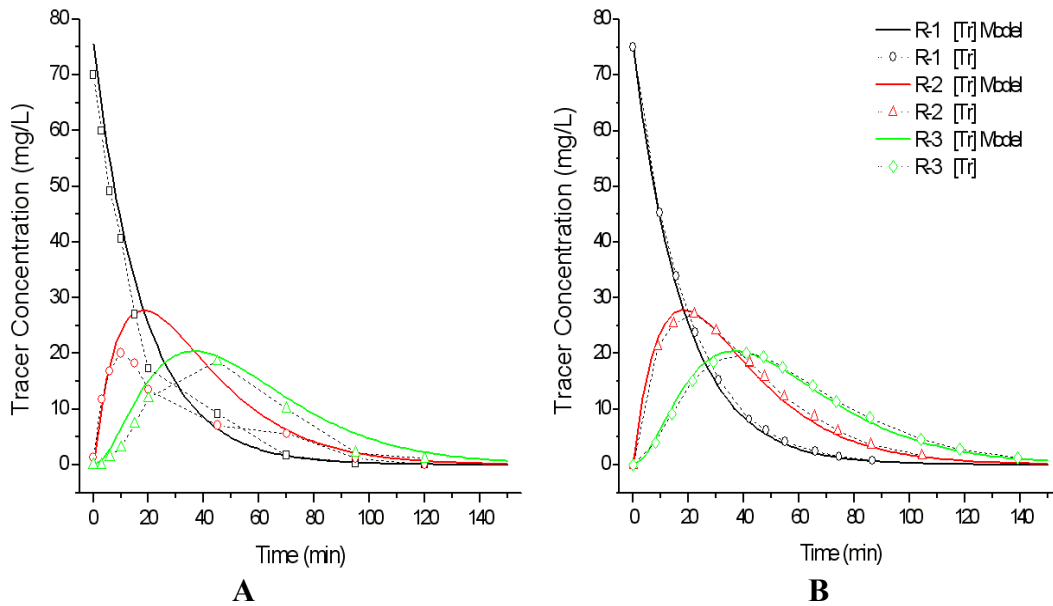


Figure 7 Theoretical and actual tracer test response curves for a three reactor circuit with (A) 1.5” marine type impellers and (B) 2.5” Lightnin A-310 type impellers.

For a step change, the theoretical response curve is similar to start-up conditions and is known as the approach to steady-state. By evaluating this response, it is possible to determine the amount of time required to operate the circuit before steady-state conditions are obtained. The time to steady-state is a relative feature that is dependant on the number of stages, as well as the flow rate and reactor volume. To generalize, for a system of equally sized reactors, the time to steady-state can be expressed as a number of residence times (τ), where the residence time is defined as:

$$\tau = \frac{V}{F} = \frac{\text{Reactor volume (mL)}}{\text{Flow rate (mL} \cdot \text{min}^{-1})} = \text{min} \quad 2.6$$

Table 5 Normalized time required to achieve steady-state for a continuous circuit

No. of reactors in circuit	Time required to achieve SS
1	5 τ
2	6.5 τ
3	8 τ

Table 5 summarizes the operating time required to achieve steady-state for a circuit with a variable number of stages.

2.4 Feed Solution Preparation

A stock solution of arsenic was made by dissolving 100g of reagent grade arsenic pentoxide (Sigma-Aldrich) into 4 L of de-ionized water. Similarly, stock solutions of iron and aluminium were made by dissolving 500g of reagent grade ferric sulphate or aluminium sulphate (Sigma Aldrich) into 4 L of de-ionized water with 86g of reagent grade sulphuric acid (98%, Fisher Scientific). Stock solutions were analyzed for iron, aluminium and arsenic content by ICP-AES.

Solutions of base were made by dissolving reagent grade NaOH pellets (Fisher) or slaking reagent grade CaO (Fisher) in de-ionized water to provide a solution or slurry equivalent to 1 N.

The feed solution required for each experiment (17-21 L), was generated by adding a calculated volume of stock solution to 12 L of de-ionized water to achieve the target Fe/As ratio. The solution was analyzed by ICP-AES to determine the elemental concentrations and Fe/As ratio. Corrections were made, if required, by adding stock solution. The feed solution was then diluted with de-ionized water to attain the target arsenic concentration (1400 mg/L).

2.5 Batch Coprecipitation

Ambient temperature (22°C) batch coprecipitation was accomplished by neutralization of feed solution with base at a constant rate so as to provide neutralization to pH 8 within 10 minutes. For a feed volume of 300 mL, the base was added at a rate of

2.5 mL every 15 seconds. After coprecipitation the slurry was agitated for a period of 1 hour, during which the pH was adjusted to the target as necessary.

2.6 Continuous Coprecipitation Circuit

The ambient temperature (22°C) continuous circuit consisted of the following equipment, depicted schematically in Figure 8.

- Feed pump: Masterflex variable speed peristaltic pump with Tygon tubing
- Reactor: 2 L glass beaker with acrylic baffles and discharge spout (effective volume 1.65L)
- Agitation: IKA RW20 overhead mixer with a Lightning A310 impeller (2.5 in.)
- pH pump: Etatron DLX/B pH controller/pump (diaphragm positive displacement) unit with a Cole-Parmer pH electrode (2-point calibration)
- Fluidization: Masterflex variable speed peristaltic pump with stackable heads for lime slurry fluidization with magnetically stirred 2L flasks dedicated to each pH pump
- pH meter: Accumet Basic AB15 meter with Accumet pH/ATC liquid filled combination electrode with Ag/AgCl reference (4-point calibration)
- Eh meter: Accumet Basic AB15 meter with Accumet platinum Ag/AgCl combination electrode

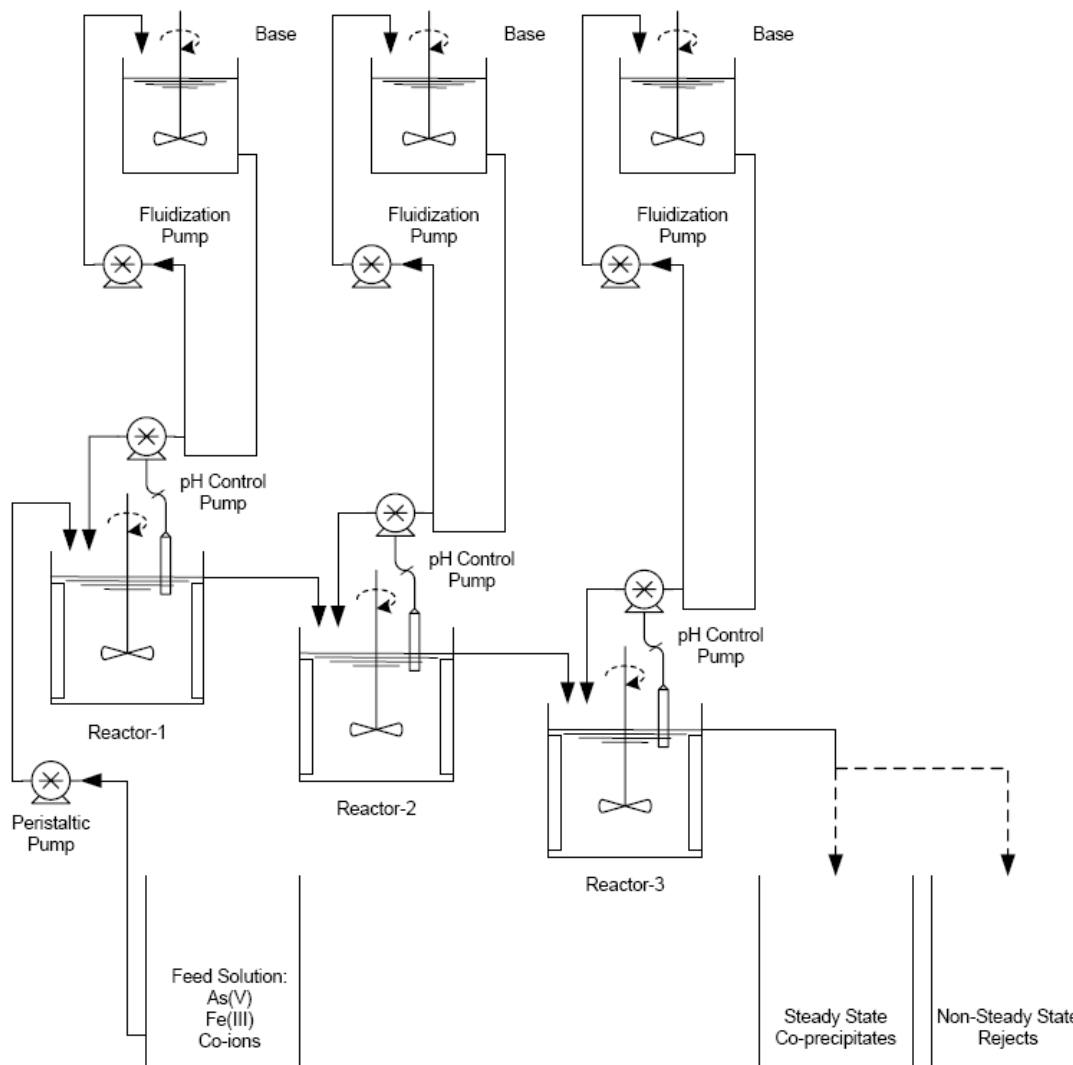


Figure 8 Schematic diagram of continuous coprecipitation circuit set-up

2.7 Continuous Coprecipitation Operation

Continuous circuit start-up involved calibration of the feed pump flow rate to provide the desired (reactor) residence time (i.e. for $\tau = 1$ h, flow rate = 27.5 mL/min). In addition, the pH controller/pump was calibrated with standards which bracketed the target set-point for the experiment. Each reactor was filled with de-ionized water and adjusted to pH 2 with sulphuric acid. The time required for the approach to steady-state varied, depending on the number of stages in the circuit. A duration of 5τ , 6.5τ and 8τ was used for one, two and three stages respectively, corresponding to 5, 6.5 and 8 hours before steady-state coprecipitates were collected for ageing. The pH controller set-point was selected based on the number of stages in the experiment. In a single stage experiment the set-point was pH 8, while for two and three stages, the set points were pH 4 & 8 or pH 2.5, 4 & 8 respectively.

During the course of steady-state operation, each reactor was sampled routinely to monitor arsenic and co-ion concentrations. The ORP and pH of each reactor were also monitored. The reactor pH fluctuated as a result of the intermittent supply provided by the pH control pump. This variation was observed to be ± 0.1 pH units with slaked lime and ± 0.4 pH units when NaOH was used for neutralization. The magnitude of the variation, which depended on the type of base was likely due to the nature of the base and the concentration gradients, outlined earlier, which are generated by the base. NaOH is a much more aggressive base owing to the fact that all of the reagent is fully dissolved, while $\text{Ca}(\text{OH})_2$ is not as aggressive because much of its acid neutralization capacity (at a concentration of 1N) is supplied in a solid state and dissolves.

Particle size distribution measurements were also taken during operation with a Horiba LA-920 laser scattering particle size analyzer. The bulk settling rate of the solids was determined by settling in a 1L graduated cylinder.

Solids recycle was simulated, in a two stage slaked lime continuous coprecipitation experiment, by simultaneously pumping feed solution and a thickened slurry of solids (at pH ~ 8) to the first reactor. Thickened solids were generated by

decanting 1 L “batches” of coprecipitation circuit effluent so as to concentrate the solids by a factor of 4 (equivalent iron content of 16.7 g/L, estimated pulp density of approximately 110 g/L total solids). A portion of the thickened slurry was returned to a stirred tank, which supplied the thickened slurry of solids pumped into the first reactor.

2.8 Coprecipitate Ageing

Following completion of the experiment, the steady-state coprecipitates were sampled, and the settling rate and particle size distribution were measured. The volume of steady-state coprecipitates produced and the volume of base used during steady-state operation were recorded. These numbers were used to determine the volume to be decanted to concentrate the solids by a factor of 2. (For example, from the initial iron concentration of 4.2 grams Fe^{3+} per litre, the concentrated slurry would then contain 8.4 grams Fe^{3+} per litre or an estimated pulp density of approximately 55 grams total solids per litre, corresponding to a solid/liquid ratio of approximately 1/25.)

Following partial decantation, the coprecipitates were re-suspended. Volumes of 1 L were measured and placed into sealed bottles for ageing at temperatures of 3, 22, 40 and 70°C with the aid of temperature controlled water baths and room temperature. For the cold water bath, the temperature was digitally controlled. For the hot water baths, the temperature was controlled by an analogue heater/circulator and verified by thermometer. The water level in the 40°C bath was maintained via a “home-made” float valve, and plastic balls were used to reduce evaporation. The 70°C bath was equipped with a stainless steel cover to reduce evaporation, and the water level was connected to the 40°C bath through a stainless steel siphon tube. The water baths were not equipped to provide continuous agitation to the bottles of ageing coprecipitates, which was deemed unnecessary as agitation is not encountered in sub-aqueous tailings management facilities. This is supported by the activation energy observed by Langmuir et al. [1999], for coprecipitate ageing (56 kJ/mol), which is above the range for diffusion controlled reactions.

To obtain samples, the coprecipitates were agitated and a slurry sample was obtained. For solution samples, the sample was pre-clarified by centrifuge and the

supernatant was filtered with a 0.02 μ m syringe filter and acidified with trace metal grade nitric acid. For solution and solid samples, the separation was achieved by using an assembled syringe filter (Millipore) and 0.025 μ m filter paper. The solids were washed with approximately 3 mL of de-ionized water prior to drying at 50°C. Solution samples were acidified with trace metal grade nitric acid.

Following sampling, the pH was measured and depending on the ageing method, either adjusted to pH 8 by addition of the same base as used during coprecipitation, or left to drift. Adjustment of pH was performed by addition of base from a small syringe into the agitated coprecipitates, followed by a period of equilibration and measurement. For NaOH, the concentration was 1 M, while for Ca(OH)₂, a slurry of base (1 N) was utilized. In all cases the target pH was approached carefully via addition of base only.

2.9 Arsenic Analysis

Arsenic analysis was accomplished by one of two techniques, depending on the arsenic concentration. For samples below 0.1 mg/L, analysis was performed using a Perkin Elmer Analyst 100 AAS equipped with a FIAS-400 hydride generator. Samples above 0.1 mg/L were analyzed with a Thermo Jarrell Ash Trace Scan ICP-AES.

Chapter 3 Coprecipitate Production

This section introduces and discusses the results of coprecipitate production experiments. Coprecipitate production results are discussed separately from ageing behavior to allow identification of process characteristics responsible for arsenic removal. Table 6 presents the steady-state concentrations obtained during different continuous circuit coprecipitation experiments, while the calculated stage removal efficiencies are shown in Table 7.

Table 6 Results of continuous circuit coprecipitation experiments (residence time 1 hr)

Exp.	Conditions	Actual Mole Ratio		No. of SS Samples	Arsenic (mg/L)				Iron (mg/L)				Co-ion (mg/L)		
		$\frac{\text{Fe}^{3+}}{\text{As}}$	$\frac{\text{Co-ion}}{\text{As}}$		Feed	Av Steady State Conc.			Feed	Av Steady State Conc.			Feed	Av SS Conc.	
						pH 2.5	pH 4	pH 8		pH 2.5	pH 4	pH 8		pH 4	pH 8
B-1	Batch, NaOH	4.00	---	---	1407	---	---	0.50	4197	---	---	BD	---	---	---
B-2	Batch, Ca(OH) ₂	4.00	---	---	1407	---	---	0.015	4197	---	---	BD	---	---	---
RP-2	1 stage, NaOH	3.44	---	6	1575	---	---	0.15	3997	---	---	BD	---	---	---
RP-4	1 stage, Ca(OH) ₂	3.36	---	5	1547	---	---	0.036	3877	---	---	BD	---	---	---
RP-4b	1 stage, Ca(OH) ₂	4.02	---	5	1442	---	---	0.026	4316	---	---	BD	---	---	---
RP-5	2 stage, Ca(OH) ₂	4.06	---	4	1418	---	0.024	0.008	4295	---	BD	BD	---	---	---
RP-9a	2 stage, batch start, Ca(OH) ₂	4.00	---	5	1403	---	0.022	0.011	4183	---	BD	BD	---	---	---
RP-6	3 stage, Ca(OH) ₂	4.03	---	5	1391	627	0.045	0.010	4177	2647	BD	BD	---	---	---
RP-11	3 stage, Ca(OH) ₂	4.01	---	6	1392	510	0.018	0.008	4160	2166	BD	BD	---	---	---
RP-9b	2 stage w/ recycle, Ca(OH) ₂	4.00	---	6	1407	---	0.021	0.016	4197	---	BD	BD	---	---	---
RP-7	2 stage w/ Ni ²⁺ , Ca(OH) ₂	4.00	0.42	6	1398	---	0.018	0.008	4168	---	BD	BD	460	416	11.4
RP-8	2 stage w/ Al ³⁺ , Ca(OH) ₂	3.07	0.91	6	1408	---	0.150	0.010	3226	---	BD	BD	459	117	BD
RP-12	2 stage w/ Fe ²⁺ , Ca(OH) ₂	4.01	1.0	6	1399	---	0.079	0.182	4181	---	633	5.4	1050	633	5.4

All steady state concentration values represent the average of at least four samples obtained during steady state operation. In all cases the standard deviation was less than 25% of the average concentration.
BD = below detection (<0.05 mg/L)

The standard deviations of the arsenic concentration values presented in Table 6 are consistently below 10% of the concentration value. The low standard deviation provides indication of the stable nature of the continuous circuit steady-state. In addition, the low concentration in the final stage of the two- and three-stage circuits appears to be readily reproducible.

Table 7 presents additional data from coprecipitate production. The base usage corresponds to the volume of base consumed (in each stage) during steady-state circuit operation. The stage arsenic removal has been calculated for each stage on an absolute basis, thereby eliminating the dilution effect caused by the addition of base. The calculation utilizes volumetric and concentration data found in Table 6 and Table 7 (where available).

Table 7 Stage removal percentages (absolute basis, to account for dilution effect of base)

Exp.	Conditions	SS Op Time (min)	Stage Base Consumption during SS Operation (mL)			SS Stage Arsenic Removal Percentage			SS Stage Iron Removal Percentage		
			pH 2.5	pH 4	pH 8	pH 2.5	pH 4	pH 8	pH 2.5	pH 4	pH 8
B-2	Batch, NaOH	300 mL	---	---	100	---	---	99.953	---	---	>99.999
B-2	Batch, Ca(OH) ₂	300 mL	---	---	100	---	---	99.999	---	---	>99.999
RP-2	1 stage, NaOH	159	---	---	1704	---	---	99.987	---	---	>99.999
RP-4	1 stage, Ca(OH) ₂	168	---	---	1765	---	---	99.997	---	---	>99.999
RP-4b	1 stage, Ca(OH) ₂	229	---	---	2197	---	---	99.998	---	---	>99.999
RP-5	2 stage, Ca(OH) ₂	244	---	294	2029	---	99.998	57.01	---	>99.999	>99.999
RP-6	3 stage, Ca(OH) ₂	258	693	544	1217	50.52	99.992	73.73	30.439	>99.999	>99.999
RP-11	3 stage, Ca(OH) ₂	225	n/a	n/a	n/a	n/a	n/a	n/a	n/a	n/a	n/a
RP-9a	2 stage batch start, Ca(OH) ₂	333	---	350	2819	---	99.998	35.175	---	>99.999	>99.999
RP-9b	2 stage w/ recycle, Ca(OH) ₂	277	---	n/a	n/a	---	n/a	n/a	---	n/a	n/a
RP-7	2 stage w/ Ni ²⁺ , Ca(OH) ₂	314	---	500	2605	---	99.999	42.88	---	>99.999	>99.999
RP-8	2 stage w/ Al ³⁺ , Ca(OH) ₂	309	---	532	2224	---	99.989	91.69	---	>99.999	>99.999
RP-12	2 stage w/ Fe ²⁺ , Ca(OH) ₂	230	---	n/a	n/a	---	n/a	n/a	---	n/a	n/a

n/a base consumption data for these experiments were not available

3.1 Effect of Base

To accomplish coprecipitation, base is used to raise the solution pH and induce precipitation of solids which contain arsenic. Most previous laboratory work has utilized NaOH to perform this task, while slaked lime, $\text{Ca}(\text{OH})_2$, is most commonly utilized by industry. Previous laboratory work has preferred the use of NaOH, as divalent ions are capable of affecting surface complexation phenomena. In addition, the use of $\text{Ca}(\text{OH})_2$ with sulphate media results in the formation of gypsum, which complicates solids characterization. To illustrate the difference between the two types of base, batch experiments were performed. The results, shown in Table 8, illustrate that when $\text{Ca}(\text{OH})_2$ is used as the base, the process can produce a final stage effluent with considerably lower arsenic concentration as compared to NaOH.

Table 8 Comparison of effect of base on coprecipitation final stage arsenic concentrations (from Table 6)

Exp.	Conditions	As conc. (mg/L after 1 hour)
B-1	Batch, NaOH	0.50
B-2	Batch, $\text{Ca}(\text{OH})_2$	0.015

The reason for the difference in arsenic concentration as a result of the base used is not clear. There are several possible explanations: 1) The dissolution of $\text{Ca}(\text{OH})_2$ reduces the concentration gradients during the process which in turn could; a) modify the phases which form (FA or FH and hence the arsenic partitioning) or b) prevent dissolution of solids (and release of arsenic). 2) Ca^{2+} could stabilize the product over the short term through surface complexation. 3) The formation of gypsum lowers the ionic strength which is known to affect the electrical double layer (EDL) and consequently sorption equilibrium. 4) The presence of Ca^{2+} may lead to Ca^{2+} - Fe^{3+} - AsO_4 association as a one- or two-dimensional precursor to the formation of three-dimensionally coordinated minerals such as yukonite or arsenosiderite.

Regardless of the reason for the enhanced arsenic removal associated with the use of $\text{Ca}(\text{OH})_2$, it becomes evident that, to provide industrially relevant results, conditions and reagents must be used that are consistent with the industrial process.

3.2 Effect of Circuit Design

An important aspect of industrial conditions is the use of continuous processes to accomplish reactions. In this case, most previous published research has utilized batch coprecipitation. One means of controlling precipitation processes is through staged neutralization, which is capable of producing a denser, more crystalline product [Demopoulos et al., 1995, Verbaan et al., 1999]. To investigate the role of circuit design (the mode of operation and effect of staging) on arsenic removal, different coprecipitation experiments were performed.

The arsenic removal for NaOH coprecipitation, shown in Table 9, appeared to vary considerably depending on the mode of operation, with continuous operation providing improved removal, despite the lower iron to arsenic molar ratio of the continuous experiment. The reason for this is not clear however, it is likely that the presence of constantly precipitating solids during continuous circuit operation, lead to the improved removal. It also may be possible that concentration gradients resulting from the aggressive base contributed to arsenic release. In the continuous circuit, the presence of freshly precipitating solids could counteract such an effect, while in the batch system re-adsorption would likely be a slower process.

Table 9 Comparison of batch and continuous circuit final stage arsenic concentrations, for NaOH neutralization (from Table 6)

Exp.	Conditions	$\frac{\text{Fe}^{3+}}{\text{As}}$	As conc. (mg/L)
B-1	Batch, NaOH	4.00	0.50
RP-2	1 stage, NaOH	3.44	0.15

The arsenic removal for $\text{Ca}(\text{OH})_2$ coprecipitation, shown in Table 10, illustrate that batch and continuous coprecipitation provided similar removal. The use of staging is capable of improving the arsenic removal (to varying extents), and the recycle of solids (as seed) does not provide a noticeable improvement to arsenic removal.

Table 10 Comparison of batch and continuous circuit final stage arsenic concentrations, for Ca(OH)₂ neutralization (from Table 6)

Exp.	Conditions	As conc. (mg/L)
B-2	Batch, Ca(OH) ₂	0.015
RP-4b	1 stage, Ca(OH) ₂	0.026
RP-5	2 stage, Ca(OH) ₂	0.008
RP-9a	2 stage, batch start, Ca(OH) ₂	0.011
RP-6	3 stage, Ca(OH) ₂	0.010
RP-11	3 stage, Ca(OH) ₂	0.008
RP-9b	2 stage w/ recycle, Ca(OH) ₂	0.016

While batch and continuous coprecipitation provide similar results, for neutralization with Ca(OH)₂, single-stage coprecipitation provides the least effective arsenic removal. This can be explained via consideration of residence time distributions (RTD), which affect continuous stirred tank reactors. The RTD tells us that for a CSTR, the molecules or particles of material leaving the reactor have spent different times within the reactor [Fogler, 1999]. Consequently, a portion of the stage effluent may leave before it has had a chance to be adsorbed by the solids (or grown adequately), resulting in the higher final stage effluent concentration of the single-stage circuit.

It can be noted, from the data in Table 6 that despite use of a three stage circuit, with the first stage set-point of pH 2.5 (which was selected to promote the formation of ferric arsenate), the removal of arsenic in the stage did not clearly indicate the formation of a 1:1 ratio coprecipitate. In all other cases the (essentially) complete removal of iron prevented interpretation of the coprecipitate composition via mass balance.

It can also be noted, from the data in Table 7, that for two-stage coprecipitation, arsenic removal continues in the final stage of the circuit, in changing from pH 4 to 8. This additional removal occurs despite the absence of precipitating iron and at very low concentration level, and is likely the result of adsorption onto solids formed at pH 4.

3.2.1 Conceptual Reaction Mechanism

One explanation for the differences between staged coprecipitation involves assuming that the coprecipitation process is capable of producing FA. Since the first stage of the circuit is maintained at different pH values, the saturation conditions of the

feed solution with respect to both FA and FH are different. As the saturation conditions control nucleation, it is possible that adjusting the staging or pH set-points can influence the partitioning of arsenic between these two phases. If more arsenic reports as FA, then the amount of arsenic remaining to be removed (or polished) by adsorption on FH is reduced, providing a lower sorption density and lower steady-state arsenic concentrations. Using this theory, (as well as the theoretical solubility, saturation index and aqueous speciation curves presented in Figure 9, Figure 10, and Figure 11, respectively^{*}), the results of staged coprecipitation can be explained.

For a three-stage circuit, the first stage set-point was pH 2.5. At this pH, the concentrations of iron and arsenic are affected by the solubility of both FH and FA. As a result both phases should form via nucleation, which also has implications to both phases: First, given the high arsenic concentrations (~550 mg/L), any FH which is formed should adsorb arsenic. As the sorption capacity of FH is higher at lower pH, it is likely that the amount of arsenic adsorbed on the FH at pH 2.5 can not be held after the pH is increased in other stages of the process, and must be re-distributed (via desorption and adsorption) during later stages or ageing. Second, the surface complexation of arsenic would serve to reduce driving force for FA nucleation. Therefore surface complexation is competitive to FA nucleation. In terms of the partitioning of arsenic between FA and FH in the coprecipitates, the pH 2.5 set-point would likely reduce the amount of arsenic partitioned to FA (from the theoretical maximum).

^{*} Generated through the use of Excel to solve the material balance equations provided by the reactions and equilibrium constants located in appendix II and obtained from Langmuir et al., 2006 and PHREEQC.

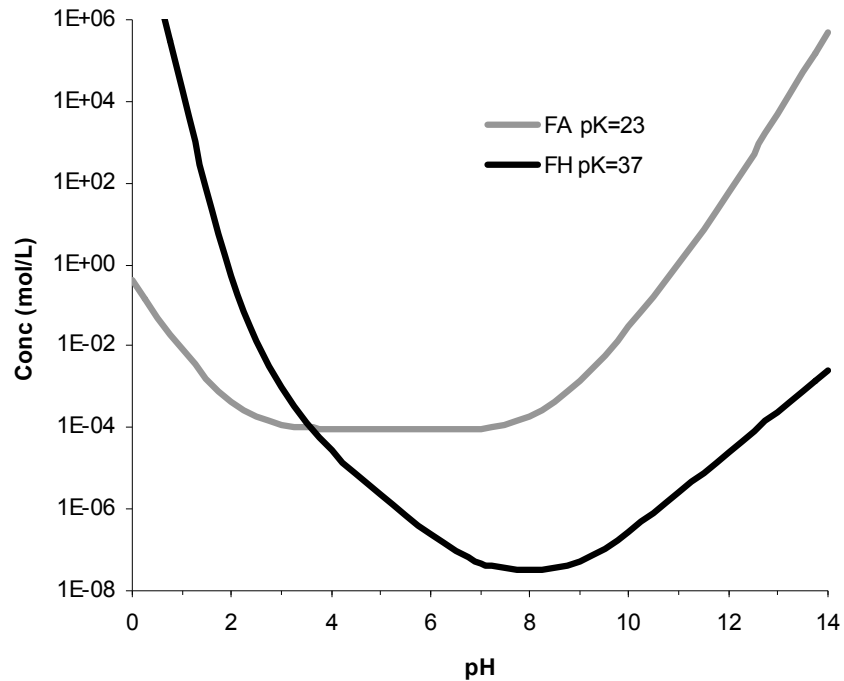


Figure 9 Theoretical solubility of Fe and/or As with respect to FA or FH (assuming congruent dissolution, not including Fe-SO₄ aqueous complexes)

For a two-stage circuit, the first stage set-point was pH 4.0, the solubility of FA approaches its minimum, while Fe³⁺ concentrations are limited by FH. At this point it becomes difficult to predict the partitioning of arsenic. As a result of the high saturation index (a measure of the degree of supersaturation) of both phases, shown in Figure 10, homogeneous nucleation should be expected to dominate. If Stranski's rule can be applied, then the meta-stable phase should form first (because it is easiest and therefore fastest to do so, as a result of the relatively lower nucleation energy barrier); that is to say, FA will be formed preferentially, after which FH will be formed, which adsorbs arsenic. This concept is supported by consideration of the aqueous speciation of the ions in solution. At low pH, the aqueous speciation is dominated by Fe-AsO₄ aqueous complexes, as shown in Figure 11. As is the case with Fe³⁺ precipitation, the phase formed is determined by the precursor complex-clusters [Demopoulos, *accepted*]

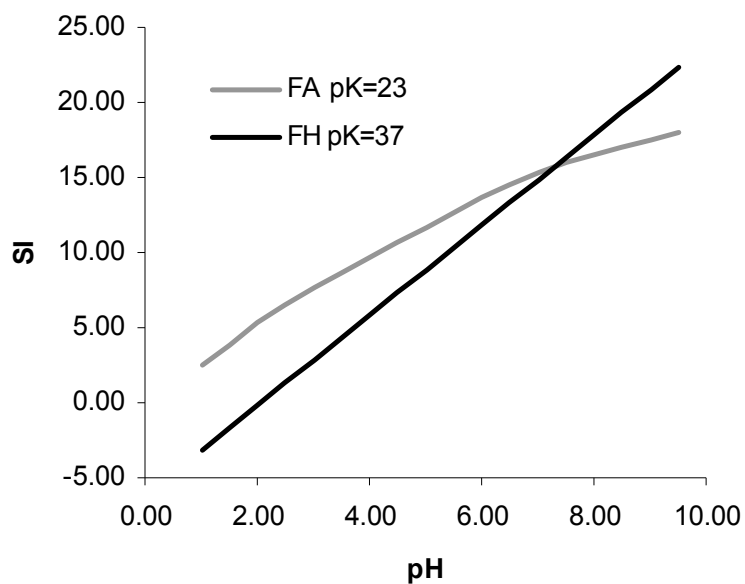


Figure 10 Calculated saturation index of FH and FA as a function of pH (1400 mg/L As, Fe/As=4, instantaneous pH change, no dilution)

At pH 8, the solubility of FA is considerably higher than at pH 4. As a result, less FA is likely to be formed via homogeneous nucleation, (than the theoretical maximum) resulting in less arsenic partitioned to this phase. Iron continues to be limited by FH solubility, and the SI of FH becomes larger than that of FA, suggesting that FH nuclei become kinetically favoured over FA.

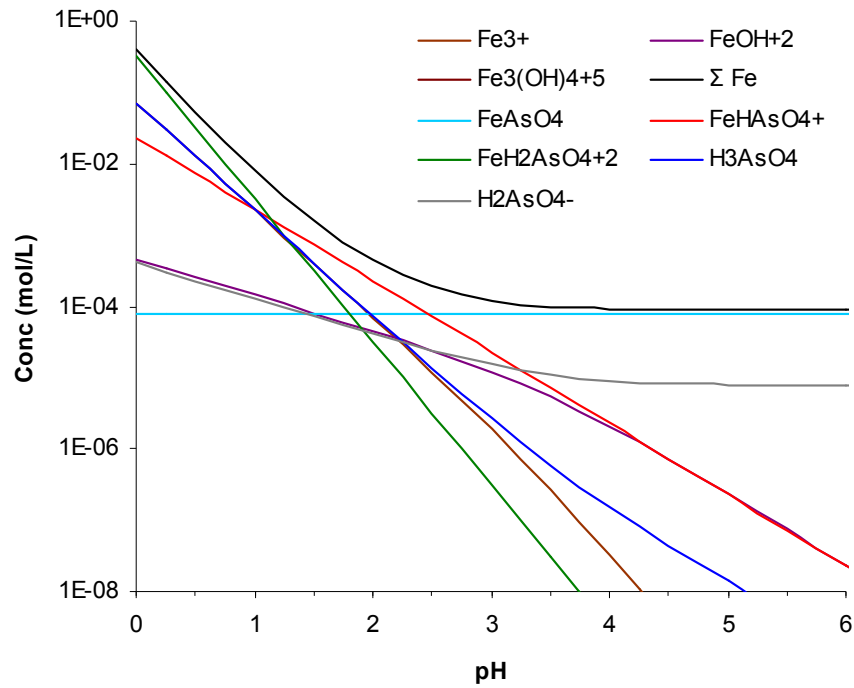


Figure 11 Aqueous speciation of Fe and As in equilibrium with FA (assuming congruent dissolution, not including Fe-SO₄ aqueous complexes)

The use of solids recycle in precipitation circuits is a commonly practiced technique to improve the bulk density of the solids, by increasing the available surface area where growth can occur. However, in a low temperature process, at the conditions used in this study (where homogeneous nucleation dominates), the major mode of growth can be expected to occur through aggregation [Demopoulos, *accepted*]. The increase in final stage effluent arsenic concentration is not clear, however it could be due to a lower surface area of FH (owing to ageing and/or growth), which is responsible for arsenic polishing.

Alternatively, it remains possible that the different pH values of initial stage coprecipitation produce FH with different nano-domain properties, which account for the variations in process effluent arsenic concentrations.

3.3 Effect of Co-ions

Another important aspect of industrial conditions is the presence of additional cations in the coprecipitation feed, which can have an affect on arsenic removal. This includes aluminium and ferrous iron. In addition, other base metal cations (such as Ni^{2+}) may also require removal. While the effect of some of these ions has been investigated, including calcium [Emett & Khoe, 1994, Jia & Demopoulos, 2005, 2008], nickel [Jia & Demopoulos, 2008], aluminium [Robins et al. 2005, Hohn et al. 2006] and combined cations of copper, cadmium and zinc [Harris & Monette, 1988], the effect of Fe^{2+} has not yet been investigated. To evaluate the effect of these ions on the coprecipitation process, continuous two-stage coprecipitation was performed with these co-ions present in the coprecipitation feed. The results, in comparison to two-stage coprecipitation without additional co-ions, are shown in Table 11. It should be noted that nickel was present in addition to arsenic (in this work it was considered an impurity which must also be removed), as opposed to aluminium and ferrous iron which were present as a substitute for ferric iron.

Table 11 Comparison of batch and continuous circuit final stage arsenic concentrations (from Table 6)

Exp.	Conditions	Actual mole ratio		As conc. (mg/L)	Co-ion conc. (mg/L)
		Fe^{3+}/As	Co-ion/As		
RP-5	2 stage	4.06	---	0.008	---
RP-7	2 stage w/ Ni^{2+}	4.00	0.5	0.008	11.4
RP-8	2 stage w/ Al^{3+}	3.07	0.91	0.010	< 0.1
RP-12	2 stage w/ Fe^{2+}	2.99	1.01	0.182	5.4

As the staging and pH conditions in the first reactor remained the same in all experiments, it can be expected that the arsenic partitioning to FA should remain consistent. The presence of other ions may however impact the arsenic polishing, which is accomplished by surface complexation.

The results indicate that Ni^{2+} does not compete for adsorption sites on FH (i.e. displace adsorbed arsenic). In addition, the 1:1 substitution of Al^{3+} for Fe^{3+} provides a suitable adsorbing material for polishing arsenic. However, the 1:1 substitution of Fe^{2+} for Fe^{3+} does not provide an effective adsorption material for arsenic polishing. The results of the two-stage experiment with Fe^{2+} also indicates that without a sufficient

Fe³⁺/As ratio, the effluent As concentration can increase as the pH is raised after the initial stage(s). This could be the result of: a) alteration of FA characteristics including the possible formation of ferrite (Fe³⁺₂Me²⁺O₄) phases; b) inadequate surface area of FH to accommodate soluble arsenic, and/or c) lack of a strong surface complexation reaction of arsenate (AsO₄) on the ferrous hydroxide surface.

3.4 Characterization

Characterization of the coprecipitates was performed by a variety of techniques. Those aimed at identifying the phases present were not as successful as desired, as a result of the poorly crystalline nature of the material. Others, which measured the physical properties of the material, were not so helpful in explaining the chemical differences between the coprecipitates. However, there was a technique from the field of colloid and surface chemistry that provided interesting insights into the nature of the coprecipitates and the behavioral differences between them. This technique was the measurement of the point of zero charge.

3.4.1 Settling Rate

The physical properties of tailings are important to deposition and downstream operations that must thicken and separate the solids. One such property is known as the settling rate, which quantifies the ability to separate the solids from a clear supernatant solution and is related to the particle/agglomerate size and other particle properties. This measurement was performed at ambient temperature (22°C) using a glass 1L graduated cylinder.

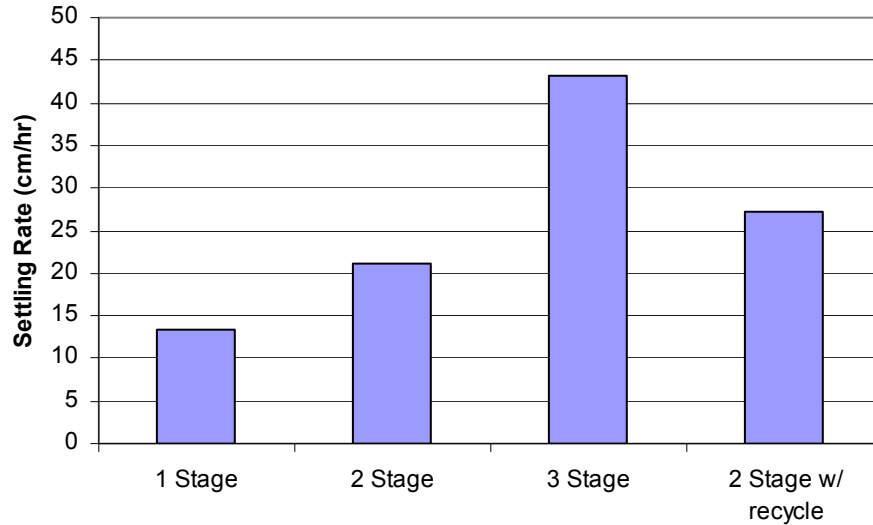


Figure 12 Initial settling rate of coprecipitates

The results of settling rate measurements indicated that staging has a significant effect on the settling rate, with an increased number of stages providing a larger settling rate. In addition, the use of solids recycle can be seen to increase the settling rate.

3.4.2 Particle Size Distribution

Particle size analysis was performed using an Horiba LA-920 laser scattering particle size analyzer. De-ionized water was used as the dispersion medium. Due to the composite nature of the samples, multiple refractive index values were available for processing of the laser scattering spectrum. In addition, there were also “shape factors” available for correction of non-spherical particles. As the instrument can only utilize a single refractive index and shape correction value, the refractive index of gypsum (1.14) with a “mild” shape correction factor was selected, as gypsum represents the bulk of the material present in the coprecipitate. Other options included hematite (2.18) or scorodite. The results presented should be taken as an indicator only, due the complications including: composite nature of the coprecipitate, the tendency for suspensions of small particle size to agglomerate as well as the dissolution of gypsum, which could be expected to occur in the de-ionized water dispersion medium.

The results of particle size analysis are shown in Figure 13 and are separated according to primary variables which affect the coprecipitate. Figure 13A illustrates the differences which arise from the use of NaOH and Ca(OH)₂ in a single stage circuit. The

appearance of a bimodal distribution becomes a trend which is observed in other $\text{Ca}(\text{OH})_2$ coprecipitation experiments. The large range in the size distribution for NaOH coprecipitation provides indication of agglomeration of particles, which could not be separated by ultrasonic dispersion.

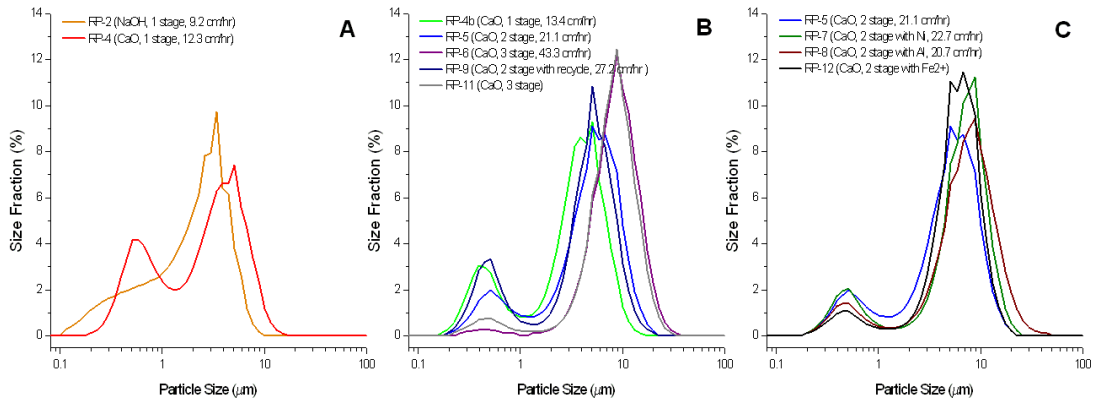


Figure 13 Particle size distribution of coprecipitates
A) effect of base, B) effect of circuit design and C) effect of co-ions

The results of Figure 13B indicate the effect of circuit design on the particle size distribution. Also shown in the legend is the initial settling rate of the coprecipitate. The distributions support the settling rate observations and indicate that the use of staging and recycle serve to increase the average size of the particles. As gypsum is the material most affected by growth, it can be expected that the second peak of the bimodal distribution is due to gypsum. Similarly, it becomes evident that the first peak in the distribution does not change significantly with respect to particle size, but it does shift in terms of the percentage that it represents. This could be interpreted as several factors, but most likely represents the agglomeration to the more dominant and larger sized gypsum material.

The results of Figure 13C indicate that the substitution or presence of other co-ions in the coprecipitation feed did not significantly affect the size distribution. As a result, the size distribution and settling rate of the precipitate are most strongly affected by the circuit design.

3.4.3 X-Ray Diffraction

X-ray diffraction was performed on the coprecipitate solids using a Philips PW1710 diffractometer equipped with a copper target ($\text{Cu K}\alpha_1$ radiation, $\lambda=1.54060\text{\AA}$), a crystal graphite monochromator and a scintillation detector. The scan was performed at 40kV and 20mA, with a step size of 0.1 degrees for a count of 3 seconds per step from 5 to 100 degrees two-theta. The pattern of coprecipitate solids produced via a two-stage circuit with Ca(OH)_2 as base is shown in Figure 14.

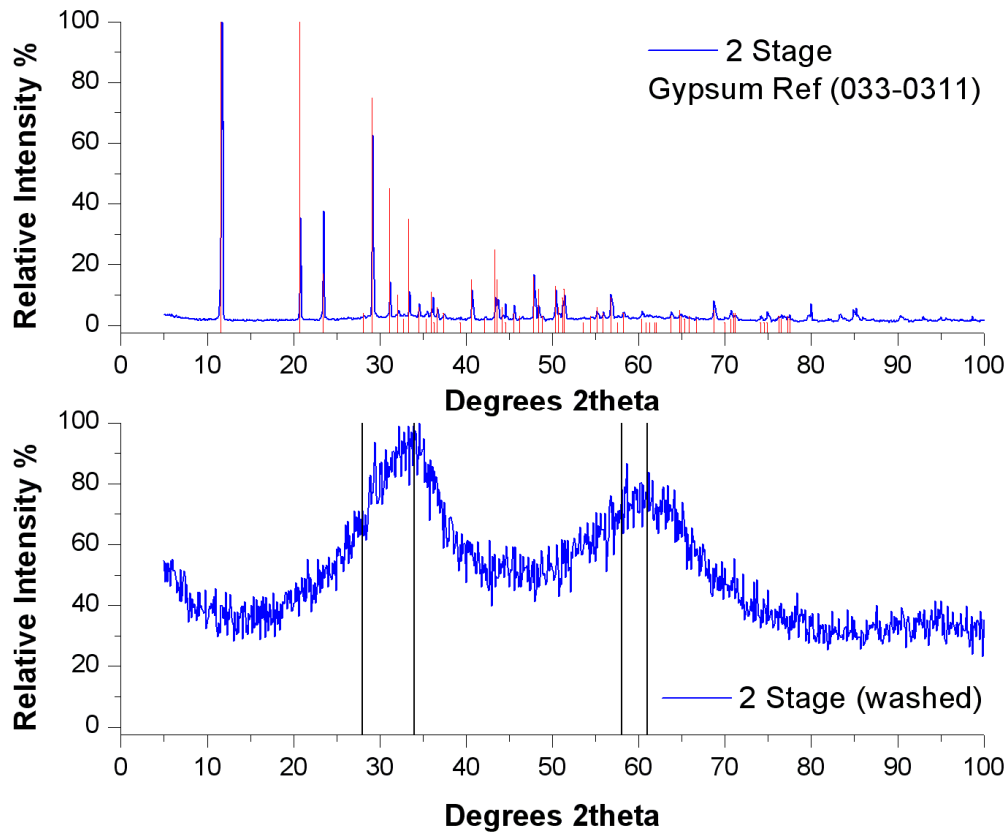


Figure 14 XRD pattern of 2 stage coprecipitates (experiment RP-5, patterns obtained before and after washing to remove gypsum)

The first pattern reveals that gypsum is the dominant crystalline phase in the product. Removing the gypsum, by washing the solids in de-ionized water, produces an XRD pattern with two broad peaks. Other researchers have observed similar XRD patterns from coprecipitates [Krause & Ettl, 1989, Jambor & Dutrizac, 1998, Jia et al., 2003, 2007, Le Berre et al. 2007, Pactunc et al. 2008] isolation of pure phases of both FA

and FH have revealed that the location of the broad peaks can be used to distinguish between the two poorly crystalline phases. FA has peaks at 28° & 58° while FH has peaks at 34° & 61°. To facilitate interpretation of the XRD pattern, these angles have been marked with vertical lines. Returning to the XRD pattern of washed two stage coprecipitates, the first peak is centered on 34° corresponding to FH, with a shoulder located at approximately 30°, which may represent FA. The second peak is located at 60° another indicator that the coprecipitate consists of a mixture of two phases.

3.4.4 Measurement of PZC via Batch Equilibration

As a result of the composite nature of the coprecipitates and the complications resulting from the presence of potential determining ions (Ca^{2+} , SO_4^{2-} , AsO_4^{3-} and Ni^{2+}), measurement of the surface properties by electrophoretic techniques was unreliable. Other techniques for determining the point of zero charge (PZC) of solids were investigated and a technique known as batch equilibration was found [Milonjić & Ruvarac, 1975].

The batch equilibration technique is mentioned by Kosmulski [2001] to provide acceptable results. The procedure involved equilibration of solids, for a period of 24 hours, at 10g/L in HDPE bottles, with solutions of 0.1M NaNO_3 adjusted to various initial pH values between 4 and 10, with HNO_3 or NaOH . The solids used were previously dried at 50°C to constant weight. After agitation, the solution pH was measured and recorded. A plot of either: a) pH_{final} versus $\text{pH}_{\text{initial}}$ or b) ΔpH versus pH_{final} or c) $\Delta[\text{H}^+]$ and $\Delta[\text{OH}^-]$ versus pH_{final} , reveals the PZC of the solid. To aid in obtaining a homogeneous sample, the solids were slurried in a small volume of de-ionized water before being split into the separate bottles and contacted with pH adjusted liquid. The results of batch equilibrations are shown in Figure 15, and the plateau in the pH_{final} represents the PZC of the solids.

The results shown indicate that the bulk PZC of the coprecipitate material varies significantly depending on the conditions by which it was produced. This observation can be used to provide information about the composition of the coprecipitate that can not be obtained by other techniques which rely on either crystalline or pure phases.

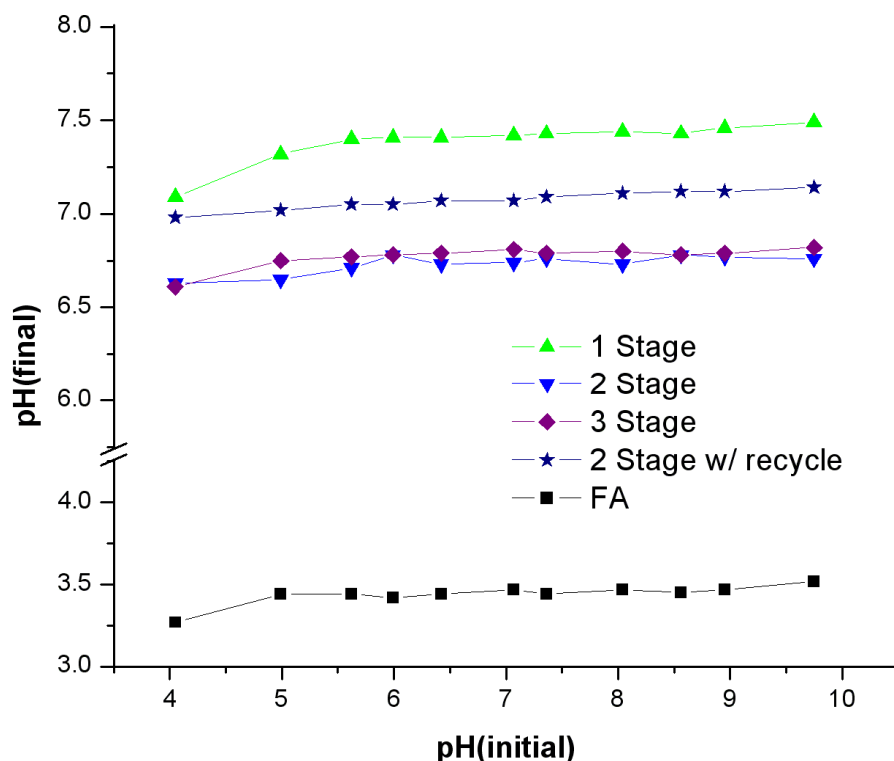


Figure 15 Bulk PZC of coprecipitates (as indicated by the plateau in pH(final) after batch equilibration at 22°C)

To provide a comparison, literature was searched for published PZC values of iron oxides and hydroxides. The PZC of FH was reported to occur at pH 8.5 [Kosmulski, 2001]. Reported values for the PZC of FA or scorodite were not found. Parks & De Bruyn, [1962] have reported that the PZC of oxides and hydroxides can be expected to occur near the pH of minimum solubility. Given the knowledge of FA and scorodite solubility, the PZC was predicted to occur between pH 3 & 4. To provide evidence, FA was synthesized from an equimolar solution (0.133 M) of ferric sulphate and arsenic pentoxide, via neutralization with $\text{Ca}(\text{OH})_2$ to pH 2.5 (initial pH 0.75 by H_2SO_4 , room temperature). The solids produced were filtered, washed (with a small volume of de-ionized water to flush out the pore water), dried and subjected to batch equilibration. The results are shown in Figure 15 and indicate that the PZC of FA occurs at pH 3.5, the center of the predicted range.

Returning to the PZC data of Figure 15, it can be seen that staging is capable of modifying the PZC values associated with different coprecipitates. This is interpreted to

be the result of the presence of FA in the final product, given its low PZC. Apparently at pH 4 or lower, a significant amount of FA is formed and reports to the final product, as opposed to the coprecipitates from a single-stage system at pH 8, where FA constitutes a lower fraction of the final product. Calculation of the FA content is specifically addressed in Section 4.2.1.

3.4.5 Fourier Transform Infrared Spectroscopy

Infrared spectra were obtained using a Perkin Elmer FTIR spectrometer with a Miracle single bounce diamond ATR cell. Spectra were collected over the range of 4000 to 550 cm^{-1} at a resolution of 4 cm^{-1} , co-addition of scans was performed to improve the signal to noise ratio. All spectra were normalized and background corrected using the Spectrum software (version 5.02). The spectrum for two-stage coprecipitates is shown in Figure 16, as well as a comparison spectrum for gypsum.

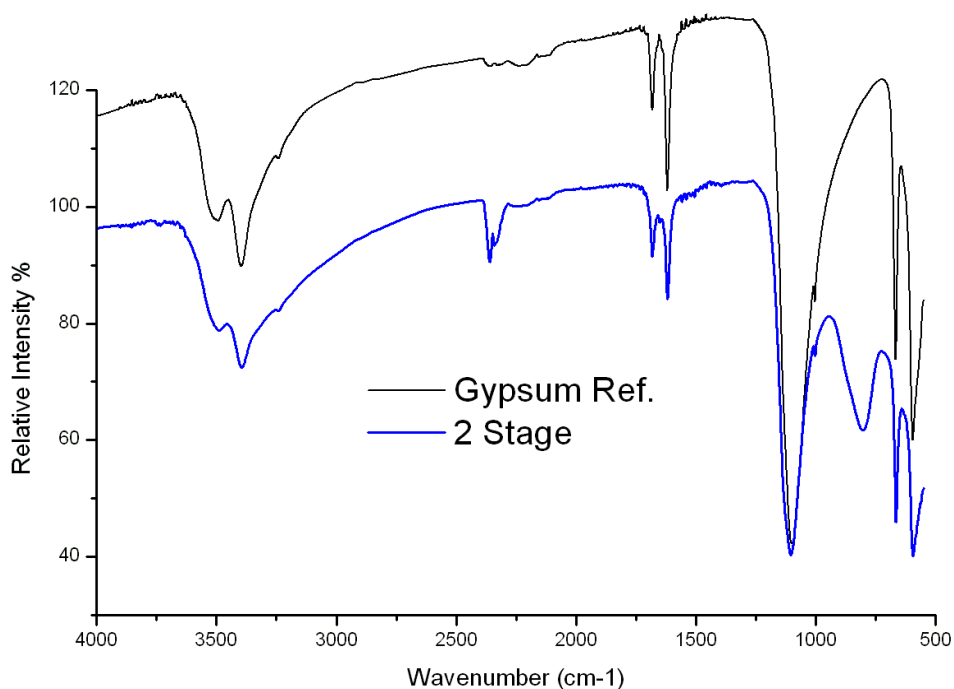


Figure 16 FTIR spectra of coprecipitates

FTIR spectroscopy can be used to identify the different function groups within the material and the bonding environment of the functional group (refer to Table 12). For the

coprecipitate material, the majority of the observable peaks are common to gypsum, namely those of OH and SO₄. Other functional groups are also visible, including CO₂, which occurs in the range of 2000 to 2500 cm⁻¹. The presence of CO₂ could be due to atmospheric CO₂ as a result of improper background correction or the presence of adsorbed carbonate on the solid surface. The presence of carbonate in solution is possible via multiple sources including: 1) the presence of CaCO₃ as an impurity in the lime used as base, 2) the dissolution of atmospheric CO₂ into either the water or the alkaline solutions used as base. Finally, a peak at 800 cm⁻¹ is also present, which corresponds to the arsenate functional group.

Table 12 FTIR absorption frequencies for various functional groups

Functional Group Vibration Mode	Range (cm ⁻¹)	Intensity	Assignment	Ref
hydroxide/water				
stretching	3580-3650	var	O-H (free), usually sharp	Nakamoto
	3200-3550	s	O-H (H-bonded), usually broad	
bending	1600-1630	s	H-O-H bending	Nakamoto
	1330-1430	m	O-H bending (in-plane)	Nakamoto
	2500-3300	s	O-H (very broad)	
Sulphate (S=O)				
bridging/chelating	1000-1200	s-vs	bridging or chelating	Nakamoto
	610-650	s		
complexed	970-1000	vw-m		Nakamoto
Arsenate (As=O)				
	800-1000			Myneni

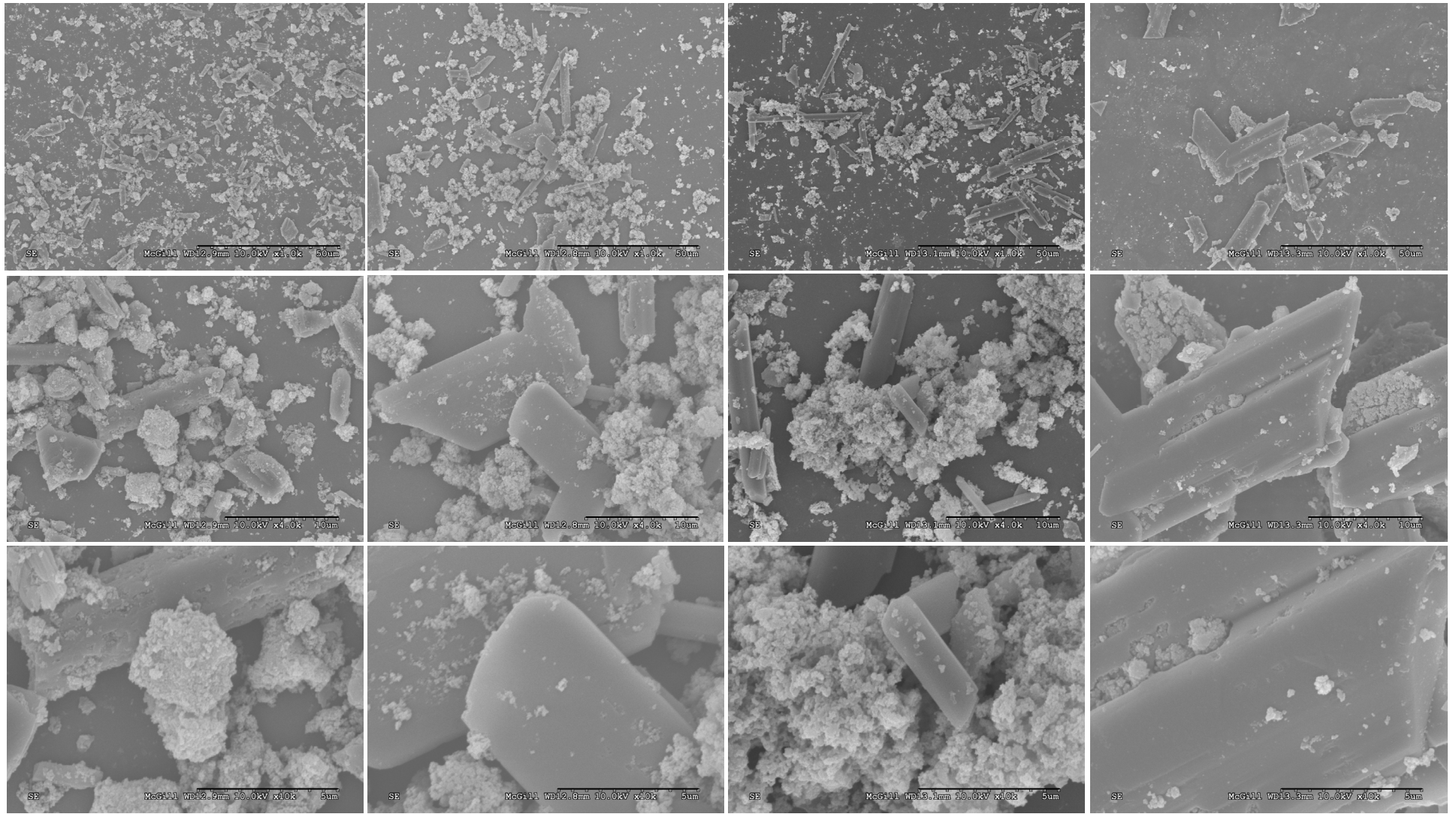
3.4.6 Scanning Electron Microscopy

Electron microscopy was performed using an Hitachi S-3000N scanning electron microscope. Prior to microscope work, all samples were filtered, washed with de-ionized water and dried at 50°C in an oven. The solids were lightly ground and dispersed in alcohol, via the use of ultrasonics, prior to being placed on a silicon wafer and coated with a thin layer of AuPd. Several micrographs at increasing magnification are shown in Figure 17, for coprecipitates produced under various circuit configurations.

The images reveal the heterogeneous nature of the coprecipitates which consist of long angular particles, consistent with gypsum, as well as clustered agglomerates of very small particle size, presumably that of the iron and arsenic bearing phases.

One trend which can be observed is the increased size of the gypsum particles (either through length or width) with increased number of stages in the circuit and with recycle of solids, an observation in agreement with previous research findings [Verbaan et al. 1994].

Another trend which can be observed is the roughly spherical agglomeration of small particles, which have individual sizes less than 0.5 μm . In addition, the agglomerates can be observed on the surface of the gypsum, which may contribute to the rough surface texture of gypsum observed in some of the micrographs. Also of note is the apparent growth of gypsum particles around agglomerates on the surface of gypsum, as can be seen in the highest magnification image of coprecipitates produced in the two-stage circuit with solids recycle.



1 Stage

2 Stage

3 Stage

2 Stage w/recycle

Figure 17 SEM images of coprecipitates

3.5 Discussion

The results presented in this section indicate that arsenic can be removed to very low concentrations by coprecipitation with an Fe/As mole ratio of 4. The role of base, circuit design and industrially relevant co-ions was investigated to see how it influenced arsenic removal. Arsenic removal was most significantly affected by: 1) the Fe/As molar ratio or to be more specific, the Fe(III)/As(V) molar ratio, as well as 2) the presence of calcium (type of base). While other parameters affected arsenic removal, their contribution was minor.

The use of staged continuous circuit operation provided observation of the coprecipitation reactions at stage pH values. While the observations do not represent the full picture, they indicate that the coprecipitation process is complex and can not be described by a single mechanism; either ferric arsenate or arsenate adsorption on ferrihydrite. Consistent with observations and the theories of crystallization and surface complexation, a dual mechanism explanation has been proposed (but not proven) in an effort to explain, understand and predict the behavior of the process.

As a result of the nature of the coprecipitates, which consist of a mixture of phases, ranging in crystallinity from very poorly crystalline (arsenic bearing phases) to crystalline (gypsum), characterization efforts were complicated and did not provide as much information as desired. However, it may be concluded that the coprecipitates consist of a mixture of ferric arsenate and arsenic bearing iron(III) oxyhydroxide.

Chapter 4 Coprecipitate Ageing

This section introduces and discusses the results of coprecipitate ageing experiments. These results are discussed separately to allow identification of process characteristics that provide improved arsenic retention.

The primary means of characterizing the coprecipitates was through observation of the arsenic retention behavior during ageing. Two ageing techniques were employed; a) solution-controlled forced equilibrium at pH 8, which could be considered as an open system with respect to base addition and b) solids-controlled “natural” equilibrium without pH control, which would correspond to a closed system.

The first method relied on routine addition of base, as the solution pH had a tendency to decrease. This routine adjustment forced the solids to re-equilibrate with the solution. It remains possible that the addition of base (as either $\text{Ca}(\text{OH})_2$ or NaOH) caused short-term, irreversible dissolution of solids as a result of concentration gradients (discussed in Section 2.1). For this reason, the second ageing method, inspired by conditions encountered in a tailings management facility, did not involve pH adjustment, instead allowing the solids and liquid to come to equilibrium with each other.

In both methods, the solid content was approximately 8.4 grams Fe^{3+} per litre (or an estimated pulp density of approximately 55 grams total solids per litre, corresponding to a solid/liquid ratio of approximately 1/25). All solution samples were filtered with either a 0.025 μm or 0.02 μm syringe filter. The pH-controlled ageing experiments are discussed first.

It should be noted that the concentrations presented are those of arsenic only. Analysis for iron was also performed on occasion, however the results were consistently below the detection limit of the ICP-OES instrument (0.05 mg/L) and as a result they are not presented. During ageing of coprecipitates produced via NaOH , the supernatant developed a brown color with time, most notably at higher temperatures. Upon filtration with a 0.02 μm syringe filter, the coloration was removed and iron concentrations were below detection, indicating the presence of colloidal fines. These fines were not observed during the ageing of coprecipitates produced with $\text{Ca}(\text{OH})_2$.

4.1 Ageing with pH Control

The results of ageing coprecipitates (produced via coprecipitation with slaked lime) at pH 8 and temperatures of 3, 22, 40 and 70 °C are shown in Figure 18. Additionally, data from preliminary ageing tests involving single-stage coprecipitates are provided in Appendix III. The results of coprecipitate ageing indicate that short and long term arsenic stability, as indicated by initial release rates and “equilibrium” stability, was affected by the manner in which the coprecipitates were produced. The arsenic retention trend follows the order: 1 stage < 3 stage < 2 stage \approx 2 stage with recycle and exhibits consistency at different temperatures. The consistency between data produced via the two-stage circuit, with and without recycle, serves as an indicator of the reproducibility of the measurements.

The results of ageing also indicate that the presence of additional cations (besides calcium), can affect the initial release rates and “equilibrium” stability during ageing. The substitution of Al^{3+} for Fe^{3+} , as well as the presence of Ni^{2+} , appears to improve the arsenic retention capacity/ability of the coprecipitates relative to two-stage coprecipitates produced under similar conditions.

It can be noticed that the stability of arsenic during ageing is also dependant on temperature. The direction of the temperature dependence indicates that at lower temperatures, arsenic stability is improved. This is significant as most sub-aqueous tailings management facilities have low temperatures, typically 3-20°C, which is advantageous to the reduction of arsenic source terms to the environment.

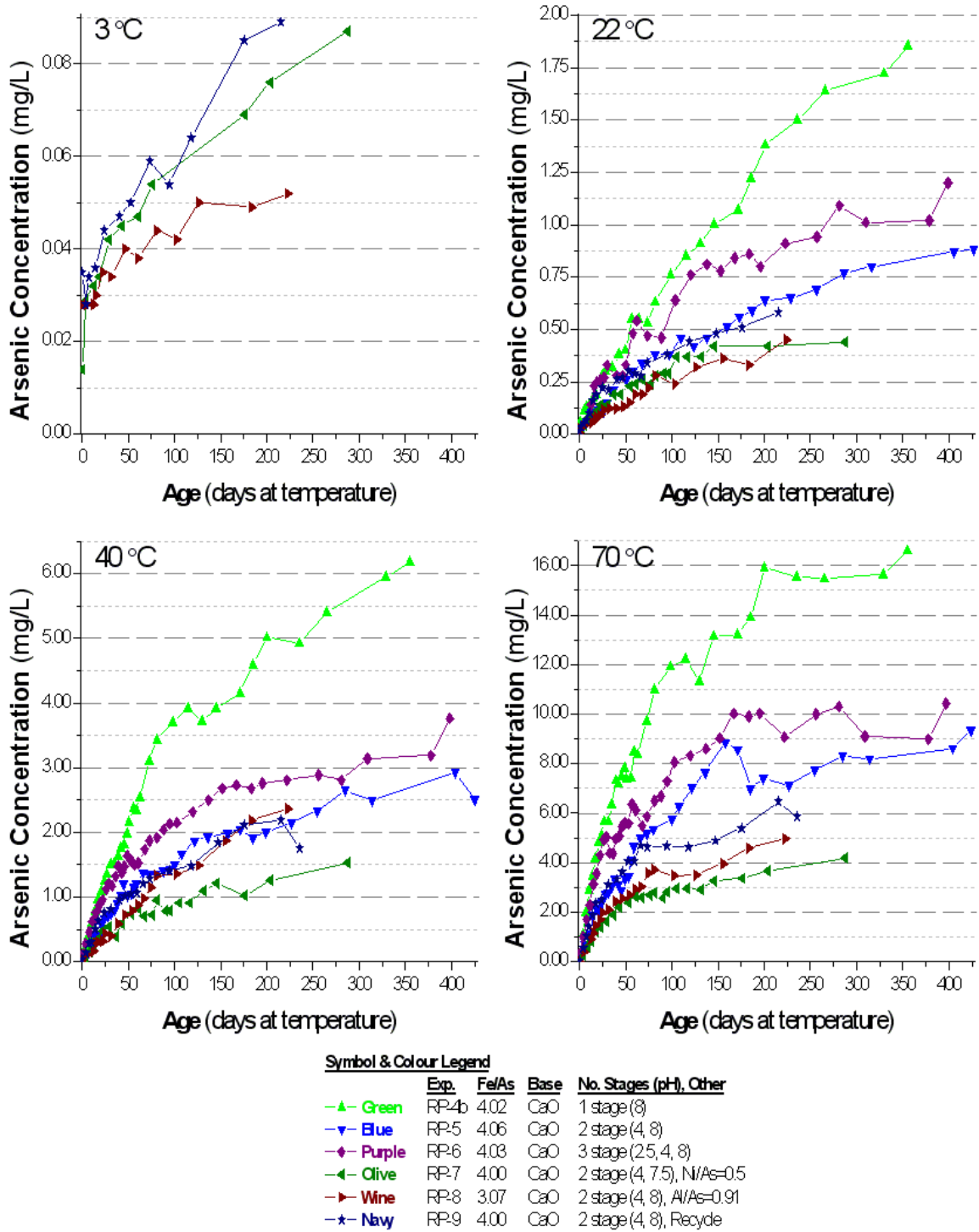


Figure 18 Coprecipitate arsenic retention during ageing (pH 8 and temperatures of 3, 22, 40 & 70 °C)

4.1.1 Effect of Base

As shown in Section 3.1, the choice of base can affect the arsenic removal during the coprecipitation process. In addition, several researchers have also demonstrated that the presence of Ca^{2+} improves coprecipitate retention [Emett & Khoe, 1994, Jia & Demopoulos, 2005, 2008]. These observations were confirmed by ageing batch coprecipitates (with pH control). The data is provided in Figure 19.

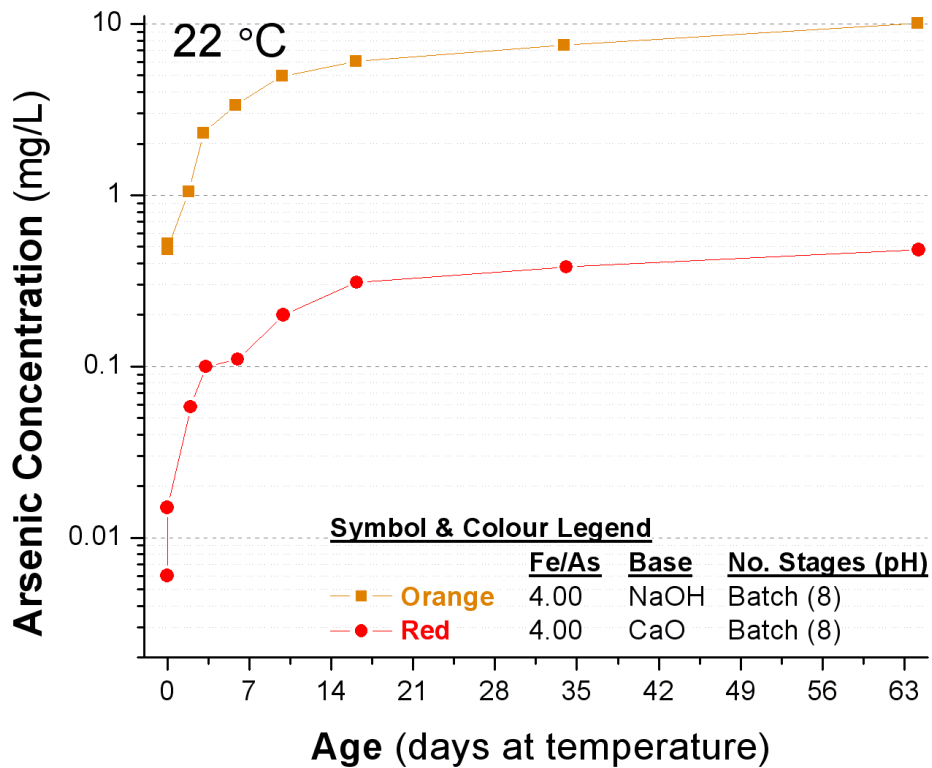


Figure 19 Arsenic retention differences resulting from the type of base (pH 8, 22°C)

The reasons for the variation are not clear. Some of the possible explanations outlined in Section 3.1, that relate to coprecipitated ageing were investigated further (such as the effect of ionic strength and the formation of complexes) and are reported in Appendix I and II. The most important observation was that Ca^{2+} has a significant influence on the stability of arsenic in the coprecipitate during ageing. Therefore, to achieve results consistent with industry and to provide industrially relevant data for model development, it was important to use $\text{Ca}(\text{OH})_2$ as a base.

4.1.2 Effect of Coprecipitation Circuit Design

The results of ageing coprecipitates at pH 8 indicate that the circuit design has an impact on arsenic retention, as evidenced by the initial arsenic release rates, as well as the “equilibrium” stability. These differences can be attributed to variations in the relative amounts of arsenic bearing phase formation/partitioning as outlined in Section 3.2. According to the mechanism proposed, a greater amount of FA should be present in the solids following two-stage coprecipitation, owing largely to the saturation conditions which initiate precipitation at pH 4. By connecting the proposed mechanism to the ageing results, it would appear that the coprecipitates were stabilized through an increased partitioning of arsenic to FA.

4.1.3 Effect of Aluminium

For aluminium, the improved retention could be attributed to either the formation of an Al-AsO₄ phase or a surface complexation mechanism. The former is less likely, as Le Berre et al. [2007a,b] have shown mansfieldite (AlAsO₄·2H₂O) and aluminium substituted scorodite to be less stable than scorodite, and it can be assumed that a poorly crystalline precursor would exhibit similar behavior.

Concerning the surface complexation mechanism, several possibilities exist, including the formation of a structurally modified ferrihydrite which may provide enhanced adsorption properties. This possibility has been mentioned by other researchers [Robins et al., 2005, Hohn et al. 2006, Jambor & Dutrizac, 1998].

Alternatively, since adsorption is driven by specific and electrostatic interactions, the total bond strength can be affected by surface properties. As a result, an adsorbent with a lower specific interaction (g_i) could be compensated by a stronger electrostatic interaction ($zF\Psi_d$). Notably, the PZC of most aluminium (hydr)oxide phases are higher than those of their iron counterparts, indicating a stronger electrostatic interaction with anions. It should be noted that this phenomena alone does not always make aluminium a better candidate for adsorption processes, owing to other properties which affect adsorption.

4.1.4 Effect of Nickel

For nickel, the mechanism by which the improved retention is accomplished is not known. Observations from the coprecipitation process indicate that the bulk arsenic and iron coprecipitation is accomplished separately (i.e. in a different reactor) from that of nickel. This reduces the possibility of the formation of nickel-arsenic compounds, such as annabergite ($\text{Ni}_3(\text{AsO}_4)_2 \cdot 4\text{H}_2\text{O}$) [Yuan et al. 2005], or nickel-iron spinel like phases and indicates that the interaction of nickel most likely occurs through surface complexation. As the solids consist of both FA and FH phases, it may be possible for nickel to interact with either one. If the interaction were with FA, through the formation of Ni-AsO₄ or Ni-O-Fe surface complexes, the FA phase may be stabilized against dissolution. If the interaction were with FH, the effect on the surface properties (i.e. surface charge) would serve to reverse the reduction in surface charge that accompanies the surface complexation of anions.

Additionally, it can be observed that during ageing at pH 8, the ageing profiles of experiments with Al³⁺ and Ni²⁺ switch positions, relative to one another, between temperatures of 22 and 40°C. The reason for this is not certain, but it is likely related to the thermodynamics of surface complexation of arsenic on aluminium, and the role of nickel on the coprecipitates. Most interestingly, this switch only occurs during ageing at pH 8 (i.e. it was not observed during “drift ageing” – see next section – but in this case the presence of nickel leads to significantly lower pH than aluminium).

At this point, it is interesting to link the removal/retention of arsenic to that of nickel. In an industrial process, both elements must be removed to concentrations below the regulatory levels (currently 0.5 mg/L) as required by the Metal Mining Effluent Regulations [Fisheries Act, 2002]. The behavior of nickel during ageing is exemplified in the data of Figure 20 at 22°C (the data for other temperatures are provided in Figure 23 in Section 4.2.3). As can be seen, while arsenic is released from the original coprecipitates, nickel is slowly removed from solution, reaching steady (“equilibrium”) values of approximately 0.4 mg/L arsenic and 1.0 mg/L nickel. The terminal stable concentration of arsenic and nickel for ageing at other temperatures are summarized in Table 13. As can be seen, the concentration of nickel is reduced with increased

temperature, which is opposite to that of arsenic. This implies that nickel uptake is an endothermic process, which is common behavior for the surface complexation of cations [Machesky, 1990]. The slow rate of nickel uptake by the coprecipitates however, may reflect structural incorporation (including surface precipitation) following the initial step of surface complexation.

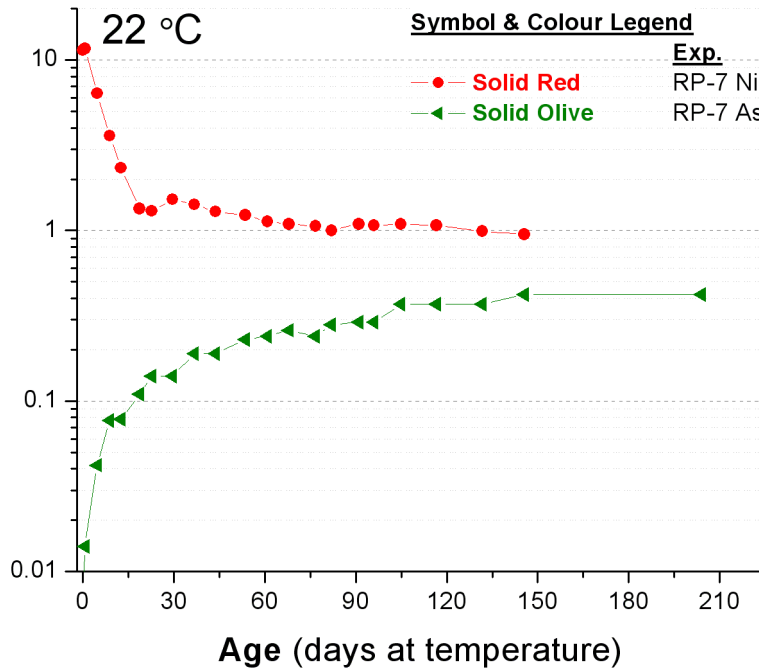


Figure 20 Arsenic retention differences resulting from the type of base (pH 8, 22°C)

Table 13 Summary of equilibrium stability concentration data observed during ageing of coprecipitates (pH 8)

Temperature (°C)	Concentration (mg/L)	
	Arsenic	Nickel
3	---	3.0
22	0.4	1.0
40	1.2	0.4
70	3.5	0.2

4.2 Ageing without pH Control: “Drift”

The second ageing treatment applied to the coprecipitates involved equilibration without pH adjustment. Since this technique was a late development, it was not applied to coprecipitates at all temperatures. Its value was quickly realized, and the technique was applied to the coprecipitates on a reduced sampling frequency. The results of this ageing treatment are shown in Figure 21.

The results show consistency in their trends (between temperature) and indicate that the initial arsenic release rates and “equilibrium” stability can be affected by the manner in which the coprecipitates were produced. The arsenic retention trend follows the order: 1 stage < 3 stage < 2 stage \approx 2 stage with recycle. Interestingly, the trends were identical to those of ageing with pH control (pH 8), shown in Figure 18, however the initial rates and “equilibrium” stability concentrations observed were lower, which were most likely the result of the lower pH values obtained during “drift” ageing.

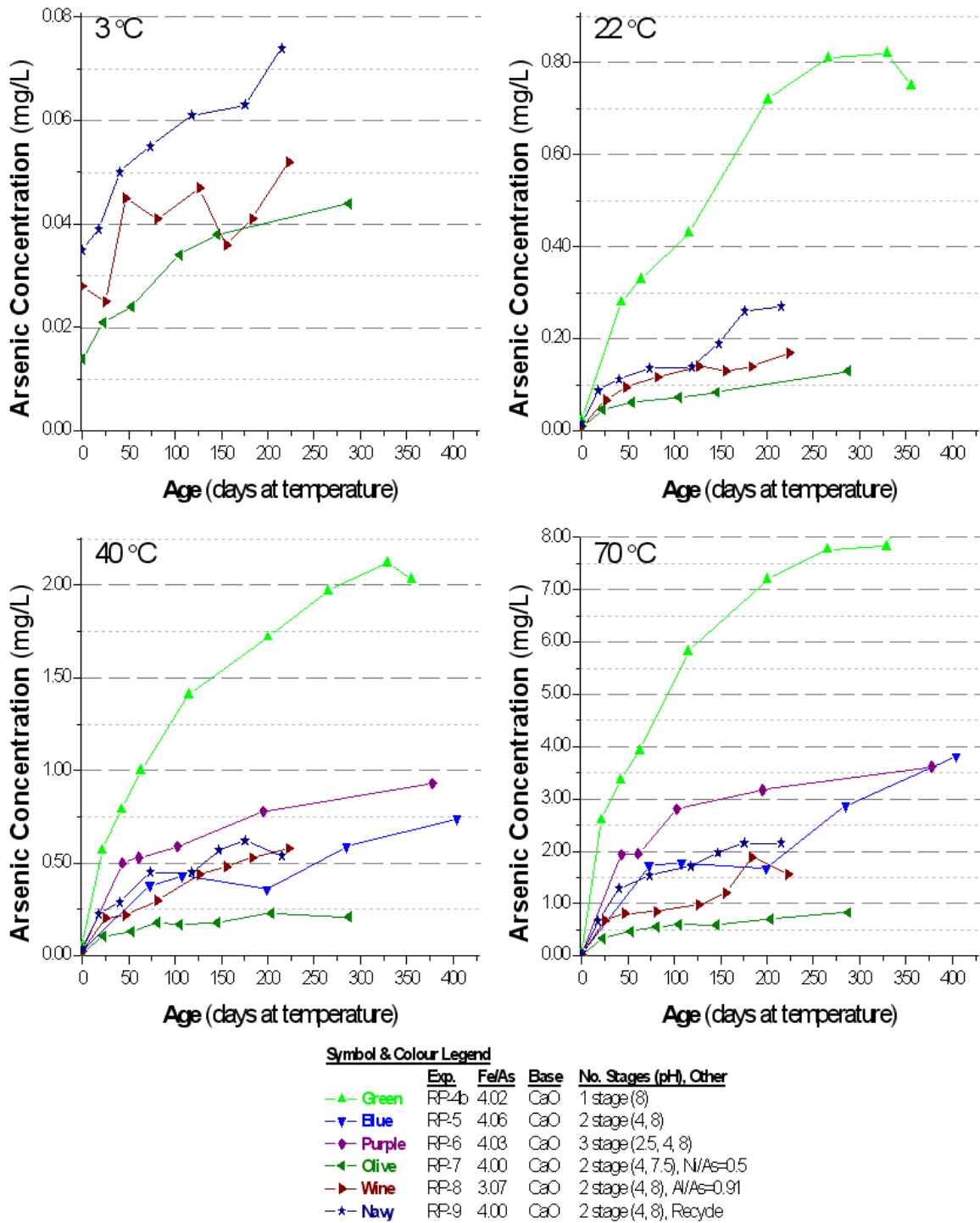


Figure 21 Coprecipitate arsenic retention during ageing (pH unadjusted and temperatures of 3, 22, 40 & 70 °C)

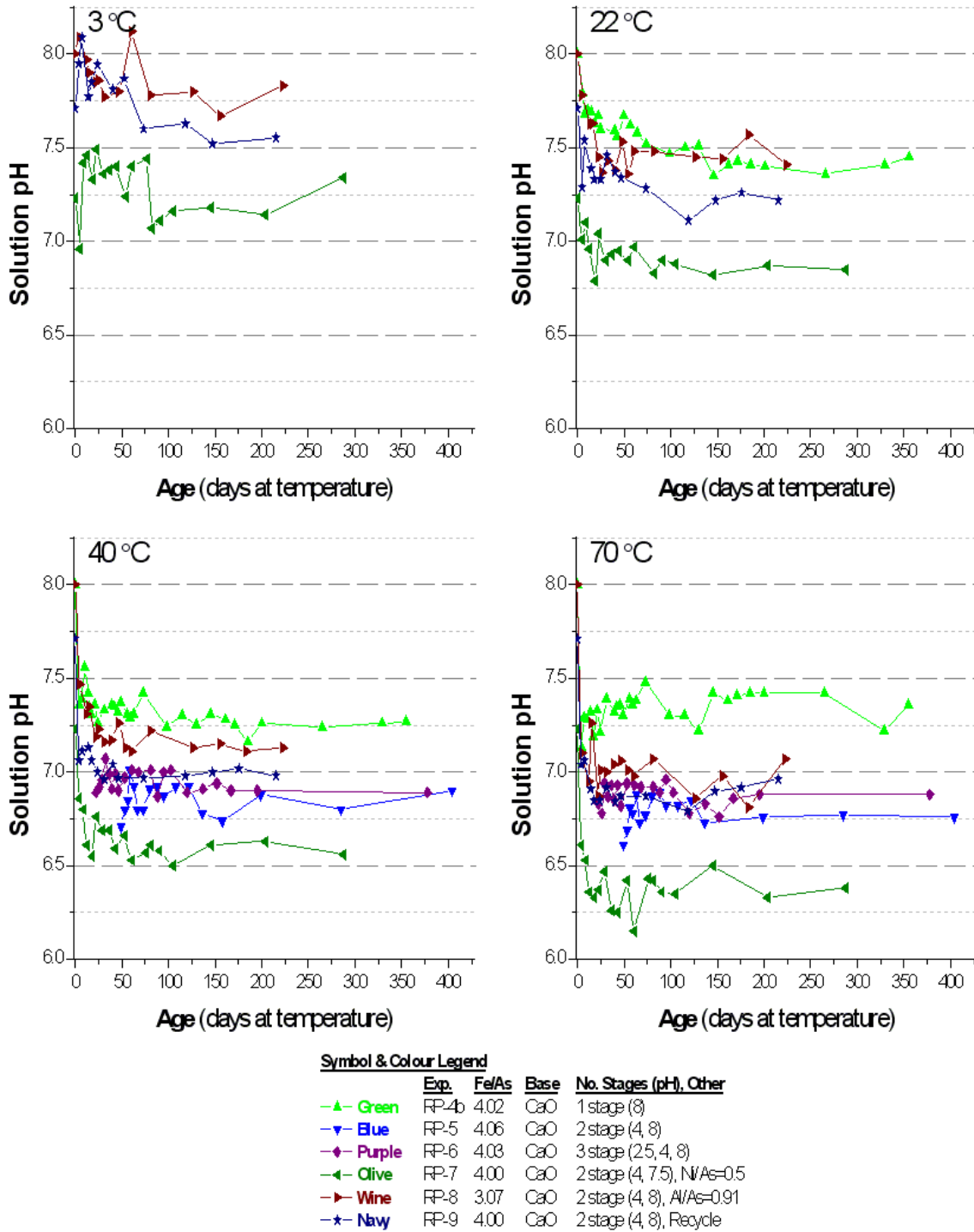


Figure 22 Solution pH during coprecipitate ageing (pH unadjusted and temperatures of 3, 22, 40 & 70 °C)

It is worthy to comment on the observed pH evolution with time for the coprecipitates produced under different conditions, as shown in Figure 22. It can be seen

that the single-stage coprecipitates exhibit the least pH drop while those produced by a two-stage circuit with nickel present, exhibit the highest pH drop. As already discussed, single-stage coprecipitation appears to favor the partitioning of arsenic to adsorption onto ferrihydrite as opposed to ferric arsenate. Hence the difference in pH change may be a reflection of the difference in the solid | liquid interface reactivity (pH_{PZC}) associated with the two arsenic-bearing phases of FA and FH. The effect of nickel in the coprecipitates, which caused a significant decrease on the observed pH_{PZC} , is unclear.

It is also interesting to observe that the coprecipitates containing aluminium consistently exhibited higher pH_{PZC} values than those of aluminium-free coprecipitates. This is likely the result of the contribution of aluminium phases to the “bulk” point of zero charge (as aluminium is also an amphoteric material and is capable of buffering solution pH to the PZC in the same manner as other solids such as ferrihydrite).

While the results of this type of ageing are perhaps more complex, they are more representative of tailings management facility conditions. Unfortunately, the nature of the ageing process does not allow one to de-couple the effect of pH on arsenic retention, as can be done with the results of constant pH ageing. As a result, lower equilibrium concentrations were (at least in part) the result of the lower pH values encountered during this type of ageing. However, there is a distinct advantage when it comes to consideration of the role that concentration gradients may have on the coprecipitates during long term ageing (i.e. the periodic addition of base is not necessary and does not contribute to increasing arsenic concentrations, introduced in Section 2.1).

The results of drift ageing also indicate that the presence of additional cations can affect the release rates and “equilibrium” stability. The trends are identical to those of ageing with pH control: a) substitution of Al^{3+} for Fe^{3+} provides improved retention over coprecipitates produced under comparable conditions; b) Ni^{2+} provides a more significant improvement to arsenic retention.

4.2.1 Effect of Circuit Design on Equilibrium pH

In addition to the preliminary discussion offered on the observed pH evolution during the “drift” ageing tests, further analysis of the behavior is presented through the use of surface chemistry concepts.

As was found (Figure 22), each coprecipitate reached a different “equilibrium” pH value. Further investigation revealed that this pH value corresponded to the PZC of the “bulk” mixture. Research in the field of colloid chemistry has indicated that the “bulk PZC” exhibited by a mixture of phases can be related to its composition [De Faria & Trasatti, 2003]. Assuming the coprecipitates represent a physical mixture of phases, the PZC can be given by a balance of surface charges, weighted according to the surface area fraction of each phase, given by:

$$0 = \sum Y_i \Psi_{o,i} \quad 4.1$$

where Y_i is the fraction of surface area which belongs to phase i
 $\Psi_{o,i}$ is the surface charge of phase i , at the equilibrium pH

For a two component mixture of FA and FH, this equation takes the form:

$$0 = Y_{FA} \Psi_{o,FA} + (1 - Y_{FA}) \Psi_{o,FH} \quad 4.2$$

Correcting for the temperature effect on the surface potential (Ψ_o) with the aid of the Nerstian equation (eqn 1.1) presented in Section 1.1. Rearranging, gives the surface area fraction of FA (Y_{FA}) as:

$$Y_{FA} = \frac{\text{pH}_{\text{PZC,FH}} - \text{pH}}{\text{pH}_{\text{PZC,FH}} - \text{pH}_{\text{PZC,FA}}} \quad 4.3$$

Using this equation, estimates of the surface area fraction of FA were produced from the equilibrium pH values for each temperature during drift ageing. The average and standard deviation were computed and the results are shown in Table 14.

**Table 14 Calculated FA content of coprecipitates
(assuming $pH_{PZC,FA}=3.5$, $pH_{PZC,FH}=8$)**

Conditions	Equilibrium pH			FA Content (as % surface area)
	22°C	40°C	70°C	
1 stage	7.36	7.24	7.42	14.7 ± 2.0%
2 stage	-	6.80	6.77	27.0 ± 0.5%
3 stage	-	6.90	6.88	24.7 ± 0.3%
2 stage w/ recycle	7.22	7.00	6.90	21.3 ± 3.6%

The calculated results indicate that the surface area fraction of FA produced under the conditions investigated varies between approximately 14% and 27%. When coupled with the arsenic retention data (either pH 8 or drift), the results provide a strong indication that the ability of the coprecipitate to retain arsenic is dependent upon the arsenic partitioning between FA and FH. When more FA is produced during the coprecipitation process, the arsenic retention capacity of the coprecipitate (during ageing) improves. In addition, the results also provide indication of the conditions which produce the largest fraction of FA, namely two-stage coprecipitation.

The only anomaly in the results is that of two-stage with recycle, wherein the surface area fraction of FA is reduced. The reason for this is not clear; however it may be possible that due to recycling, the FA particles have had the opportunity to grow, which could have provided an equal FA partitioning but lower surface area. The lower arsenic concentration of the two-stage with recycle experiment may also be an indicator of particle growth as a consequence of the Gibbs-Thompson effect (or Kelvin effect) outlined in Section 1.2.5. Alternatively it is possible that some of the FA was “encapsulated” by gypsum during solids recycling, a phenomenon indicated through SEM imaging (Section 3.4.6).

While the physical mixture assumption may over-simplify the system, it provides an illustrative interpretation to the differences between the coprecipitates. In addition, the PZC results indicate that the improved arsenic retention is not a result of “smaller” FH crystals that might provide larger surface area for adsorption. If this were the case, the PZC values would not decrease with improved stability, but would shift in the opposite direction.

In regards to gypsum, it is likely that it behaves as a salt (i.e. it is not composed of hydronium or hydroxide species), and so its PZC is not dependent on pH but on the concentration of calcium and sulphate (i.e. PZC occurs when $[Ca^{2+}] = [SO_4^{-2}]$). As a result, it should be safe to assume that the surface potential of gypsum is negligible, or at the very least, that it affects each coprecipitate equally.

4.2.2 Effect of Aluminium

The second observation which can be made involves a comparison between the equilibrium pH values of ageing with the substitution of Al^{3+} for Fe^{3+} . For example, at 22°C the drift ageing pH of coprecipitates from a two-stage with recycle circuit was at 7.22, while the pH for two-stage with Al^{3+} was at pH 7.44. The effect of the Al^{3+} on the bulk pH_{PZC} can be used to reinforce the arsenic retention mechanism proposed in the earlier section, namely; the presence of a material with a higher PZC and similar surface complexation capabilities should provide improved arsenic retention (of the adsorbed fraction) as a result of more favorable electrostatic interactions between the surface and the arsenate anion.

4.2.3 Effect of Nickel

The third observation brings to attention the nature of retention compromise in industrial conditions. While it is well documented that arsenic retention is markedly improved at lower pH conditions, the use of lower pH conditions is not always possible because of requirements to remove and retain cations in addition to anions. Figure 23 shows the arsenic and nickel retention during ageing of identical coprecipitates under “drift” (equilibrium pH 6.9) and controlled pH conditions (pH 8).

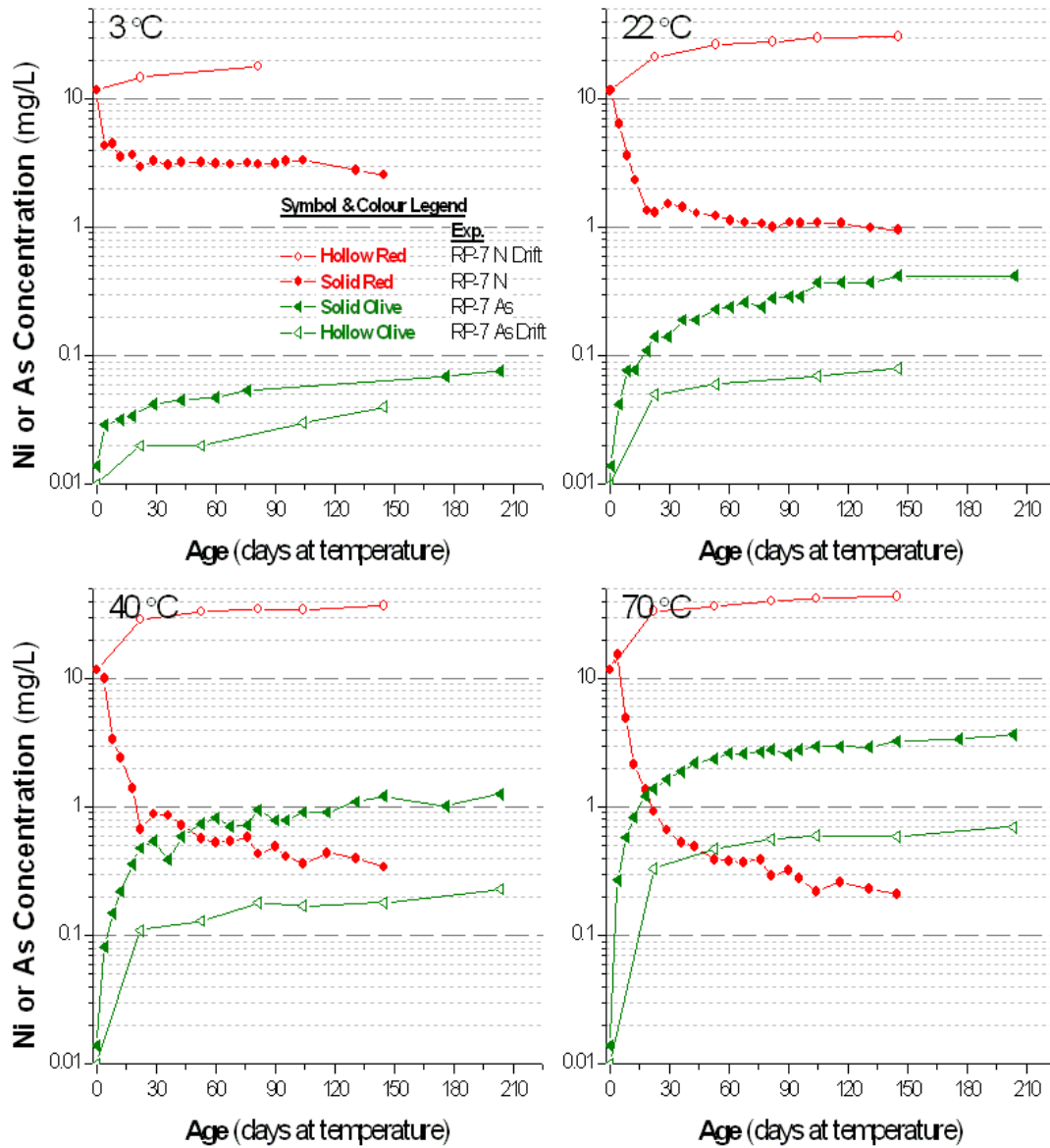


Figure 23 Nickel & arsenic retention during constant pH and drift ageing (pH 8.0 and 7.1 (3°C), 6.9 (22°C), 6.6 (40°C), and 6.4 (70°C) respectively)

The results (at all temperatures) indicated that, although ageing under drift conditions provides lower “equilibrium” arsenic concentrations, nickel concentrations increase and remain at unacceptable levels as compared to falling, during ageing at pH 8.

4.3 Evaluation of Transformation to Crystalline Phases

As the coprecipitation process produces iron oxyhydroxide phases with low crystallinity and small particle size, there is concern that the material will weather in the natural environment and transform into more crystalline phases over time. This process could occur via either dissolution-precipitation or dehydration/internal-rearrangement mechanisms to form goethite or hematite respectively [Cornell & Schwertmann, 2003]. The fate of the arsenic bound to the surface of these particles is a matter of concern, as changes to the surface area and surface properties, as a result of transformation processes, could negatively impact arsenic retention [Ford, 2002, Hohn et al. 2006].

To evaluate the role of transformation on the retention of arsenic in the coprecipitates, Ford [2002] has adapted a procedure to evaluate the transformation of poorly crystalline iron to more crystalline phases, (i.e. time dependant dissolution in weak acid) to interpret its effect on coprecipitated arsenic. The procedure also provides interpretation of the amount of arsenic incorporated into the crystalline solids.

The procedure involved selective extraction of poorly crystalline material and was performed by digesting the solids for 30 minutes at 1 g/L, in 0.4 M HCl. The digestion vessel was a 125 mL HDPE bottle, which was tumbled end-over-end during digestion. After 30 minutes a sample was obtained by filtering the solution through a 0.02 μ m syringe filter. Total digestion of solids was accomplished via hot, strong acid dissolution (75°C, ~20% vol. HCl). The solutions were analysed for Fe, As, Ca and S via ICP-OES and the interpreted results are shown in Figure 24.

Selective extraction via HCl was performed on two-stage coprecipitate solids aged at 70°C for up to 285 days under constant pH conditions (pH 8). It can be seen that the ratio of iron dissolved during selective extraction to total iron decreased only slightly, indicating that the transformation of iron to more crystalline phases occurred only to a minor extent. In addition, the total Fe/As molar ratio increased only slightly above 4 during ageing. This is likely due to the release of arsenic from the solids during ageing, which would affect the ratio remaining in the solids.

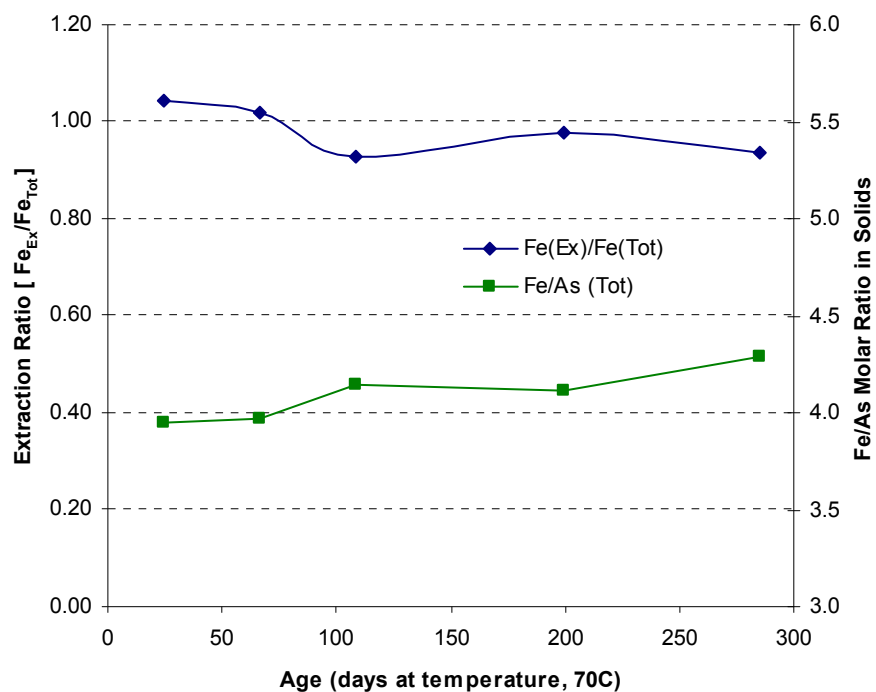


Figure 24 HCl digestion of two-stage coprecipitate solids aged at 70°C, indicating the extent of transformation of iron to crystalline phases

Given the affect of temperature on kinetics, the rate of transformation of iron to more crystalline phases at lower temperatures, under the time investigated, can be expected to be insignificant. The reason for the low transformation rates can be attributed to disruption of the elementary reactions in the overall transformation mechanism (i.e. dissolution, for the formation of goethite), brought about by the presence of adsorbed ions such as multivalent cations (Ca^{2+}) and oxoanions (AsO_4) [Stumm, 1997, Baltpurvins et al. 1997, Jambor & Dutrizac, 1998, Ford, 2002].

4.4 Discussion

Two ageing techniques were applied to the coprecipitates and provided different insights into their behavior during ageing. In both cases, the release of arsenic was accompanied by a reduction in solution pH. The first indicated that if a supply of OH⁻ was made available (to keep the solution at pH 8), the coprecipitates continued to release arsenic at a slow rate until “equilibrium” was attained which was dependent upon the precipitation circuit design. The second ageing technique indicated that without a supply of OH⁻, the solution pH rapidly stabilized to the bulk PZC (related to the composition of the coprecipitates), after which the arsenic release rate was significantly reduced. Here also, the bulk PZC (solution pH), and hence arsenic concentration, was dependant upon the precipitation circuit design.

The variation of equilibria indicated that the coprecipitation circuit design can have a significant affect on the stability of the coprecipitates. The evidence would suggest that this is accomplished via changes in the partitioning of arsenic between FA and FH (i.e. the mechanisms of precipitation and surface complexation).

In addition, the results also indicate that co-ions such as Ca²⁺, Ni²⁺ and Al³⁺, which may be present during coprecipitation, also affect the stability of the coprecipitates. The mechanisms of the interaction have not been confirmed but are likely related to surface properties that are involved in surface complexation.

Finally, it was observed that the slow uptake of nickel occurs during constant pH ageing. The influence of temperature on its uptake indicates an endothermic reaction. It is not clear if the slow uptake is due to structural incorporation or a surface complexation mechanism.

Chapter 5 Modelling of Coprecipitate Ageing

The development of predictive tools is an important final objective for the results of coprecipitate ageing. To be most universal, these models should be based on parameters with physical significance. As a result, the basis of the model was developed using kinetic and thermodynamic relationships and is outlined below. While the data for ageing is not all complete, development of the model was performed using data available at the time of writing.

As a starting point, any reaction is affected by temperature, which is known to influence both the rate, through kinetics, as well as the equilibrium, that is to say thermodynamics. The effect of temperature on kinetics is given by the Arrhenius equation, while the effect of temperature on equilibrium can be given by an integrated form of the van't Hoff equation (assuming constant ΔH).

$$k(T_{eq}) = k(T_1) \exp \left[\frac{E_A}{R} \left(\frac{1}{T_1} - \frac{1}{T_{eq}} \right) \right] \quad 5.1$$

where $k(T)$ is the rate at temperature T

E_A is the activation energy

R is the gas law constant

$$C(T_{eq}) = C(T_1) + \exp \left[\frac{\Delta H}{R} \left(\frac{1}{T_{eq}} - \frac{1}{T_1} \right) \right] \quad 5.2$$

where $C(T)$ is the equilibrium concentration at temperature T

ΔH is the enthalpy of reaction

R is the gas law constant

5.1 Calculation of Kinetic & Thermodynamic Terms

The *apparent* activation energy for the ageing of arsenic bearing coprecipitates was determined via the method of initial rates. The natural logarithm of the initial rate of total arsenic release was plotted versus the inverse temperature, as shown in Figure 25 (log₁₀ y-axis shown). The slope of the line was then evaluated, representing E_A/R . The initial rates as well as the calculated activation energy are provided in Table 15.

Table 15 Initial rate data and calculated apparent activation energy (E_A) for coprecipitate ageing

Exp	Conditions	Initial Rate (mg/L·day)			Activation Energy (E_A) kJ/mol
		22°C	40°C	70°C	
RP-2	1 stage, NaOH, Fe/As=3.4	0.553	2.55	11.50	52.6
RP-4	1 stage, Ca(OH) ₂ , Fe/As=3.4	0.0158	0.0934	0.3348	52.4
RP-4b	1 stage, Ca(OH) ₂	0.0087	0.0436	0.1976	54.1
RP-5	2 stage, Ca(OH) ₂	0.0052	0.0238	0.1052	52.1
RP-6	3 stage, Ca(OH) ₂	0.0078	0.0333	0.1981	55.5
RP-9	2 stage w/ recycle, Ca(OH) ₂	0.0088	0.0316	0.1341	65.0
RP-7	2 stage w/ Ni ²⁺ , Ca(OH) ₂	0.0045	0.0220	0.0630	60.5
RP-8	2 stage w/ Al ³⁺ , Ca(OH) ₂	0.0029	0.0148	0.0759	68.0
Average (kJ/mol)					57.5

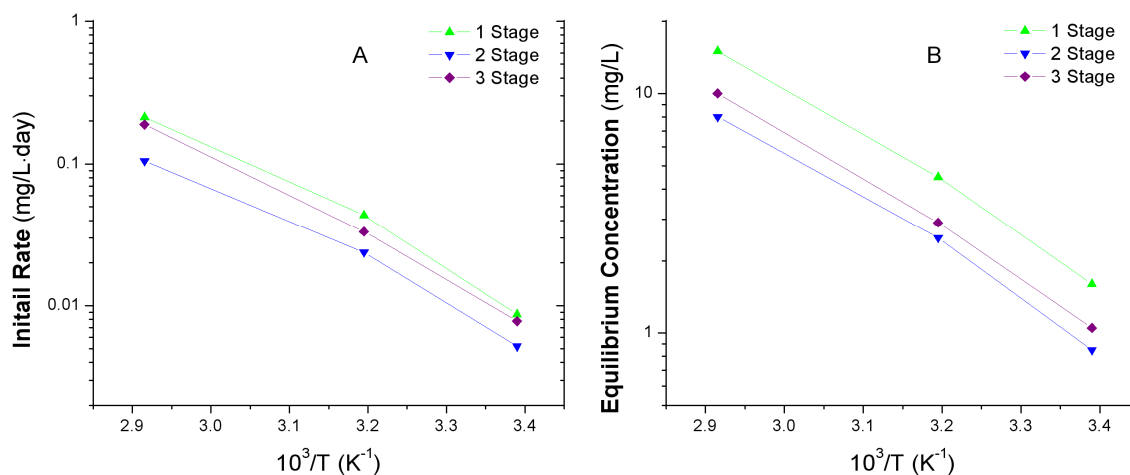


Figure 25 Effect of temperature on A) the initial reaction rate (Arrhenius plot) and B) the “equilibrium” concentration (van’t Hoff plot)

As ageing progressed, the arsenic release behavior exhibited by the coprecipitates appeared to reach stable “equilibrium” arsenic concentration values (refer to Figure 18).

These values are summarized in Table 16, and were used to determine the enthalpy of reaction by plotting the natural logarithm of the equilibrium concentration versus the inverse temperature, as shown in Figure 25 (\log_{10} y-axis shown). The results of such calculations, where “equilibrium” values were available are shown in Table 16.

Table 16 “Equilibrium” concentration data and calculated enthalpy (ΔH) for coprecipitate ageing

Exp	Conditions	Equilibrium Conc. (mg/L)			Enthalpy (ΔH) kJ/mol
		22°C	40°C	70°C	
RP-2	1 stage, NaOH, Fe/As=3.4	(55)	(180)	(500)	-38.1
RP-4	1 stage, Ca(OH) ₂ , Fe/As=3.4	(2)	(7)	(19)	-38.8
RP-4b	1 stage, Ca(OH) ₂	1.6	4.5	15.0	-39.0
RP-5	2 stage, Ca(OH) ₂	0.85	2.5	8.0	-39.0
RP-6	3 stage, Ca(OH) ₂	1.05	2.9	10.0	-39.3
RP-9	2 stage w/ recycle, Ca(OH) ₂	---	---	---	n/a
RP-7	2 stage w/ Ni ²⁺ , Ca(OH) ₂	---	---	---	n/a
RP-8	2 stage w/ Al ³⁺ , Ca(OH) ₂	---	---	---	n/a

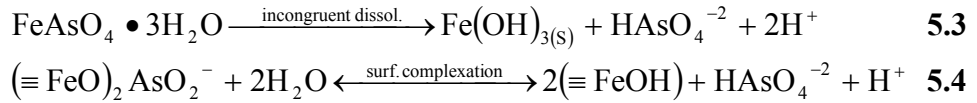
Values in parenthesis were assumed based on near-equilibrium concentrations

A cursory examination of the values of the *apparent* activation energy reveals an average value of 57.5 kJ/mol. Langmuir [1997] indicates reaction mechanisms can be generalized by the magnitude of the activation energy and that dissolution via surface reaction control is usually accompanied by activation energies of 42-84 kJ/mol, while diffusion controlled processes exhibit activation energies in the range of 21-25 kJ/mol. This would indicate that the process controlling arsenic release involves a chemical reaction, as opposed to the physical process of diffusion. Possible reactions include; a) dissolution of FA or, b) desorption of arsenic bound by surface complexation on FH. For comparison purposes, Langmuir et al. [1999] have calculated activation energies for coprecipitate ageing with an average of 56 kJ/mol, while Bluteau and Demopoulos [2007] have determined activation energies ranging from 60 to 100 kJ/mol for the dissolution of crystalline scorodite.

Examination of the enthalpy of reaction (-38.5 kJ/mol) indicates that arsenic release is an exothermic reaction. The consistency in the enthalpy values would suggest that despite the use of different types of base and different precipitation conditions, the same bond(s) were being broken (i.e. the same reaction was controlling arsenic

release/retention). For comparison, Langmuir et al. [1999] have calculated enthalpies for coprecipitate ageing averaging -35.2 ± 6.7 kJ/mol, while Bluteau and Demopoulos [2007] found the enthalpy for the dissolution of crystalline scorodite to be -59 kJ/mol. The magnitude of the calculated values appears to be consistent with the bidentate surface complexation of anions such as phosphate and selenite [Machesky, 1990].

The kinetic and thermodynamic terms calculated in this section, cannot be assigned to a specific reaction. However, there are two reactions that could contribute to the release of arsenic, notably; a) the incongruent dissolution of FA, as well as b) the release of arsenic bound as a bidentate surface complex. For the surface complexation reaction, the aqueous and surface arsenic species are those predicted to dominate at pH 8 [Langmuir et al. 1999, Fukushi & Sverjenski, 2007].



where $\equiv \text{FeO}$ or $\equiv \text{FeOH}$ represents the FH surface

As an analogous material to FA, the enthalpy for the incongruent dissolution of scorodite has been determined to be 59 kJ/mol [Bluteau & Demopoulos, 2007]. If the dissolution of FA has a comparable enthalpy, it would suggest that the dissolved arsenic concentration is not controlled by the incongruent dissolution of FA. Consequently, if more arsenic becomes partitioned as FA, the coprecipitates should exhibit improved arsenic retention characteristics, as observed with coprecipitate ageing (Section 4.1.2), quantified via PZC based calculations (Section 4.2.1) and in accordance with the proposed reaction mechanism (Section 3.2). This conclusion can be used to provide a link between the long-term stability of the coprecipitates and the method of preparation.

5.2 Model Selection

Upon examination of the ageing data, it was recognized that the coprecipitate ageing profiles could be represented reasonably well by a first-order model (for an irreversible reaction), with an equation of the type:

$$X = 1 - \exp(-kt)$$

where $X = \frac{C_{As} - C_{As,0}}{C_{As,EQ}}$

k is the first order model fit parameter

t is the time in days

and where

C_{As} is the concentration of arsenic at time t

$C_{As,0}$ is the initial concentration of arsenic

$C_{As,EQ}$ is the "equilibrium" concentration of arsenic

To evaluate the model parameter k, the equation was rearranged to give

$$\ln(1 - X) = -kt$$

In a plot of $\ln(1-X)$ versus time, the value for the first-order model fit parameter (k) was represented by the slope. The calculated values are provided in Table 17.

Table 17 First-order model fit parameter (k) values

Exp	Conditions	Model Fit Parameter, k (day ⁻¹)			Arrhenius fit slope (kJ/mol)
		22°C	40°C	70°C	
RP-4b	1 stage, Ca(OH) ₂	0.0062	0.0105	0.0180	18.5
RP-5	2 stage, Ca(OH) ₂	0.0066	0.0109	0.0143	13.2
RP-6	3 stage, Ca(OH) ₂	0.0078	0.0174	0.0246	19.4

By attempting to correlate the model fit parameter to the inverse temperature, as with an Arrhenius type equation, the value of the slope was significantly different from the values of activation energy obtained in the previous section. There are two possible explanations for this behavior: a) multiple reactions (arising from different phases) contribute to arsenic release and the dominant mechanism may shift during ageing or b) a

single reversible reaction is primarily responsible for arsenic release, where the reverse reaction can have a significant affect near equilibrium. In addition, the variability of both the Arrhenius fit slope, as well as the fit parameter values between experiments, prevent generalization for the purposes of prediction. As a result, the use of a single, first-order irreversible model oversimplifies the system.

From a predictive perspective, the later time period, approaching “equilibrium” is of particular interest. Here the first-order model should be used as a responsive approximation tool only and not as a true predictive model. A measure of the adequacy of the first-order model can be seen with the aid of the plots presented in Figure 26. For the model fits, the “equilibrium” arsenic concentrations were predicted using the reaction enthalpy estimated in the previous section.

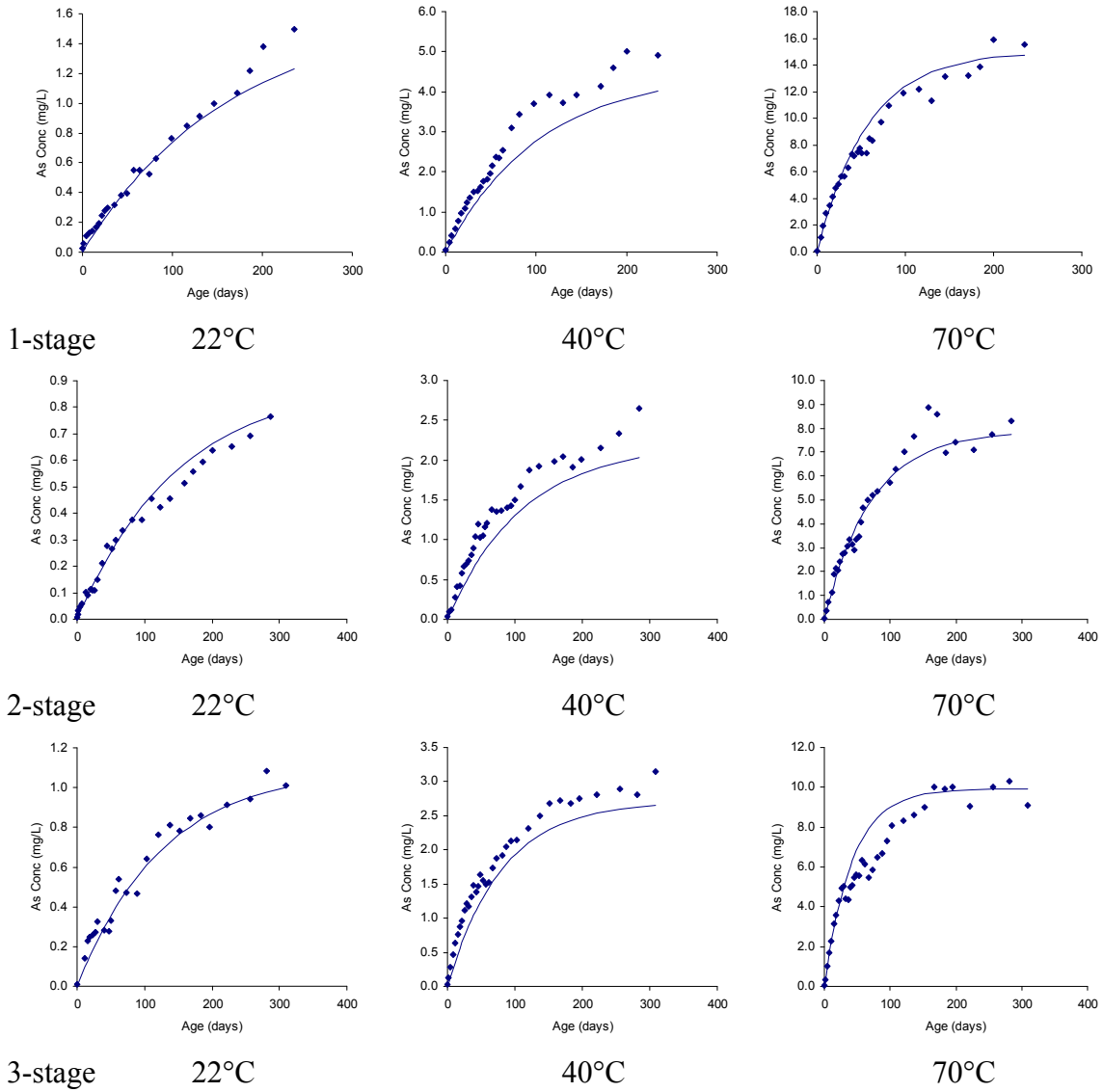


Figure 26 First-order model fits to the results of coprecipitate ageing (1- 2- and 3-stage respectively)

5.3 Discussion

Evaluation of the kinetics and “equilibrium” of coprecipitate ageing at pH 8 was performed in an effort to develop predictive tools for ageing of the coprecipitates. The reaction kinetics appeared to be variable between coprecipitates, with no clear dependency on the method of production or the co-ions present in the coprecipitates. The magnitude of the activation energy would suggest a reaction controlled dissolution mechanism.

Evaluation of the reaction thermodynamics indicated that the “equilibrium” shared the same dependency upon temperature indicating that, for all coprecipitates, the same reaction controls the retention/release of arsenic. Comparison of the calculated enthalpy indicated the controlling reaction may be consistent with a bidentate surface complexation reaction. The variability of the “equilibrium” arsenic concentration between different coprecipitates reduces the possibility that the arsenic release was controlled by a mineral solubility reaction.

The estimated reaction enthalpy may be used to predict the arsenic retention (at pH 8) for any coprecipitate, provided that the “equilibrium” is known for at least one temperature. Attempts to predict the arsenic concentration prior to “equilibrium” with a first-order model of the reaction kinetics proved only partially successful.

Chapter 6 Global Conclusions

This research, which has been aimed at understanding the link between the stability of arsenic bearing coprecipitates and the method by which they were produced, has demonstrated that the coprecipitation process is complex. Evidence indicates that the process (at high arsenic concentrations) must involve at least two mechanisms: precipitation of ferric arsenate, as well as surface complexation of arsenic onto iron(III) oxyhydroxides. While the removal of arsenic is not significantly affected by the relative contribution of the two mechanisms to the overall process, the stability of the coprecipitates is dependent on the partitioning of arsenic between the two phases, which can be affected by the precipitation circuit design.

The process of arsenic removal via coprecipitation, while still not fully understood, has been known to be affected by the Fe/As molar ratio. This work has also confirmed that coprecipitation in synthetic systems can be affected by the co-ions present (or absent) during coprecipitation. In particular, calcium has been demonstrated to have an important role in stabilization of arsenic within the coprecipitates, affecting both the immediate arsenic removal and long-term arsenic retention.

The ageing of synthetic continuous circuit coprecipitates (with adjustment of the pH) has indicated that, while arsenic concentrations in pore water have the tendency to increase during ageing, this behavior eventually approached a steady state (or an “equilibrium”), which was observed to be strongly dependent on the precipitation circuit design. For example, coprecipitates from a two-stage circuit (with or without recycling) proved superior to single-stage circuit coprecipitates, in terms of arsenic retention. This effect was attributed to increased formation of ferric arsenate. In addition, the “equilibrium” observed was also found to be dependent on co-ions present during coprecipitation, for which Ni^{2+} and Al^{3+} are reported, and have beneficial effects on arsenic stability (Fe^{2+} was also tested, but did not improve arsenic retention when used as a substitute for Fe^{3+}). The ageing of coprecipitates without routine adjustment of pH indicated that both the pH and arsenic concentrations stabilized rapidly to values consistent with those observed in industrial tailings management facilities.

The interpretation of rate and “equilibrium” data from ageing coprecipitates (at pH 8) indicated that the reaction(s) that result in the release of arsenic exhibit slow kinetics, consistent with a reaction-controlled dissolution mechanism. In addition, the effect of temperature on “equilibrium” (through enthalpy) indicated that, for all coprecipitates, the same reaction was responsible for the release of arsenic. The magnitude of the enthalpy was consistent with published bidentate surface complexation reactions.

The final objective of this research, the development of predictive tools, goes beyond the scope of this thesis: However, the kinetic and thermodynamic terms obtained by techniques and data described here, will be fundamental to the development of such predictive tools.

6.1 Recommendations for Future Research

There has been an industrial understanding that divalent cations may serve to stabilize arsenic within coprecipitates [Harris & Krause, 1993]. There is also a growing body of evidence from research with synthetic solutions (including the present work), which supports this concept [Emett & Khoe, 1994, Jia & Demopoulos, 2008]. The details and mechanism through which arsenic becomes stabilized are not yet understood. Calculations presented in appendix II indicate that, when Ca^{2+} is present in solution, the predominant species at mildly alkaline conditions changes from a simple arsenic aqueous complex to a Ca-AsO_4 aqueous complex. This behavior also occurs with other divalent metal species including Ni^{2+} and Fe^{2+} . While such thermodynamic based calculations indicate that the aqueous speciation can be changed, it raises questions as to whether the surface speciation could also be changed, with the possible formation of ternary surface complexes involving arsenic and divalent metal species.

The current understanding of arsenic surface complexation is limited to singular metal speciation stemming from the characterization of synthetic systems in background electrolytes of monovalent salts, a condition seldom encountered in industrial or geochemical conditions. There is evidence by Paktunc et al. [2004], which indicates that in tailings containing gypsum, both iron (as ferric oxyhydroxide) and calcium were intimately associated with arsenic. Such data could be interpreted as either 1) a mixture of individual Fe-As and Ca-As complexes, or 2) a ternary surface complex, prior to mineral-like association – as for example a yukonite precursor. Further investigation is encouraged.

A second area for research concerns the role of colloid properties in controlling the aqueous equilibrium observed within tailings disposal facilities. In this research, coprecipitates were subjected to ageing without pH adjustment. The solution pH in each case was found to be controlled by a colloid property known as the point of zero charge (PZC). This concept is novel and relevant to understanding the mechanism(s) which control the pH and hence “equilibrium” conditions observed in sub-aqueous tailings management facilities. This knowledge can be used to converge upon conditions at

which to evaluate the long-term stability of any material under consideration for disposal. Further application of this knowledge to tailings disposal conditions is encouraged.

A third area for future research concerns the effect of redox states on the coprecipitation process. In addition to ferric iron, the presence of ferrous iron is commonly encountered during industrial coprecipitation. While the effect of ferric iron has been well studied, the role of ferrous iron has received little attention and is not clearly understood. Further research is encouraged.

References

- Baltpurvins, K.A.; Burns, R.C.; Lawrance, G.A.; Stuart, A.D., (1997) "Effect of Ca^{2+} , Mg^{2+} and anion type on the ageing of iron(III) hydroxide precipitates," *Environmental Science & Technology*, 31(4), 1024-1032.
- Blesa, M.A.; Matijevic, E., (1989) "Phase transformations of iron oxides, oxohydroxides and hydrous oxides in aqueous media," *Advances in Colloid & Interface Science*, 29(3-4), 173-221.
- Bluteau, M.C.; Demopoulos, G.P., (2007) "The incongruent dissolution of scorodite - solubility, kinetics and mechanism," *Hydrometallurgy*, 87, 163-177.
- Chen, N.; Jiang, D.T.; Cutler, J.; Kotzer, T.; Demopoulos, G.P.; Rowson, J.W., (in review) "Structural characterization of amorphous scorodite, iron(III)-arsenate co-precipitates and uranium mill neutralized raffinate solids using x-ray absorption fine structure spectroscopy," *Geochimica et Cosmochimica Acta*, in review.
- Cornell, R.M.; Schwertmann, U., (2003) The Iron Oxides: Structure, properties reactions occurrences and uses, 2nd Edition, Wiley-VCH Verlag GmbH & Co.
- Cutler, J.N.; Chen, N.; Jiang, D.T.; Demopoulos, G.P.; Jia, Y.; Rowson, J.W., (2003) "The nature of arsenic in uranium mill tailings by x-ray absorption spectroscopy." *J. Phys. IV France*, 107, 337-340.
- Davis, J.A.; Kent, D.B., (1990) "Surface complexation modeling in aqueous geochemistry," *Reviews in Mineralogy (Miner.-Water Interface Geochem.)*, 176-260.
- De Faria, L.A.; Trasatti, S., (2003) "Physical versus chemical mixtures of oxides: the point of zero charge of Ni+Co mixed oxides," *Journal of Electroanalytical Chemistry*, 554-555, 355-359.
- Demopoulos, G.P. (accepted) "Aqueous precipitation and crystallization for the production of particulate solids with desired properties," *Hydrometallurgy*, accepted.
- Demopoulos, G.P.; Zinck, J.M.; Kondos, P.D., (1995) "Production of super dense sludges with a novel neutralization process," In *Waste Processing and Recycling in Mineral and Metallurgical Industries II, Proceedings of the International Symposium on Waste Processing and Recycling in Mineral and Metallurgical Industries*, (Rao, S.R., Amaratunga, L.M., Richards, G.G. and Kondos, P.D. Eds.), CIM, 401-411.
- Donahue, R.; Hendry, M.J.; Landine, P. (2000) "Distribution of arsenic and nickel in uranium mill tailings, Rabbit Lake, Saskatchewan, Canada," *Applied Geochemistry*, 15(8), 1097-1119.
- Emett, M.T.; Khoe, G.H., (1994) "Environmental stability of arsenic bearing hydrous iron oxide," In *EPD Congress 1994*, (Warren, G. Ed.), TMS, 153-166.
- Fisheries Act, (2002) "Metal Mining Effluent Regulations," In *Canada Gazette, Part II*, 136(13), Queen's Printer for Canada.
- Ford, R.G., (2002) "Rates of hydrous ferric oxide crystallization and the influence on coprecipitated arsenate," *Environmental Science & Technology*, 36(11), 2459-2463.
- Fogler, H.S., (1999) Elements of Chemical Reaction Engineering. Prentice Hall, Inc.
- Fourest, B.; Hakem, N.; Guillaumong, R., (1994) "Characterization of colloids by measurement of their mobilities," *Radiochimica Acta*, 66/67, 173-179.

- Fuerstenau, M.C.; Han, K.N., (2003) Principles of Mineral Processing, SME.
- Fukushi, K.; Sverjenski, D.A., (2007) "A predictive model (ETLM) for arsenate adsorption and surface speciation on oxides consistent with spectroscopic and theoretical molecular evidence," *Geochimica et Cosmochimica Acta*, 71, 3717-3745.
- Han, K.N., (2002) Fundamentals of Aqueous Metallurgy. SME.
- Harris, G.B.; Krause, E., (1993) "The disposal of arsenic from metallurgical processes: its status regarding ferric arsenate." In *Extr. Metall. Copper, Nickel Cobalt, Proc. Paul E. Queneau Int. Symp.*, (Reddy, R.G. and Weizenbach, R.N. Eds.), TMS, 1, 1221-1237.
- Harris, B., (2003) "The removal of arsenic from process solutions: Theory and industrial practice," In *Hydrometallurgy 2003*, (Young, C.A., Alfantazi, A.M., Anderson, C.G., Dreisinger, D.B., Harris, B. and James, A. Eds.), TMS, 1889-1902.
- Harris, G. B.; Monette, S., (1988) "The stability of arsenic-bearing residues," In *Arsenic Metallurgy: Fundamentals & Applications*, (Reddy, R.G.; Hendrix, J.L.; Queneau, P.B., Eds.), TMS, 469-488.
- Harris, G. B.; Monette, S. (1989) "The disposal of arsenical solid residues," In *Productivity and Technology in the Metallurgical Industries*, (Koch, M., Taylor, J.C. Eds.), TMS, 545-559.
- Hohn, J.; Twidwell, R.; Robins, R.G., (2006) "A comparison of ferrihydrite and aluminum-modified ferrihydrite for the removal of arsenate from aqueous solution by co-precipitation," In *Iron Control in Hydrometallurgy*, (Dutrizac, J.E. Ed.), CIM, 911-926.
- Jambor, J.L.; Dutrizac, J.E., (1998) "Occurrence and constitution of natural and synthetic ferrihydrite, a widespread iron oxyhydroxide," *Chemical Reviews*, 98(7), 2549-2585.
- James, R.O.; Parks, G.A., (1982) "Characterization of aqueous colloids by their electrical double-layer and intrinsic surface chemical properties," In Surface and Colloid Science. (Matijevic, E., Ed.), Plenum Press, 12, 119-216.
- Jia, Y.F.; Demopoulos, G.P., (2008) "Coprecipitation of arsenate with iron(III) in aqueous sulfate media: Effect of time, lime as base and co-ions on arsenic retention," *Water Research*, 42(3), 661-668.
- Jia, Y.; Xu, L.; Wang, X.; Demopoulos, G.P., (2007) "Infrared spectroscopic and X-ray diffraction characterization of the nature of adsorbed arsenate on ferrihydrite," *Geochimica et Cosmochimica Acta*, 71(7), 1643-1654.
- Jia, Y.F.; Xu, L.; Fang, Z.; Demopoulos, G.P., (2006) "Observation of surface precipitation of arsenate on ferrihydrite," *Environmental Science & Technology*, 40(10), 3248-3253.
- Jia, Y.F.; Demopoulos, G.P.; Chen, N.; Cutler, J., (2005) "Coprecipitation of As(V) with Fe(III) in sulfate media: solubility and speciation of arsenic," In *Arsenic Metallurgy*, (Reddy, R.G.; Ramachandran, V., Eds.), TMS, 137-148.
- Jia, Y.F.; Demopoulos, G.P., (2005) "Adsorption of arsenate onto ferrihydrite from aqueous solution: Influence of media (sulfate vs. nitrate), added gypsum, and pH alteration," *Environmental Science & Technology*, 39, 9523-9527.
- Jia, Y.F.; Demopoulos, G.P.; Chen, N.; Cutler, J.N.; Jiang, D.-T., (2003) "Preparation, characterization and solubilities of adsorbed and co-precipitated iron (III)-arsenate solids," In *Hydrometallurgy 2003 Volume 2: Electrometallurgy and Environmental Hydrometallurgy*, (Young, C.A.; Alfantazi, A.M.; Anderson, C.G.; Dreisinger, D.B.; Harris, B.; James, A., Eds.), TMS, 1923-1935.

- Kosmulski, M.; (2001) Chemical Properties of Material Surfaces. Marcel Dekker, Inc.
- Krause, E.; Ettl, V.A., (1989) "Solubilities and stabilities of ferric arsenate compounds," *Hydrometallurgy*, 22, 311-337.
- Langmuir, D.; Mahoney, J.; Rowson, J., (2006) "Solubility products of amorphous ferric arsenate and crystalline scorodite ($\text{FeAsO}_4 \cdot 2\text{H}_2\text{O}$) and their application to arsenic behavior in buried mine tailings," *Geochimica et Cosmochimica Acta*, 70(12), 2942-2956.
- Langmuir, D., (1997) Aqueous Environmental Geochemistry. Prentice Hall, Inc.
- Langmuir, D.; Mahoney, J.; MacDonald, A.; Rowson J., (1999) "Predicting arsenic concentrations in the porewaters of buried uranium mill tailings," *Geochimica et Cosmochimica Acta*, 63(19-20), 3379-3394.
- Le Berre, J.F.; Cheng, T.C.; Gauvin, R.; Demopoulos, G.P., (2007a) "Hydrothermal synthesis and stability evaluation of mansfieldite in comparison to scorodite," *Canadian Metallurgical Quarterly*, 46(1), 1-10.
- Le Berre, J.F.; Cheng, T.C.; Gauvin, R.; Demopoulos, G.P., (2007b) "Hydrothermal synthesis and stability evaluation of iron(III)-aluminium(III) arsenate solid solutions," *Metallurgical and Materials Transactions B: Process metallurgy and Materials Processing Science*, 38B(2), 159-166.
- Le Berre, J.F.; Gauvin, R.; Demopoulos, G.P., (2007c) "Characterization of poorly-crystalline ferric arsenate precipitated from equimolar Fe(III)-As(V) solutions in the pH range 2 to 8," *Metallurgical and Materials Transactions B: Process metallurgy and Materials Processing Science*, 38B(5), 751-762.
- Lyklema, J.; (1987) "Electrical double layers on oxides: Disparate observations and unifying principles." *Chemistry & Industry*, 21, 741-747.
- Machesky, M.L., (1990) "Influence of temperature on ion adsorption by hydrous metal oxides," In *Chemical Modeling of Aqueous Systems II*, (Melchior, D.C. and Bassett, R.L., Eds.), ACS Symposium Series, 282-292.
- Mahoney, J.; Langmuir, D.; Gosselin, N.; Rowson, J., (2005) "Arsenic readily released to pore waters from buried mill tailings," *Applied Geochemistry*, 20(5), 947-959.
- Moldovan, B. J.; Hendry, M. J., (2005) "Characterizing and quantifying controls on arsenic solubility over a pH range of 1-11 in a uranium mill-scale experiment," *Environmental Science & Technology*, 39(13), 4913-4920.
- Moldovan, B.J.; Jiang, D.T.; Hendry, M.J., (2003) "Mineralogical characterization of arsenic in uranium mine tailings precipitated from iron-rich hydrometallurgical solutions," *Environ. Sci. Technol.*, 37(5), 873-879.
- Milonjić, S.K.; Ruvarac, A.L., (1975) "The heat of immersion of natural magnetite in aqueous solutions." *Thermochimica Acta*, 11, 261-266.
- Myerson, A.S., (2002) Handbook of Industrial Crystallization, 2nd Edition. Butterworth Heinemann.
- Myneni, S.C.B.; Traina, S.J.; Waychunas, G.A.; Logan, T.J., (1998) "Experimental and theoretical vibrational spectroscopic evaluation of arsenate coordination in aqueous solutions, solids and at mineral-water interfaces," *Geochimica et Cosmochimica Acta*, 62(19/20), 3285-3300.

- Nakamoto, K., (1986) Infrared and Raman Spectra of Inorganic and Coordination Compounds, 5th Edition. Wiley.
- Paktunc, D., Dutrizac, J., Gertsman, V., (2008) "Synthesis and phase transformations involving scorodite, ferric arsenate and arsenical ferrihydrite: Implications for arsenic mobility," *Geochimica et Cosmochimica Acta*, 72(11), 2649-2672.
- Paktunc, D.; Foster, A.; Heald, S.; Laflamme, G., (2004) "Speciation and characterization of arsenic in gold ores and cyanidation tailings using X-ray absorption spectroscopy," *Geochimica et Cosmochimica Acta*, 68(5), 969-983.
- Paktunc, D.; Foster, A.; Laflamme, G., (2003) "Speciation and characterization of arsenic in Ketzka River mine tailings using X-ray absorption spectroscopy," *Environmental Science and Technology*, 37(10), 2067-2074.
- Parkhurst, D.L., Appelo, C.A.J., (1999) "User's guide to PHREEQC (Version 2), A computer program for speciation, batchreaction, one-dimensional transport, and inverse geochemical calculation," U.S. Geol. Surv. Water-Resour. Invest. Rep., 99-4259.
- Parks, G.A.; De Bruyn, P.L., (1962) "Zero point of charge of oxides," *Journal of Physical Chemistry*, 66, 967-973.
- Parks, G.A., (1990) "Surface energy and adsorption at mineral-water interfaces: An introduction," In Reviews in Mineralogy: Vol 23. Mineral-Water Interface Geochemistry, (Hochella, M.F. and White, A.F., Eds.), Mineralogical Society of America, 133-175.
- Parks, G.A., (1965) "The isoelectric points of solid oxides, solid hydroxides and aqueous hydroxo complex systems," *Chemical Reviews*, 65(2), 177-98.
- Perry, R.H.; Green, D.W.; (1999) Perry's Chemical Engineers Handbook: 7th Edition. McGraw-Hill.
- Pichler, T.; Hendry, M.J.; Hall, G.E.M., (2001) "The mineralogy of arsenic in uranium mine tailings at the Rabbit Lake In-pit Facility, northern Saskatchewan, Canada," *Environmental Geology*, 40(4-5), 495-506.
- Robins, R.G.; Singh, P.; Das, R.P., (2005) "Coprecipitation of arsenic with Fe(III), Al(III) and mixtures of both in a chloride system," In *Arsenic Metallurgy*, (Reddy, R.G.; Ramachandran, V., Eds.), TMS, 113-128.
- Robins, R.G.; Huang, J.C.Y.; Nishimura, T.; Khoe, G.H., (1988) "The adsorption of arsenate ion by ferric hydroxide," In *Arsenic Metallurgy: Fundamentals and Applications*, (Reddy, R.G.; Hendrix, J.L.; Queneau, P.B., Eds.), TMS, 99-112.
- Schindler, P.W., (1990) "Co-adsorption of metal ions and organic ligands: Formation of ternary surface complexes," In Reviews in Mineralogy: Vol 23. Mineral-Water Interface Geochemistry, (Hochella, M.F. and White, A.F., Eds.), Mineralogical Society of America, 281-305.
- Schwartz, A.M.; Myerson, A.S., (2002) "Solutions and solution properties," In Handbook of Industrial Crystallization, 2nd Edition (Myerson, A.S., Ed.) Butterworth Heinemann, 1-30.
- Stumm, W., (1997) "Reactivity at the mineral-water interface: dissolution and inhibition," *Colloids & Surfaces A: Physicochemical and Engineering Aspects*, (1997), 120, 143-166.
- Söhnel, O.; Garside, J., (1992) Precipitation: Basic principles and industrial applications, Butterworth-Heinemann Ltd.

- Swedlund, P. J.; Webster, J. G. (2001) "Cu and Zn ternary surface complex formation with SO₄ on ferrihydrite and schwertmannite," *Applied Geochemistry*, 16(5), 503-511.
- Twidwell, L.G.; Robins, R.G.; Hohn, J.W., (2005) "The removal of arsenic from aqueous solution by coprecipitation with iron(III)," In *Arsenic Metallurgy*, (R.G. Reddy and V. Ramachandran, Eds.), TMS, 3-24.
- Verbaan, C.M.; Omelon, S.J.; Demopoulos, G.P., (1999) "The effect of staging and seeding/recycling on the density and cleanliness of gypsum produced in simulated zinc plant wastewater treatment circuits," In *Solid/Liquid Separation Including Hydrometallurgy and the Environment*, (Harris, G.B.; Omelon, S.J., Eds.), CIM, 251-264.
- Wey, J.S.; Karpinski, P.H.; (2002) "Batch crystallization," In Handbook of Industrial Crystallization, 2nd Edition (Myerson, A.S., Ed.), Butterworth Heinemann, 231-248.
- Wilkie, J.A.; Hering, J.G., (1996) "Adsorption of arsenic onto hydrous ferric oxide: effects of adsorbate/adsorbent ratios and co-occurring solutes," *Colloids and Surfaces, A: Physicochemical and Engineering Aspects*, 107, 97-110.
- Yuan, T.C.; Jia, Y.F.; Demopoulos, G.P., (2005) "Synthesis and solubility of crystalline annabergite (Ni₃(AsO₄)₂·8H₂O)," *Canadian Metallurgical Quarterly*, 44(4), 449-456.

Appendix I Effect of Ionic Strength (on As retention)

Ionic strength is known to affect the electrical double layer (i.e. the solid | liquid interface, discussed in Section 1.1). Since the use of $\text{Ca}(\text{OH})_2$ for coprecipitation results in the formation of gypsum and causes a reduction of the ionic strength, it remains possible that the improved stability of $\text{Ca}(\text{OH})_2$ versus NaOH could be due to ionic strength effects. The use of different reagents, as well as background electrolyte concentrations by other researchers, has resulted in variations in the ionic strength of published coprecipitation work (Section 1.4).

Table I-1 summarizes the estimated residual ionic strength after coprecipitation of “identical” solutions made using different reagents and coprecipitated with either NaOH or $\text{Ca}(\text{OH})_2$. The estimated values indicate a difference in the ionic strength, as a result of the ions remaining in solution, which ranges from 0.4 to 0.76.

Table I-1 Estimated ionic strength after coprecipitation (1400mg/L As, Fe/As=4, sulphate media)

Arsenic Reagent	As_2O_5		Na_2HAsO_4	
	NaOH	$\text{Ca}(\text{OH})_2$	NaOH	$\text{Ca}(\text{OH})_2$
Ionic Strength	0.70	0.40	0.76	0.46

To evaluate the role of ionic strength, batch coprecipitation and ageing was performed with $\text{Ca}(\text{OH})_2$ and a background electrolyte (NaNO_3), in varying concentrations. The results of coprecipitation and ageing are shown in Figure I-1, which indicates that, while ionic strength does affect the arsenic retention behavior during ageing, it does not fully explain the observed stability associated with the presence of calcium. Hence, it becomes apparent that there is a specific interaction between calcium and the arsenic bearing solids (i.e. FA and FH). It is likely that this interaction occurs between calcium and the ferric arsenate surface, which has a low PZC (pH 3.5) and would have a significant negative surface charge at the ageing conditions of pH 8.

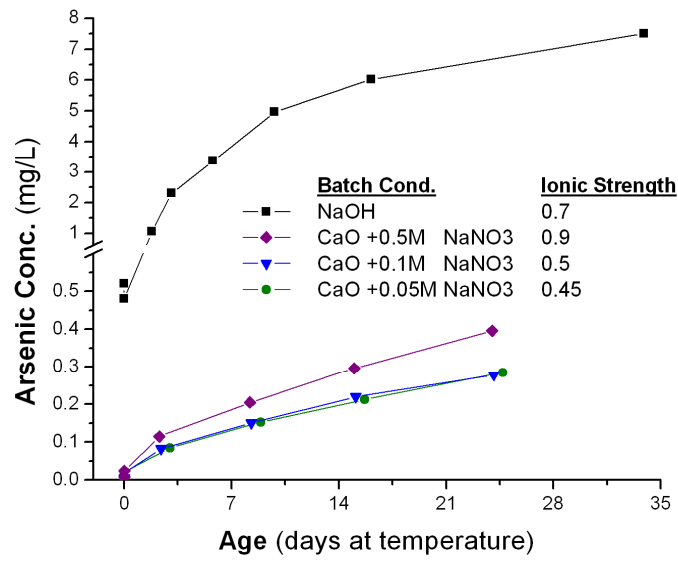


Figure I-1 Effect of ionic strength on arsenic coprecipitation and ageing behavior

Appendix II Equilibrium Constants (As Speciation)

The following table presents the equilibrium constants used to construct the theoretical speciation and solubility plots for FH and FA* (with and without the presence of Ca²⁺, at gypsum saturation) of figures II-1 and II-2 as well as those of Section 3.2.1.

Table II-1 Equilibrium constants used for calculation of

Aqueous Species	Reaction	Equilibrium Constant log K	Ref.
As(V)			
H ₃ AsO ₄	H ₃ AsO ₄ = H ₃ AsO ₄	0	
H ₂ AsO ₄ ⁻	H ₃ AsO ₄ = H ₂ AsO ₄ ⁻ + H ⁺	-2.24	Langmuir
HAsO ₄ ⁻²	H ₃ AsO ₄ = HAsO ₄ ⁻² + 2H ⁺	-9.20	Langmuir
AsO ₄ ⁻³	H ₃ AsO ₄ = AsO ₄ ⁻³ + 3H ⁺	-20.70	Langmuir
Fe(III)			
Fe ⁺³	Fe ⁺³ = Fe ⁺³	0	
FeOH ⁺²	Fe ⁺³ + H ₂ O = FeOH ⁺² + H ⁺	-2.19	Parkhurst
Fe(OH) ₂ ⁺	Fe ⁺³ + 2H ₂ O = Fe(OH) ₂ ⁺ + 2H ⁺	-5.67	Parkhurst
Fe(OH) ₃	Fe ⁺³ + 3H ₂ O = Fe(OH) ₃ + 3H ⁺	-12.56	Parkhurst
Fe(OH) ₄ ⁻	Fe ⁺³ + 4H ₂ O = Fe(OH) ₄ ⁻ + 4H ⁺	-21.6	Parkhurst
Fe ₂ (OH) ₂ ⁺⁴	2Fe ⁺³ + 2H ₂ O = Fe ₂ (OH) ₂ ⁺⁴ + 2H ⁺	-2.95	Parkhurst
Fe ₃ (OH) ₄ ⁺⁵	3Fe ⁺³ + 4H ₂ O = Fe ₃ (OH) ₄ ⁺⁵ + 4H ⁺	-6.3	Parkhurst
Fe(III)-As(V)			
FeH ₂ AsO ₄ ⁺²	Fe ⁺³ + H ₃ AsO ₄ = FeH ₂ AsO ₄ ⁺² + H ⁺	1.8	Langmuir
FeHASO ₄ ⁺	Fe ⁺³ + H ₃ AsO ₄ = FeHASO ₄ ⁺ + 2H ⁺	0.66	Langmuir
FeAsO ₄	Fe ⁺³ + H ₃ AsO ₄ = FeAsO ₄ + 3H ⁺	-1.8	Langmuir
Ca(II)-As(V)			
CaH ₂ AsO ₄ ⁺	Ca ⁺² + H ₃ AsO ₄ = CaH ₂ AsO ₄ ⁺ + H ⁺	-1.18	Langmuir
CaHASO ₄	Ca ⁺² + H ₃ AsO ₄ = CaHASO ₄ + 2H ⁺	-6.51	Langmuir
CaAsO ₄ ⁻	Ca ⁺² + H ₃ AsO ₄ = CaAsO ₄ ⁻ + 3H ⁺	-14.48	Langmuir
Fe(III)-SO₄			
FeSO ₄ ⁺	Fe ⁺³ + SO ₄ ⁻² = FeSO ₄ ⁺	4.04	Parkhurst
FeHSO ₄ ⁺²	Fe ⁺³ + HSO ₄ ⁻ = FeHSO ₄ ⁺²	2.48	Parkhurst
Fe(SO ₄) ₂ ⁻	Fe ⁺³ + 2SO ₄ ⁻² = Fe(SO ₄) ₂ ⁻	5.38	Parkhurst
Phases			
Ferric Arsenate	FeAsO ₄ ·xH ₂ O = Fe ⁺³ + AsO ₄ ⁻³ + xH ₂ O	-23	Langmuir
Ferrihydrite	Fe(OH) ₃ = Fe ⁺³ + 3OH ⁻	-37 (-39)	Langmuir
Scorodite	FeAsO ₄ ·2H ₂ O = Fe ⁺³ + AsO ₄ ⁻³ + xH ₂ O	-25.83	Langmuir

Langmuir, D.; Mahoney, J.; Rowson, J., (2006) "Solubility products of amorphous ferric arsenate and crystalline scorodite (FeAsO₄·2H₂O) and their application to arsenic behavior in buried mine tailings," *Geochimica et Cosmochimica Acta*, 70(12), 2942-2956.

Parkhurst, D.L., Appelo, C.A.J., (1999) "User's guide to PHREEQC (Version 2), A computer program for speciation, batchreaction, one-dimensional transport, and inverse geochemical calculation," U.S. Geol. Surv. Water-Resour. Invest. Rep., 99-4259.

* Generated through the use of Excel to solve the material balance equations provided by the reactions and equilibrium constants located in appendix II and obtained from Langmuir et al. 2006 and PHREEQC.

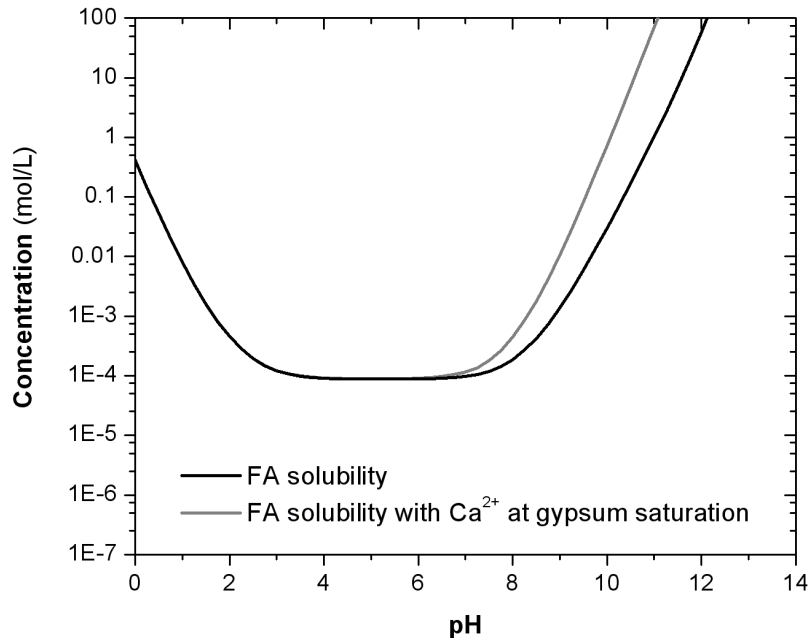


Figure II-1 Effect of Ca^{2+} on the theoretical solubility of Fe and As with respect to FA (assuming $\text{pK}=23$, no Fe- SO_4 complexes, congruent dissolution)

Figure II-1 illustrates the results of the theoretical congruent solubility of FA, as well as the solubility of FA in solution with a calcium concentration equal to that of gypsum solubility. (While it is understood that the assumption of congruent dissolution is not valid for a quantitative explanation, the results obtained serve the purpose for qualitative discussion.) According to these results, the computed solubility should increase when Ca^{2+} is present. To explain this effect, the distribution of the aqueous complexes was calculated and is presented in figure II-2. It becomes evident that in the alkaline pH region, Ca-AsO_4 aqueous complexes begin to dominate, hence contributing to the observed increase in solubility. However, the ageing results showed the opposite affect, that is to say, a reduction in arsenic release (enhancement of stability) with the presence of calcium.

As a result, it may be possible for the Ca-AsO_4 aqueous complexes to remain intact during surface complexation, resulting in ternary surface complexes which are less charged than arsenate species (i.e. CaHAsO_4^0 and CaAsO_4^- as opposed to HAsO_4^{2-}). The concept of ternary surface complexes[†] was proposed by Schindler [1990] and is being

[†] $\equiv \text{SOH} + \text{L}^- + \text{M}^{z+} \longleftrightarrow \equiv \text{S} - \text{L} - \text{M}^{z+} + \text{OH}^-$ or $\equiv \text{SOM} - \text{L}^{(z-2)+} + \text{H}^+$

explored in ferric iron [Swedlund & Webster, 2001] (and other) systems using surface complexation modeling and advanced characterization techniques. The possibility of ternary Ca-AsO₄ complexes also fits with the observed association of As with Fe and Ca in industrial tailings [Paktunc et al. 2003, Pichler et al. 2001, Donahue et al. 2000] and can be conceptualized as a transition between single element surface complexation and the formation of minerals such as yukonite or arsenosiderite.

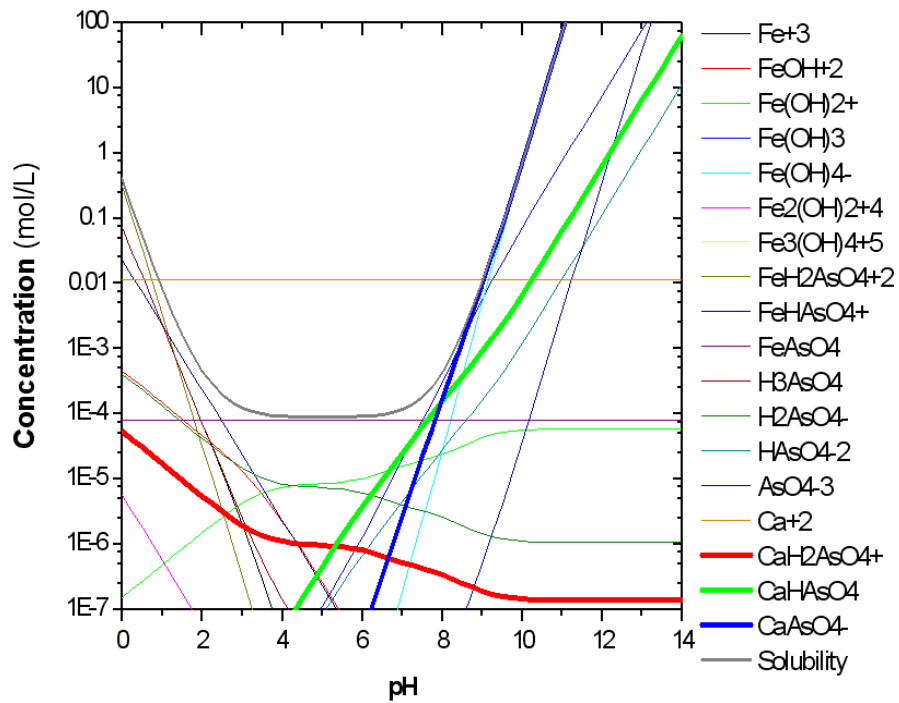
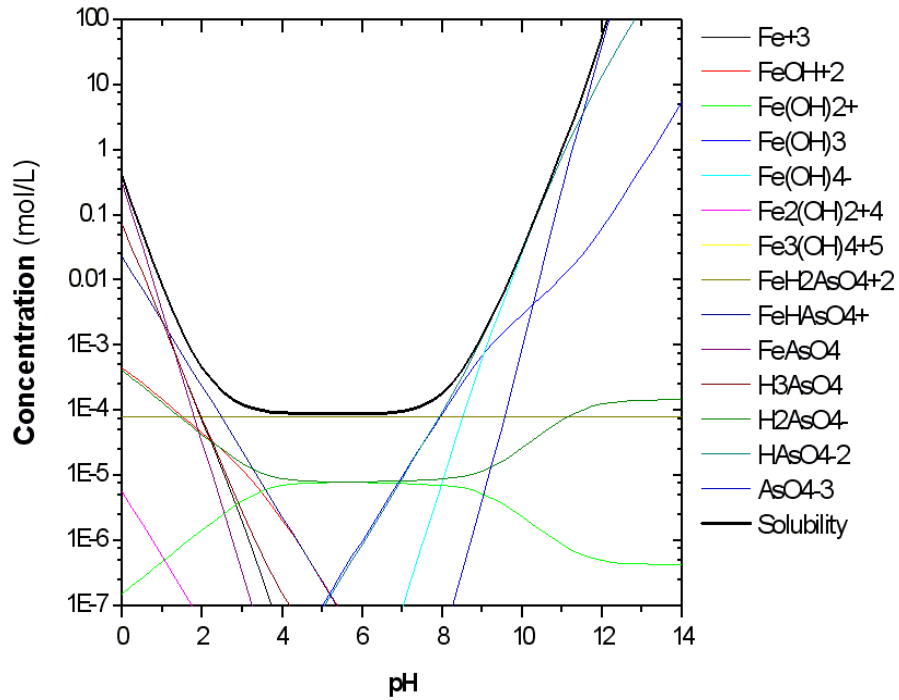


Figure II-2 Distribution of aqueous complexes that affect FA solubility (top) FA and (bottom) FA with Ca^{2+} present at a concentration corresponding to gypsum saturation

Appendix III Additional Data from Coprecipitate Production and Ageing

Table III-1 presents ORP measurements obtained from each reactor, as well as the feed solution, during coprecipitate production. The values indicate the average of at least two measurements during steady-state operation.

Table III-1 Continuous circuit operation ORP readings

Exp.	Conditions	Feed		SS Operation ORP*		
		pH	ORP (mV)	pH 2.5 (mV)	pH 4 (mV)	pH 8 (mV)
RP-2	1 stage, NaOH	n/a	n/a	---	---	n/a
RP-4	1 stage, Ca(OH) ₂	n/a	n/a	---	---	n/a
RP-4b	1 stage, Ca(OH) ₂	1.21	677	---	---	330
RP-5	2 stage, Ca(OH) ₂	1.16	692	---	474	452
RP-6	3 stage, Ca(OH) ₂	1.30	692	680	527	360
RP-11	3 stage, Ca(OH) ₂	1.18	672	690	590	305
RP-9a	2 stage batch start, Ca(OH) ₂	n/a	n/a	---	500	300
RP-9	2 stage w/ recycle, Ca(OH) ₂	1.20	679	---	500	315
RP-7	2 stage w/ Ni ²⁺ , Ca(OH) ₂	1.19	664	---	515	365
RP-8	2 stage w/ Al ³⁺ , Ca(OH) ₂	1.20	670	---	505	305
RP-12	2 stage w/ Fe ²⁺ , Ca(OH) ₂	1.20	474	---	270	-255

*ORP values obtained with an electrode reading 44 mV relative to the calomel electrode

Figure III-1 presents some additional coprecipitate ageing data from single stage coprecipitates with different Fe/As molar ratios which were not shown in Figure 18 (experiments RP-2 and 4, Fe/As~3.4). The data for ageing of single stage coprecipitates with an Fe/As molar ratio of 4 are also shown for comparison (experiment RP-4b). For experiment RP-4, the higher arsenic concentrations are the result of the lower Fe/As ratio while for experiment RP-2, the higher arsenic concentrations are due both the lower Fe/As ratio as well as the to the use of NaOH as base, as opposed to Ca(OH)₂.

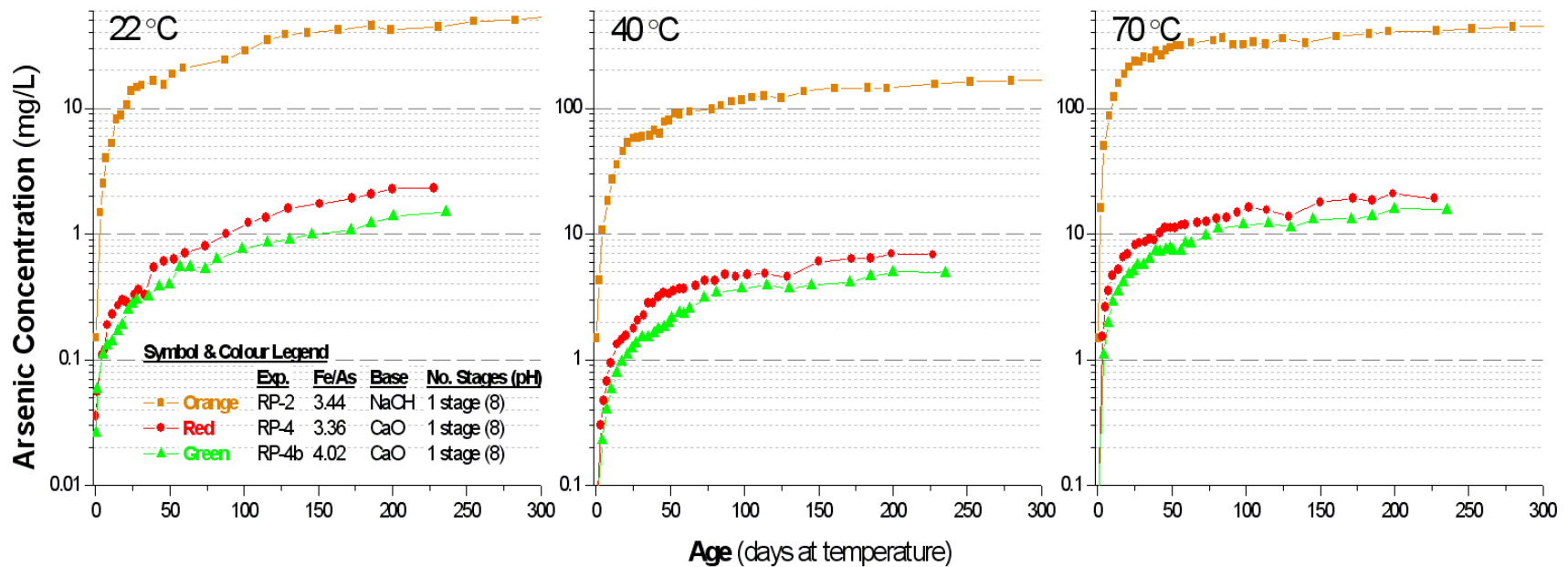


Figure III-1 Ageing profiles for experiments RP-2, 4 & 4b